Electronic Theses and Dissertations                    Theses, Dissertations, and Major Papers

2007

# Chemical and biochemical aspects of protein disulfide isomerase denitrosation/nitrosation activities, and the role of vicinal thiols

Inga Sliskovic
*University of Windsor*

Follow this and additional works at: https://scholar.uwindsor.ca/etd

Chemical and Biochemical Aspects of

Protein Disulfide Isomerase Denitrosation/Nitrosation

Activities, and the Role of Vicinal Thiols

by

Inga Slišković

A Dissertation

Submitted to the Faculty of Graduate Studies

through Chemistry and Biochemistry

in Partial Fulfillment of the Requirements for

the Degree of Doctor of Philosophy at the

University of Windsor

Windsor, Ontario, Canada

2007

# Canada

# ABSTRACT

Protein disulfide isomerase (PDI) is involved in isomerization, reduction and oxidation of disulfide bonds. Recent studies from our lab showed that cell-surface PDI is also involved in transport of nitric oxide (•NO) inside the cells. •NO is a small signaling molecule involved in many cellular processes.

We have utilized S-nitrosoglutathione (GSNO) as a substrate for PDI in order to characterize its denitrosation activity. Our results suggested that final product of PDI-mediated GSNO denitrosation is •NO. We have shown that PDI stores •NO released from GSNO, probably in the form of $N_2O_3$ and can transfer it to intra- and intermolecular thiols. Our findings suggest that PDI could have an important role in both efflux and influx of S-nitrosothiols (RSNO)-bound •NO.

We have shown that platelet surface PDI (psPDI) was able to mediate GSNO denitrosation thus inhibiting platelet aggregation. Animal models of the pre-diabetic state indicated that psPDI activity was diminished, platelet ROS production and aggregation rates were enhanced compared to controls. Treatment of animals with rosuvastatin, an inhibitor of HMG-CoA reductase, showed efficacy in normalizing activities monitored in this animal model of diabetes. Monitoring the dynamic thiol and disulfide states provides an insight for evaluating PDI-dependent processes. We have shown, using ICAT-MALDI technology, that the PDI **a** domain active site thiols undergo spontaneous oxidation, while the **a'** domain thiols are present in an oxidized state.

The presence of PDI on the ghost membranes of RBC suggested that it may play a role in NO-efflux from RBC. We have shown that ghost-associated PDI disulfide reductase activity is inhibited in the presence of NO donors, accompanied by a decrease in thiol concentration, due to the S-nitrosation of PDI active site thiols. These findings strongly suggest the NO transport in RBC could be mediated by PDI present on the ghost membranes.

We have shown that iron(III) is a potent inhibitor of caspase-3 activity. Our results suggest that PDI is capable of activating caspase-3 inhibited by iron(III), probably by formation of iron-sulfur complexes through its active site thiols. We propose a physiological role for Fe(III) and PDI dependent caspase-3 activation in the process regulating apoptosis.

**Posvećeno mojoj Mami,**

**za sve što je učinila za mene**

# ACKNOWLEDGEMENTS

First and foremost, I would like to thank my supervisor, Dr. Bulent Mutus, for his invaluable support and guidance over the years. I would also like to thank my committee members Dr. Lana Lee, Dr. Siryam Pandey, Dr. William Crosby and external examiner Dr. Guy Guillemette for their contributions. I would like to thank Dr. Sirinart Ananvoranich and Dr. Panayiotis Vacratsis for all their help over the years.

My deepest appreciation goes to Arun Raturi and Shane Miersch, for all their help throughout the years and indispensable contribution to my thesis. I would also like to thank both previous and current members of the Mutus lab: Paul Root, Jiyun Wang, Arzu Akarca, Ruchi Chaube, Harmanpreet Kaur, Suzie Durocher and Patrick Walsh. Many thanks to Una Lee, Anna Kozarova, Denis Tetreault and Monica Radulescu for always being there for me. My thanks extend to all of the other graduate students in the department who have made this journey pleasurable both academically and socially.

I would like to extend my gratitude to all other faculty and staff of the department for providing assistance and entertainment over the years. Special thanks to Marlene Bezaire for all her help during my studies.

Finally, I would like to thank my family for all their support, understanding and encouragement. Most importantly I would like to thank my mom, for being my prime inspiration throughout the years.

# TABLE OF CONTENTS

# LIST OF FIGURES

# LIST OF SCHEMES

# LIST OF ABBRIVIATIONS

| | |
|---|---|
| ACD: | Acid Citrate Dextrose |
| Ac-TEMPO: | 4-((9-acridinecarbonyl)-amino)-2,2,6,6-tetramethylpiperidine-1-oxyl |
| ADP: | Adenosine diphosphate |
| ATP: | Adenosine triphosphate |
| $BH_4$: | Tetrahydrobiopterin |
| BSA: | Bovine serum albumin |
| BSA-NO: | S-nitroso albuin |
| CaM: | Calmodulin |
| cGMP: | Cyclic guanosine monophosphate |
| csPDI: | Cell surface PDI |
| DAN: | Diaminonaphthaline |
| DEA-NO: | Diethylamine NONOate |
| DFO: | Desferoxamine |
| Dieosin-GSSG: | Dieosin glutathione disulfide |
| DMF: | N, N,-Dimethyl formamide |
| DMSO: | Dimethylsulfoxide |
| DNA: | Deoxyribonucleic acid |
| DTNB: | 5, 5'-dithiobis(2-nitrobenzoic acid) |
| DTT: | Dithiothreitol |
| EDTA: | Ethylene diamine tetraacetic acid |

| | |
|---|---|
| ER: | Endoplasmic reticulum |
| FAD: | Flavin adenine dinucleotide |
| FDA: | Food and Drug Administration |
| GC: | Guanylate cyclase |
| GP: | Glycoprotein |
| GSH: | Reduced glutathione |
| GSNO: | S-nitrosoglutathione |
| GSSG: | Oxidized glutathione |
| Hb: | Hemoglobin |
| HMG-CoA reductase: | 3-hydroxy-3-methylglutaryl Coenzyme A reductase |
| IAA: | Iodo acetic acid |
| ICAT: | Isotope coded affinity technology |
| IPA: | Isopropyl alcohol |
| IPTG: | Isopropyl $\beta$-D-1-thiogalactopyranoside |
| $IP_3$: | Inositol 1, 4, 5 biphosphate |
| MALDI-TOF: | Matrix assisted laser desorption/ionization time of flight |
| MS: | Mass spectrometry |
| NADPH: | Nicotinamide adenine dinucleotide phosphate |
| NAT: | Napthatriazole |
| NEM: | N-ethylmaleimide |
| NO•: | Nitric oxide |
| NOS: | Nitric oxide synthase |
| NOX: | NADPH oxidase |

| | |
|---|---|
| PAO: | Phenylarsine oxide |
| PBS: | Phosphate buffer saline |
| PDI: | Protein disulfide isomerase |
| PRP: | Platelet rich plasma |
| psPDI: | Platelet surface PDI |
| RBC: | Red blood cells |
| RFU: | Relative fluorescence units |
| ROS: | Reactive oxygen species |
| RS•: | Thiyl radical |
| RSH: | Thiols |
| RSNO: | S-nitrosothiols |
| SOD: | Superoxide dismutase |
| sGC: | Soluble guanylate cyclase |
| SNAP: | S-nitroso-N-acetyl-penicillamine |
| T2D: | Type 2 diabetes |

# CHAPTER 1

# Introduction to Protein Disulfide Isomerase and Nitric Oxide

## 1.1 Protein Disulfide Isomerase

Protein disulfide isomerase (PDI) was first isolated from bovine liver and characterized by Anfinsen in the 1960's (Goldberger *et al.*, 1963; DeLorenzo *et al.*, 1966). Its primary location was found to be the lumen of the rough endoplasmic reticulum (ER) where it assists in the folding of newly synthesized proteins by performing a series of disulfide isomerization reactions. PDI has been found widely distributed across eukaryotic cells where it performs a variety of functions (Turano *et al.*, 2002).

### 1.1.1 Structure and classification

PDI belongs to the PDI-like family of proteins and all of them are characterized by the multidomain arrangement. Each domain resembles the typical thioredoxin fold which is formed by the specific sequence of α-helixes and β-strands: β1–α1–β2–α2–β3–α3–β4–β5–α4 (Kemmink *et al.*, 1997; Ferrari *et al.*, 1998). PDI is ~55 kDa protein consisting of 5 domains, as shown in Figure 1.1 (Darby *et al.*, 1996). Two redox active domains, **a** and **a'** contain the active site sequence CGHC that performs reduction and oxidation reactions. Domains **b** and **b'** lack the active site, but still resemble the thioredoxin fold (Kemmink *et al.*, 1999). Domain **c** consists of highly negatively charged sequences that contribute to the low affinity, high capacity calcium binding properties of PDI (Macer and Koch, 1988), and the KDEL sequence for retention in the ER (Kemmink *et al.*, 1997).
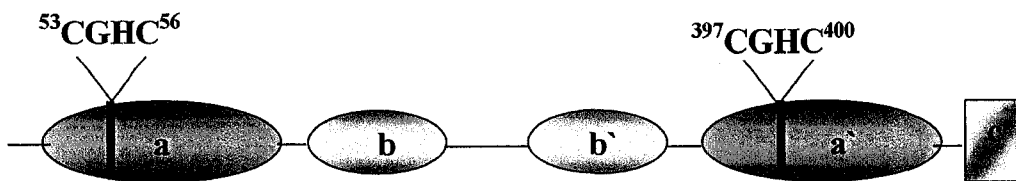
**Figure 1.1: Domain organization of PDI (Darby *et al*, 1996)**

In the recent review by Ellgaard and Ruddock (Ellgaard and Ruddock, 2005), the human

PDI-like family of proteins consists of 17 members all of which contain at least one

redox active domain as shown in Figure 1.2.
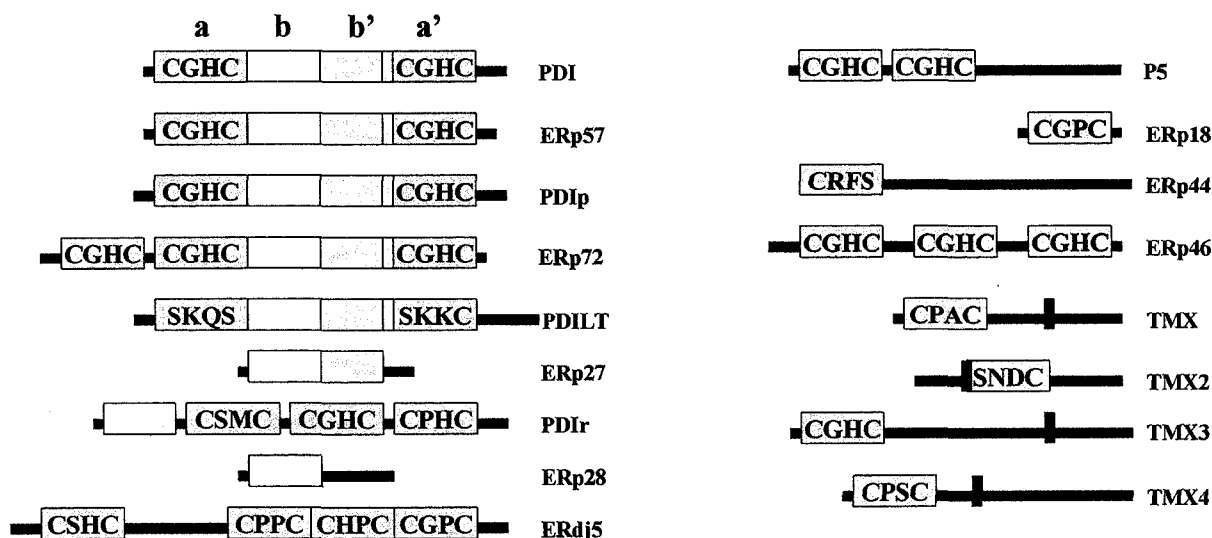


**Figure 1.2: Overview of human PDI family**

The green squares represent the active site domains (**a** and **a'**), the catalytically inactive

domains are shown in yellow and pink (**b** and **b'**, respectively), and the linker region

between **b'** and **a'** is shown in blue.

The overall role of different domains of PDI remained a mystery until the structures of individual domains (Kemmink *et al.*, 1995, 1996) were solved and most recently, the overall structure of yeast PDI was determined (Tian *et al.*, 2006). Initial structural studies of individual domains of PDI by Kemmink revealed that **a** and **b** domains share highly conserved secondary structure elements despite their low primary sequence identity (11%) (Kemmink *et al*, 1999). Besides the absence of the active site CGHC, **b** domain has β4 sheet antiparallel to the others (Figure 1.3)

**(a)**                    **(b)**
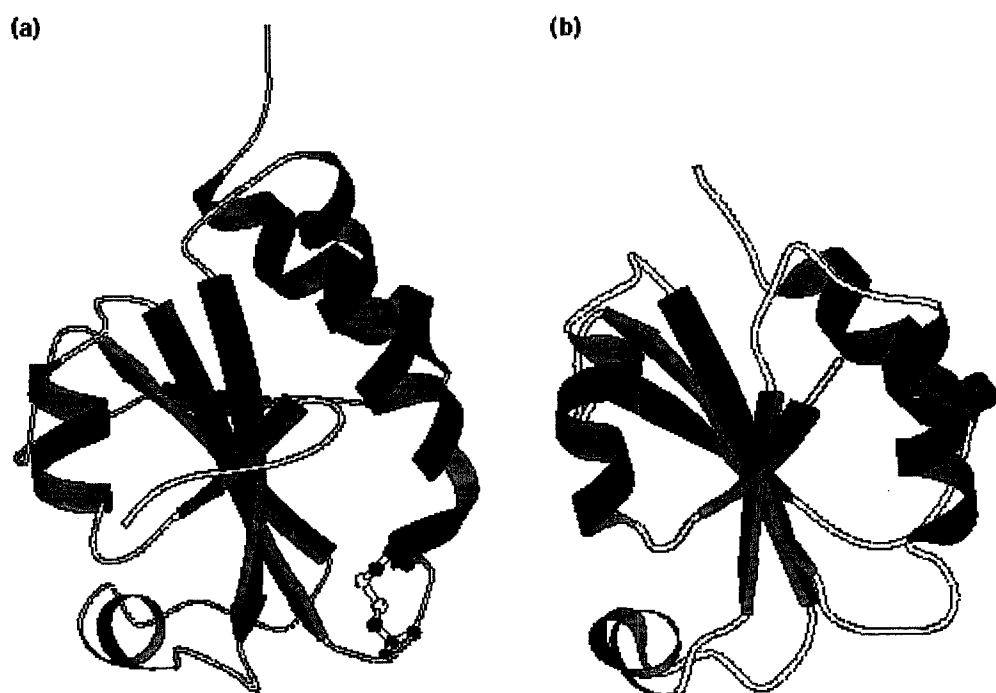
**Figure 1.3: MOLSCRIPT representation of PDI a-domain (a) and PDI-b-domain (b)**

Adapted form Kemmink *et al* (1997) with the permission from Elsevier.

The redox activity of PDI is due to reactivity of its active site cysteines in CGHC peptide, especially its N-terminal Cys which has a pKa of 4.5 and is partially stabilized by the nearby histidine imidazole group (Ferrari and Soling, 1999). Therefore, the disulfide

form of the protein is relatively unstable as compared to thioredoxin and results in oxidative rather than reductive function (Kortemme *et al,*. 1996, Freedman *et al.*, 1995). Based on these early single domain studies, it was proposed that the other domains **a'** and **b'** should resemble the **a** and **b** domains, respectively, but the overall domain arrangement was unknown until the crystal structure of yeast PDI was determined. Since the yeast and mammalian PDI share a high degree of primary structure and domain arrangement, it seems very likely that they will share the same architecture (Tian *et al.*, 2006).

### 1.1.2   Understanding the structure and function of PDI

In the absence of overall mammalian PDI structure, initial research of understanding the significance of individual domains was performed by studying multidomain constructs. Darby and coworkers (Darby *et al.*, 1998) observed that for the disulfide bond isomerization, the absence of **b'** and **a'** domains totally inhibited PDI activity, thereby suggesting that these two domains play a crucial role in substrate binding. Disulfide bond formation and reduction was significantly decreased in the absence of a full PDI construct, suggesting that the overall multidomain architecture of PDI has evolved in this way in order to achieve its versatile catalytic repertoire enabled though PDI substrate interactions.

The crystal structure of the yeast PDI and its individual domains is shown in Figure 1.4.
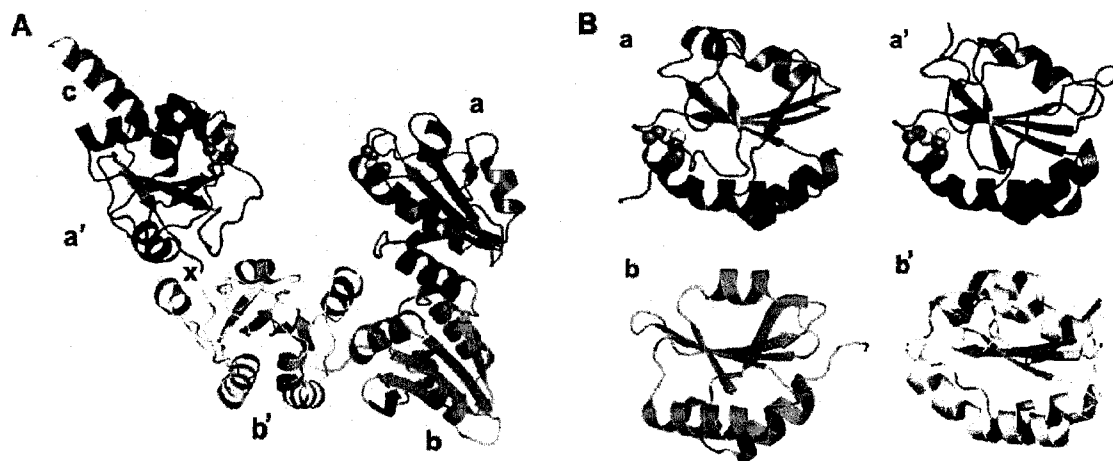
**Figure 1.4: Overall structure of yeast PDI (PDB 2B5E)**

A) Ribbon diagram of PDI. B) Ribbon diagram of individual domains.

(Tian *et al.*, 2006) with the permission from Elsevier.

As shown in Figure 1.4 (a), PDI resembles the letter "U", with the b and b' domains at the base and the a and a' domains at the ends of "U". Each of the domains appears to have a typical thioredoxin fold with minor variations. For example, b domain does not contain the third α helix and its second helix is shorter while the b' domain has an additional short helix and lacks the first β sheet. The four domains are arranged in an asymmetrical geometry which allows domain a to be in contact with both the b and b' domains, while a' interacts with b' domain only. The active sites on the a and a' domains point towards each other but are separated by the large cleft, although the interaction may be possible since a and a' domains are more flexible with respect to the rigid base consisting of b and b' domains.

a) Active site **a** and **a'** domains

Even though the **a** and **a'** domains share a high structural homology, there are a few significant differences observed in yeast PDI. First of all, the redox state of two active site domains are different in a way that **a** domain active site was found to be in its oxidized form while **a'** domain active site was detected in its reduced form. This can be explained by the corresponding standard redox potentials of -188 mV for the **a** domain and -152 mV for the **a'** domain. If these values are compared with the strongest oxidant in the thioredoxin family, DsbA that has the redox potential of -120 mV (Zapun *et al.*, 1993) and strongest reductant thioredoxin with redox potential of -270 mV (Aslund *et al.*, 1997; Moore *et al.*, 1964), it may be speculated that in yeast PDI, the active site of the **a** domain will be mainly in its oxidized form while the active site of the **a'** domain will be reduced.

Another difference lies in the location of tryptophan residue located immediately before each active site cysteine. In the **a** domain, $W_{60}$ seems to be fixed at its location while $W_{405}$ of **a'** domain is highly mobile. As a result of this, the $C_{406}$ of the **a'** domain is more exposed to the solvent than $C_{61}$, hence making the active site of **a'** domain more accessible.


b) Hydrophobic **b** and **b'** domains

The structure of PDI reveals several surface exposed hydrophobic patches. Two of them surround the active sites in **a** and **a'** domains, while **b** and **b'** domains each have one exposed hydrophobic patch at the relatively same position. As a consequence of this, the continuous hydrophobic surface is formed which plays a crucial role in the interaction

between PDI and its substrates. Retrospectively, the opening between **a** and **a'** domain and the hydrophobic pocket in **b'** domain is large enough to accommodate a folded protein of about 100 residues. This study is in agreement with the earlier observations made by Klappa and coworkers (Klappa *et al.*, 1998) where they reported the presence of highly hydrophobic pockets in the b' domain and recognized it as the primary peptide binding site. Although it could be speculated that **b** domain could share the peptide binding properties of **b'** domain, the studies using mutants **bb'a'c** and **b'a'c** showed that the **b'** domain plays a role in the refolding of proteins while **b** domain may influence the refolding rates in selected cases (Tian *et al.*, 2006)

### 1.1.3    Multifunctional aspects of PDI

PDI is a multifunctional enzyme involved in isomerization, reduction, oxidation, chaperone and other activities which will be described in the following sections.

### 1.1.3.1 Isomerazation, reduction and oxidation

One of the first studied functions of PDI was the folding of newly synthesized proteins in the ER. Since the concentrations of PDI in the ER is approximately 0.8% of the total cellular protein (Freedman *et al.*, 1994) and it interacts with a broad group of peptides (Noiva, 1994), it can be speculated that PDI is one of the most important enzymes for the correct assembly of proteins in the ER.

The major oxidizing and reducing power in the ER is thought to be combination of glutathione (GSH) and glutathione disulfide (GSSG). The ER is considered to be more

oxidative environment since the ratio of GSH to GSSG is close to 2:1, while in the cytoplasm this ratio is more reducing and it varies from 20:1 to 100:1 (Noiva, 1994). Oxidizing equivalents in the ER come from an additional source which is the Ero1 protein that is proposed to form a mixed disulfide with the reduced PDI thereby oxidizing it. The Ero1 FAD moiety would essentially allow for the constant electron transfer to $O_2$ thus completing the redox circle (Ellgaard, 2004).

The mechanism for the role of PDI in isomerization, reduction and oxidation is shown in Figure 1.5. The first step in rearrangement of misfolded disulfide bonds involves nucleophilic attack of the N-terminal cysteine in CGHC active site of PDI which results in the formation of a mixed disulfide between PDI and its substrate. The isomerization is completed by the attack of the second cysteine of PDI, which breaks a mixed disulfide bond, leaving PDI in its reduced state and the properly folded substrate. In the case where isomerization fails to proceed to completion, a series of reduction and oxidation reactions take place, until the substrate folds into the proper conformation and resists further attack by PDI (Schwaller *et al.*, 2003).
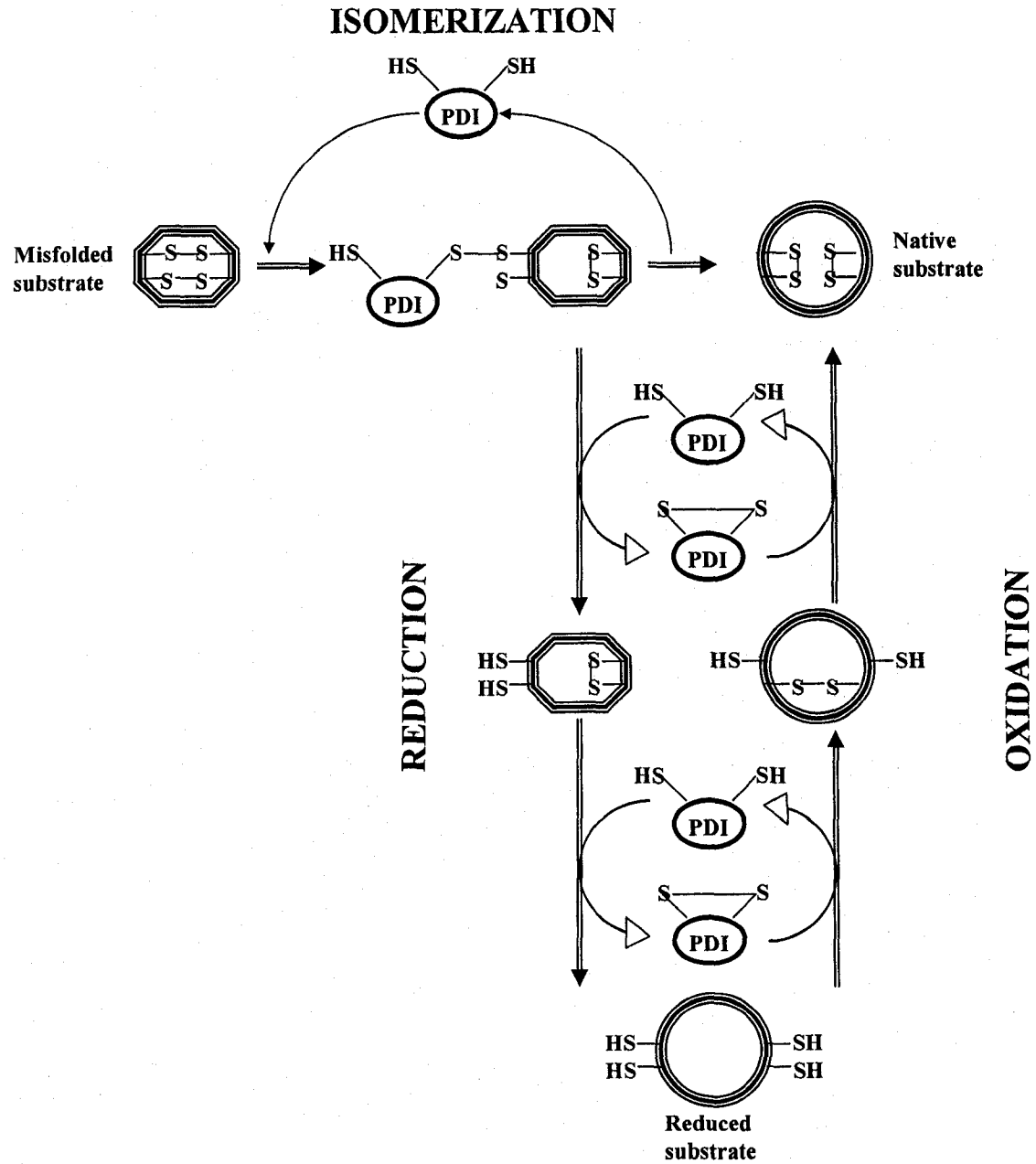
# ISOMERIZATION



Figure 1.5: Isomerization, reduction and oxidation of PDI (Schwaller *et al.*, 2003)

### 1.1.3.2 Chaperone activity

A protein is referred to as a chaperone if it is able to assist unfolded or misfolded proteins to attain the native state by providing a protective microenvironment which decreases the chance of aggregation and precipitation. PDI is a chaperone with a wide range of substrates. It chaperones proteins that contain disulfide bonds such as lysozyme (Puig and Gilbert, 1994; Hayano et al., 1996), and proteins which lack disulfide bonds such as acidic phospholipase $A_2$ (Yao et al., 1997), glyceraldehyde-3-phosphate dehydrogenase (Cai et al., 1994) and rhodanase (Song and Wang, 1995) as shown by in vitro refolding studies. The ability of PDI to act as a chaperone is shown to be independent of its isomerase activity and does not involve its active site CGHC sequence. Previous studies have shown that the acidic domain c plays a crucial role in PDI chaperone activity since the mutated PDI lacking c domain showed no chaperone activity (Dai and Wang, 1997).

### 1.1.3.3 Subunit of other enzymes

a) Prolyl 4-Hydoxylase

Prolyl 4-hydroxylase (P4H) is an enzyme located in the ER where it catalyzes the hydroxylation of proline residues of newly synthesized procollagen polypeptides (Kivirikko et al., 1989). It consists of two α and two β subunits, with α subunits being catalytically active. Protein sequencing and DNA analysis of β subunit of P4H suggested that this subunit is identical to PDI (Bulleid, 1993). There are several different proposed roles of PDI as a part of P4H. It was initially believed that the active site of PDI may play a role in the various redox steps of the hydroxylation reaction, or it may act as a

retention signal for P4H considering that P4H lacks the retention sequence at its C-terminus (Bassuk *et al.*, 1989) and finally it may provide a molecular support by keeping the enzyme in its soluble form, since earlier *in vitro* studies have shown that the α subunits of P4H aggregate when they are dissociated from the β subunits (Tuderman *et al*, 1975).

b) Microsomal Triglyceride Transfer Protein

Microsomal triglyceride transfer protein (MTP) is a heterodimer consisting of two subunits (58 kDa and 88 kDa) and catalyzes the transfer of triglycerides into lipoproteins. The 58 kDa subunit has been characterized as PDI (Wetterau *et al.*, 1990), and here it keeps the MTP complex in a soluble form since the removal of the smaller subunit results in the irreversible aggregation and inactivation (Wetterau *et al*, 1991). It is interesting that the MTP has very little PDI isomerase activity (Wetterau *et al.*, 1990), suggesting that the active site of PDI is either inaccessible or unreactive.

## 1.1.3.4 Other functions of PDI

Narindrasorasak and coworkers recently reported that PDI is capable of binding copper up to 4-10 mols of Cu(I) per mole of PDI (Narindrasorasak *et al.*, 2003). The binding of copper is thought to take place though the CGHC of **a** domain of PDI as it remarkably resembles the fold of Atox1, which is a copper chaperone. This binding results in the formation of PDI tetramer. It has been hypothesized that this copper-bound PDI may act as the copper donor for copper containing proteins during *de novo* synthesis or as a copper chelator in the cells during the binding of copper in copper toxicity. Similarly,

PDI has been shown to bind to zinc ($Zn^{2+}$) (Solovyov and Gilbert, 2004) through the coordination with cysteines in PDI **a**, **a'** and **b'** domains, resulting in dimer formation and higher order oligomers and aggregates. Surprisingly, while $Zn^{2+}$ usually coordinates with four ligands, the site directed mutagenesis studies showed that for PDI only one cysteine in the active site (CGHS) is necessary for PDI to form a dimer as efficiently as the wild type. Therefore, it has been proposed that PDI may serve as a zinc chelator and protects the cells from divalent ion toxicity. However, it is of a great importance to mention that while PDI is acting as a chelator, as in the cases of copper or zinc, its enzymatic activity significantly decreases which may cause a dysfunction in proper protein folding in the ER.

### 1.1.4 Cell surface protein disulfide isomerase

Besides its primary location in the ER, PDI is also found on the cell surface (csPDI) where it binds though electrostatic interactions (Terada *et al.*, 1995). Although PDI should theoretically remain in the ER, since it contains the ER retention sequence (KDEL), there are a couple of different hypotheses proposed for PDI's ability to escape the ER. Initially, it was believed that PDI may be able to escape the ER by saturation of the KDEL sequence, which is known to be involved in peptide binding (Bulleid, 1993). Another mechanism proposes that PDI, when associated with other secretory proteins, may escape the ER and localize itself on the surface (Johnson *et al.*, 2001). Cell surface PDI has been found in the variety of cells including platelets (Chen *et al.*, 1995), leukocytes (Bennett, *et al.*, 2000), hepatocytes (Terada *et al.*, 1995), endothelial cells

(Hotchkiss *et al.*, 1998) and pancreatic cells (Yoshimori *et al.*, 1990) where it plays a role in a variety of physiological conditions.

a) HIV entry and csPDI

The entry of HIV into human cells requires protein interaction between the viral envelope glycoprotein gp120 and the primary receptor CD4 of the host cell (Berger *et al.*, 1999). It was found that CD4 binds to csPDI resulting in a CD4-PDI-gp120 (Figure 1.6) complex that allows PDI to access and reduce gp120 disulfides leading to the gp120 conformational change necessary for viral entry into the host (Ryser and Fluckiger, 2005).
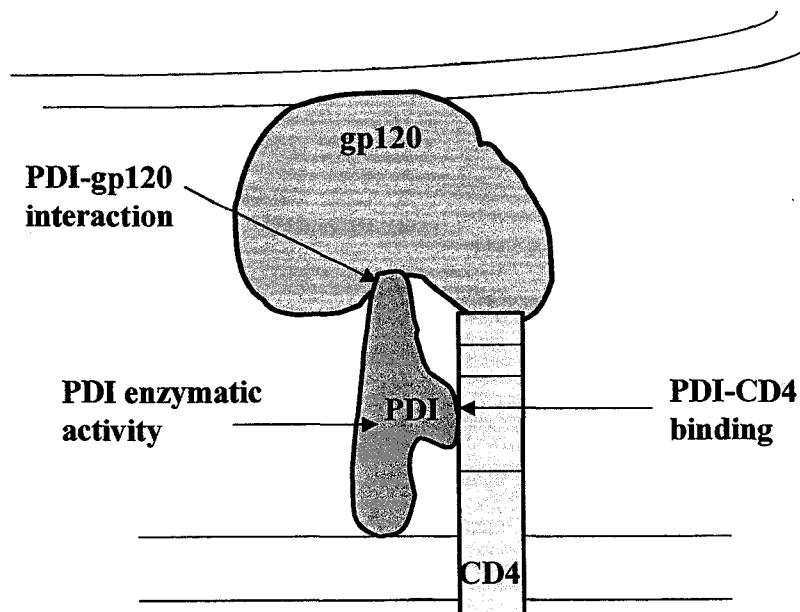


**Figure 1.6: PDI mediated HIV entry (Ryser and Fluckiger, 2005).**

Based on these findings, a novel approach for targeting HIV entry has been proposed and it involves three possibilities. One is to target the activity of PDI, which is necessary for disulfide bond shuffling. Unfortunately, since PDI is a crucial enzyme for various cellular processes as described in previous sections, targeting PDI activity may not be the most suitable approach. Instead, current research is concentrating on the binding sites between PDI-CD4 as well as PDI-gp120, which seems to be a more appropriate target (Figure 1.6).

b) Cell adhesion

Cell surface PDI plays a role in cell adhesion by shuffling surface thiols and disulfides, thereby promoting adhesion or dissociation between various cells. For example, PDI associated with the platelet surface is found to promote platelet aggregation through activation of the αIIβ3 integrin, a known fibrinogen receptor (Essex and Li, 1999).
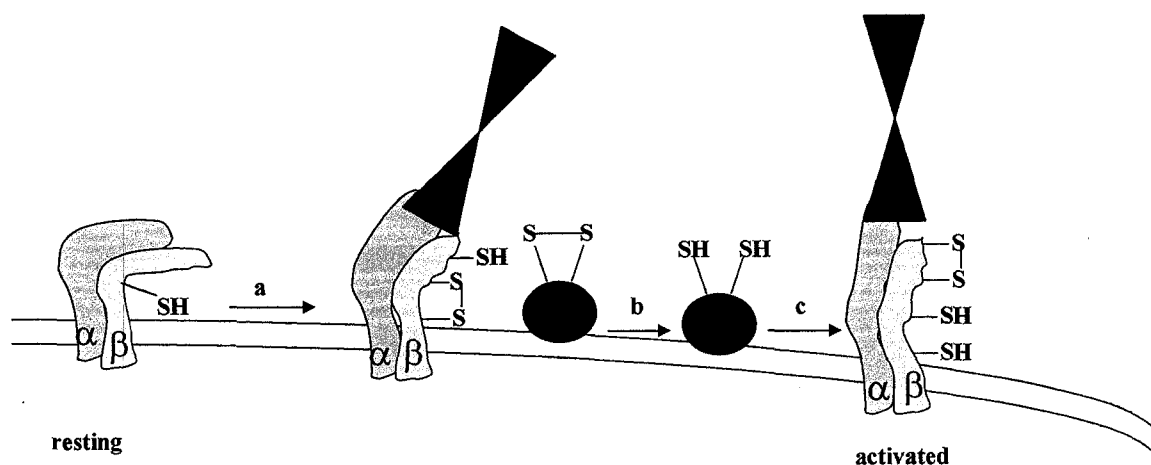


**Figure 1.7: csPDI mediated platelet aggregation (Essex, 2004)**

As shown in Figure 1.7, the platelet fibrinogen receptor ($\alpha II\beta 3$, pink and yellow) is in its reduced state under resting conditions. The first conformational change results from agonist-induced stimulation and initiates fibrinogen (blue) interaction with $\alpha II\beta 3$ (a). PDI (light blue) catalyzes disulfide exchange of $\alpha II\beta 3$ (b, c) that subsequently leads to a high affinity conformation state which results in platelet aggregation.

Another example is the role of csPDI in the regulation of L-selectin shedding. L-selectin is the membrane protein that mediates the recruitment of leukocytes to inflammatory sites (Springer, 1995). During leukocyte activation, L-selectin undergoes proteolytic cleavage which results in its release from the cell surface thus disabling leukocytes from the L-selectin dependent cell interaction (Tedder *et al.*, 1995). The idea of csPDI playing a role in cell adhesion came from the study of Bennett and coworkers (Bennett, 2000), which showed that the vicinal dithiol specific blocker phenyl arsine oxide (PAO) was able to induce L-selectin shedding. Further evidence supporting PDI involvement in L-selectin shedding was obtained by using bacitracin, a common PDI inhibitor, and PDI specific antibodies, both of which induced L-selectin shedding.
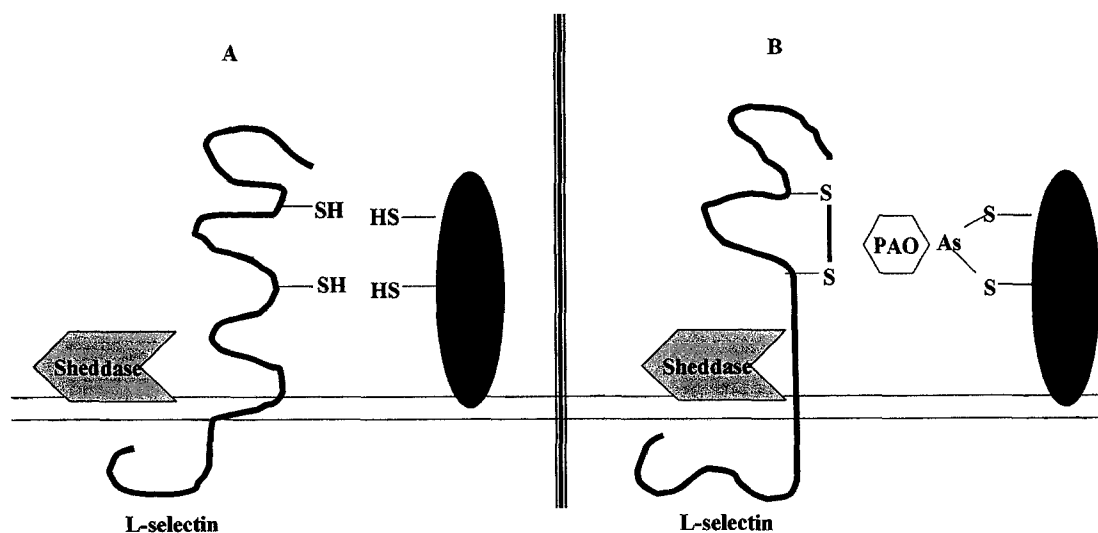
**Figure 1.8: csPDI role in L-selectin shedding (Bennette, 2000)**

Figure 1.8 A shows that csPDI maintains L-selectin in its reduced state which sustains its non-cleavable conformation, thereby resulting in its inaccessibility to the proteolytic action of sheddase (lavender). However, upon blocking PDI active site cysteines with PAO, L-selectin changes its conformation and becomes accessible to the sheddase proteolytic action.

c) PDI-mediated NO release

Besides performing disulfide exchange reactions on the cell surface, Ramachandran and coworkers showed that PDI is also involved in generation of nitric oxide (NO) from S-nitrosothiol molecules (RSNO) (Ramachandran et al., 2001).
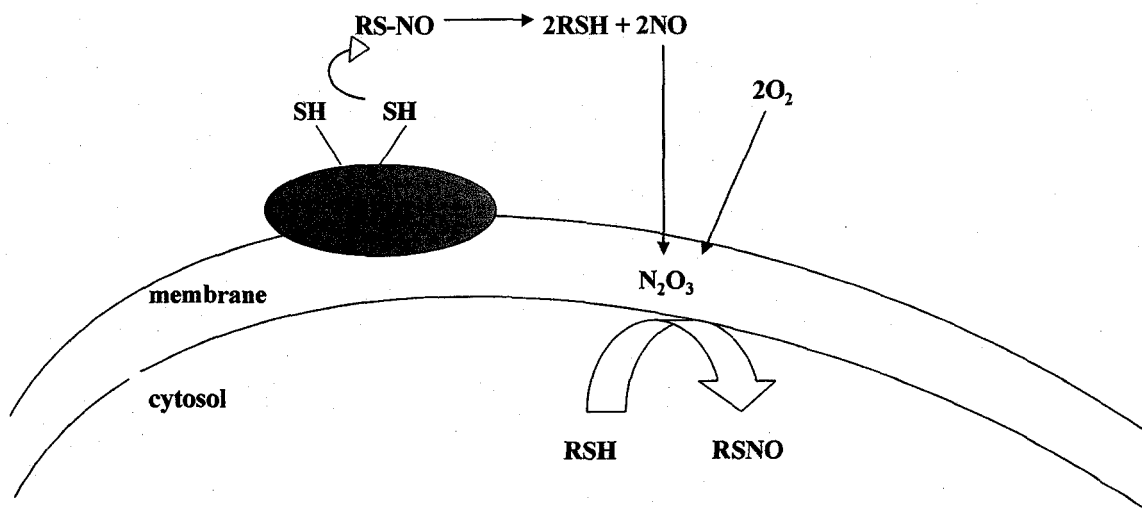
**Figure 1.9: The role of csPDI in intracellular nitrosation (Ramachandran *et al*,**

**2001)**

This study provided the first evidence that csPDI is able to catalyze NO release from RSNOs (Figure 1.9), followed by its accumulation in the membrane where it reacts rapidly with $O_2$ (Liu *et al.*, 1998) to form $N_2O_3$ at the membrane-cytosol interface which, in turn, can nitrosate intracellular thiols (Nedospasov *et al.*, 2000).

## 1.2 Nitric oxide

Nitric oxide (•NO), a diatomic free radical gas molecule, is one of the most ubiquitous substances found to be involved in a variety of physiological and pathophysiological processes. During the early 1980s, •NO was identified from what was believed to be the endothelium-derived relaxing factor (EDRF) by several independent research groups (Ignarro, Moncada and Furchgott) for which were awarded the Nobel Prize in physiology and medicine in 1998. Due to its great importance in the field of science, extensive research about •NO has been conducted in the last two decades.

### 1.2.1 Chemistry and Biology

In order to understand the behavior, nature and reactivity of •NO, the basic principles governing the chemistry and biology of •NO must be understood. The following sections will give a detailed insight into the chemistry and biology of •NO.

### 1.2.1.1 Chemical Properties of Nitric Oxide

Nitric oxide is a colorless gas at the room pressure and temperature with a maximum solubility in water of approximately 2 mM (Venkataraman, et al., 2000). The reactivity of •NO can be depicted by simply looking at its Lewis dot diagram (Figure 1.10) where •NO has one unpaired electron and thus is considered to be a free radical.

$$•\ddot{\overset{..}{N}}•\ +\ •\ddot{\overset{..}{O}}•\ \longrightarrow\ •\ddot{N}:\ :\ddot{O}•$$
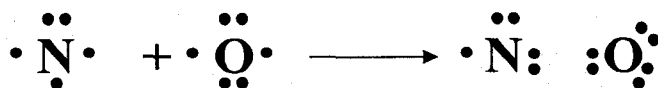
**Figure 1.10: Lewis dot structure of •NO**

The molecular orbital diagram (Figure 1.11) (Stanbury, 1989) of •NO consists of a $\sigma_s$

bonding orbital and corresponding $\sigma_s^*$ antibonding orbital, two $\pi_{x,y}$ bonding orbitals and

slightly higher in energy $\sigma_z$ bonding orbital, two $\pi_{x,y}^*$ antibonding orbitals and a high

energy $\sigma_z^*$ antibonding orbital. Therefore, •NO is a paramagnetic molecule with an

unpaired electron in a $\pi^*$ antibonding orbital. The stability of •NO as a monomer comes

from the fact that •NO has a bond order of 2.5 and formation of a dimer (O=N-N=O)

would give the overall bond order of 5, thus there is no net gain in overall bonding and

•NO exists as a monomer at room temperature and pressure.

N atomic orbitals                    O atomic orbitals
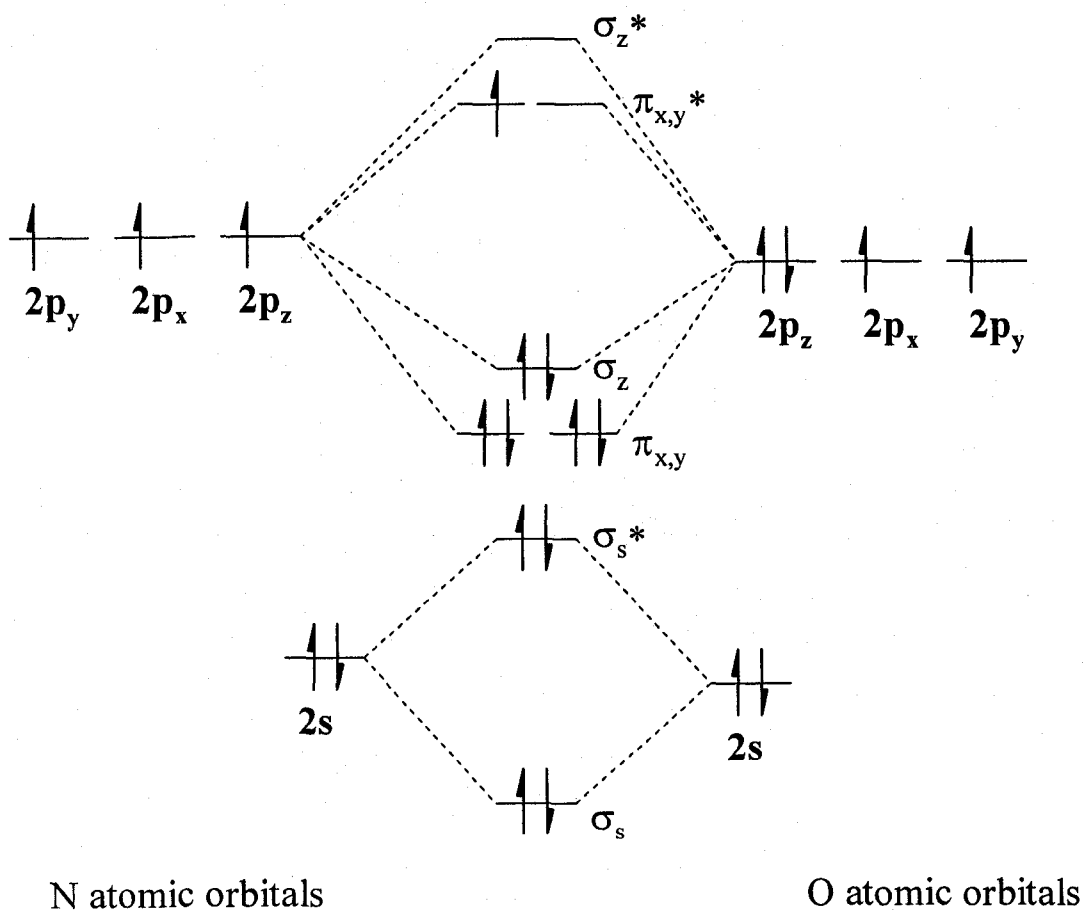
**Figure 1.11: Molecular orbital diagram of •NO (Stanbury, 1989)**

As described in the above paragraph, •NO is a free radical and based on its unique chemistry, it can undergo a variety of redox reactions generating new nitric oxide species. •NO can undergo reduction by accepting an electron to give a nitroxide species ($NO^-$), or oxidation by losing an electron resulting in nitrosonium ($NO^+$). In the presence of molecular oxygen ($O_2$), •NO undergoes a series of reactions to form higher nitric oxide species. Formation of nitrogen dioxide (•$NO_2$) involves reactions (1-3) and consumes 2 equivalents of •NO. Once •$NO_2$ is formed (3), it can react via reaction (4) with another •$NO_2$ molecule to form dinitrogen tetroxide ($N_2O_4$). Another possibility involves combination of •$NO_2$ and •NO to give a potent nitrosating agent (Gobert *et al.*, 1999) dinitrogen trioxide ($N_2O_3$) as in reaction (5).

$$•NO + O_2 \rightarrow •OONO \tag{1}$$

$$•OONO + •NO \rightarrow ONOONO \tag{2}$$

$$ONOONO \rightarrow 2 •NO_2 \tag{3}$$

$$•NO_2 + •NO_2 \rightarrow N_2O_4 \tag{4}$$

$$•NO_2 + •NO \rightarrow N_2O_3 \tag{5}$$

### 1.2.1.2 Biological Properties of Nitric Oxide

Physiologically, •NO is involved in a great variety of cellular processes including roles in vasculature, immune response and neurotransmission (Moncada *et al.*, 1991). However, the *in vivo* reactivity of •NO is determined by its chemical properties, and for simplification purposes, the •NO reactions are divided into two categories: i) direct effects, and ii) indirect effects.

i) Direct effects

Direct effects involve chemical reactions of •NO with its target which is usually a heme-containing protein. The summary of the reactions depicting direct effects is shown in Figure 1.12.



NO

| Oxidation of metals | Reduction of metals | Lipid radical reactions | Heme-NO formation |

$NO + Hb(O2) \rightarrow metHb$    $Fe(IV)=O + NO \rightarrow Fe(II)$    $LOO\bullet + NO \rightarrow LOONO$

Consumption of NO    Limits formation of oxidants and cellular oxidative stress

1. Guanylate cyclase activation
2. Reversible inhibition of Cyt P450
3. Nitric oxygen species
4. Activation of Hemoxygenase
5. Aconitase
6. Inhibition of Catalase
7. Reversible inhinibition of Cyt c oxidase
8. Binding to IRE; stimulation of Transferrin receptor; inhibition of Ferritin

**Figure 1.12: Direct effects of nitric oxide**

The most important reaction of •NO involves reaction with iron centers of the heme. In some cases, this leads to the significant activation of the target enzyme, while in others, to the reversible inhibition. The most studied nitrosylation of the heme resulting in the enzyme activation is most likely soluble guanylate cyclase (GC) (Murad, 1994). Upon •NO binding to the heme of GC, the position of iron within porphorin ring shifts in such a way that the five-coordinate nitrosyl complex becomes favoured (Stone and Marletta, 1994). This leads to a significant GC activation by •NO, with $EC_{50}$ of 100 nM,

(Forstermann and Ishii, 1996) resulting in the conversion of guanosine triphosphate (GTP) to cyclic guanosine monophosphate (cGMP) which in turn initiates a signaling cascade responsible for smooth muscle relaxation. On the contrary, nitric oxide is able to reversibly inhibit monooxygenases such as cytochrome P-450 (Wink *et al.*, 1993). Here, the same principle follows with •NO binding to the heme iron, causing a conformational change and displacement of $O_2$ that is required to facilitate oxidative chemistry.

ii) Indirect Effects

Indirect effects involve species derived from •NO; therefore it requires a higher concentration of •NO than for direct effects, as well as a supply of $O_2$ or superoxide ($O_2^-$). The summary of indirect effects is shown in Figure 1.13.
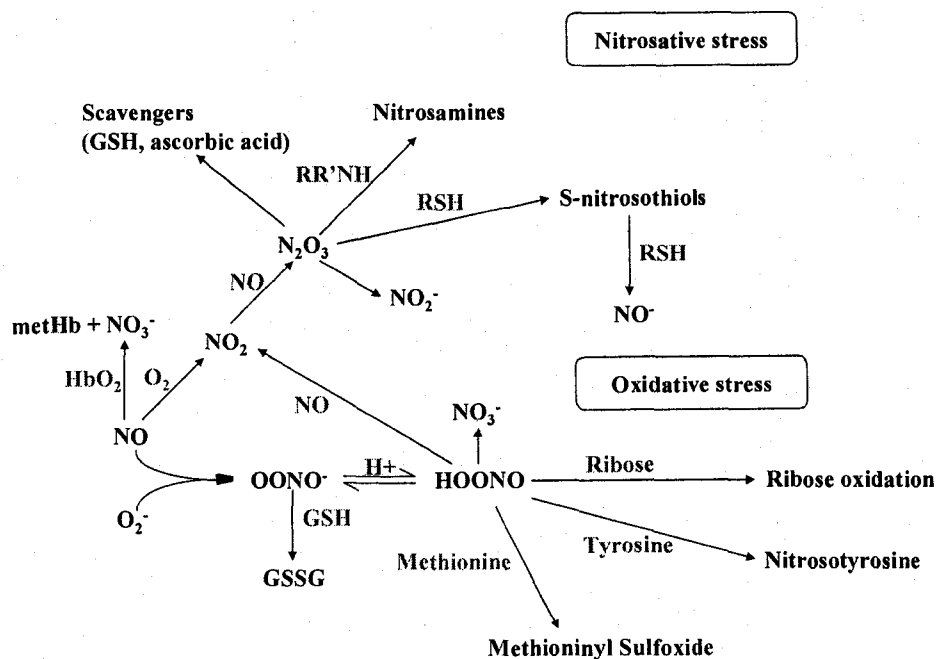


**Figure 1.13: Indirect effects of nitric oxide**

As shown in Figure 1.13, indirect effect of •NO can be subdivided into two classes. The first one involves nitrosative stress which mainly affects primary amines and thiols, while the second one, oxidative stress may result in the modification of variety of macromolecules including DNA, tyrosine residues in proteins and lipids. Therefore, indirect effects are usually associated with a variety of pathophysiological conditions, and this is thought to be due to the presence of higher nitrogen oxide species (Miranda et al., 2000).

## 1.2.2 Endogenous Nitric Oxide

Enzymes involved in endogenous •NO production are called nitric oxide synthases (NOS). There are three isoforms of NOS enzymes and all of them catalyze the five electron oxidation of L-arginine to yield one mole of nitric oxide and citrulline as shown in Figure 1.14 with the overall reaction consuming 1.5 moles of NADPH and two moles of $O_2$.
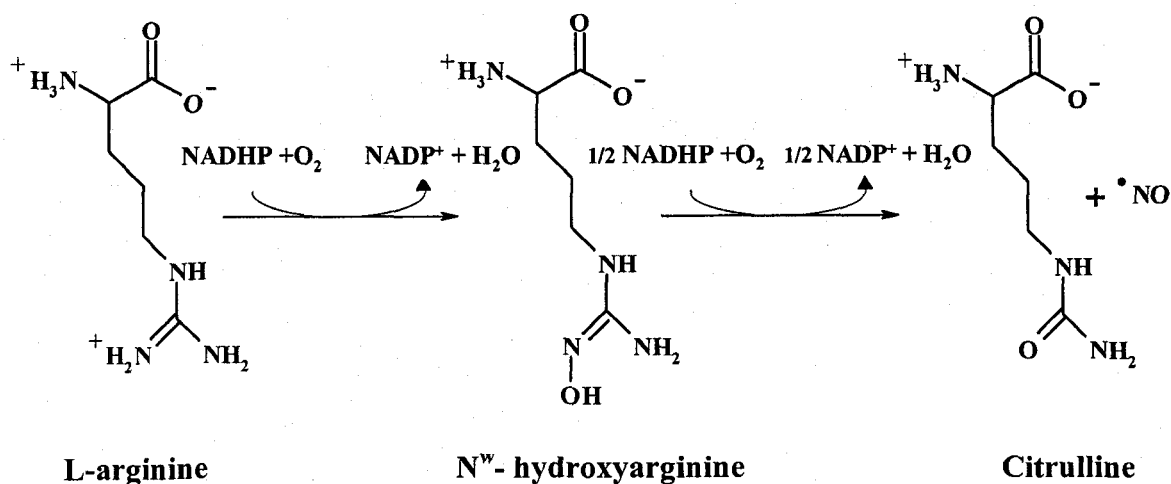
Figure 1.14: •NO synthesis from L-arginine (Hevel and Marletta, 1994)

Although the above reaction appears simple, there are numerous cofactors that play a crucial role in electron transport. Three isoforms of the NOS family of proteins include: neuronal NOS (nNOS or NOS 1), which is involved in neurotransmission and long-term potentiation; inducible NOS (iNOS or NOS 2), which regulates immune response; and endothelial NOS (eNOS or NOS 3), which mediates smooth muscle relaxation. Each isoform exists as a homodimer and consists of the C-terminus reductase domain which includes binding sites for calmodulin (CaM), flavine mononucleotide (FMN), flavin adenine dinucleotide (FAD) and nicotinamide adenine dinucleotide phosphate (NADPH). The N-terminus oxygenase domain contains a heme, tetrahydrobiopterin ($BH_4$) and an arginine binding site (Figure 1.15).
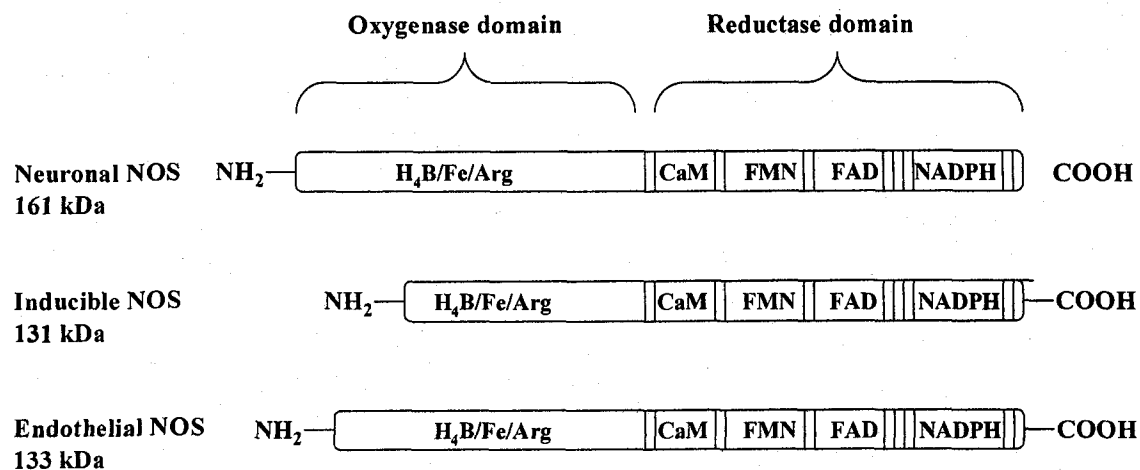


**Figure 1.15: Domain organization of three NOS isoforms (Ignarro, 2000)**

The presence of calcium ($Ca^{2+}$) initiates calmodulin binding which in turn activates the reductase domain allowing for the electron transfer from NADPH to FAD and FMN in

the reductase domain to the iron heme and $BH_4$ in the oxygenase domain (Alderton *et al.*, 2001). iNOS has a tightly bound CaM and $Ca^{2+}$ (Abu-Soud and Stuehr, 1993) and produces large amounts of nitric oxide, while nNOS and eNOS produce relatively small amounts of •NO and require $Ca^{2+}$ and calmodulin for activation.

It is now well recognized that FAD and FMN are involved in electron shuffling from NADPH, while the domain containing the iron heme is responsible for carrying out redox reactions and L-arginine binding, the role of $BH_4$ is still controversial to some extent. $BH_4$ plays a role in both steps of •NO synthesis from L-arginine (Figure 1.14), as shown by the decrease in nitric oxide production during $BH_4$ depletion in iNOS and eNOS (Kinoshita *et al.*, 1997). Also, it has been shown that $BH_4$ was able to stabilize nNOS dimer formation, this was not apparent in eNOS (Klatt *et al.*, 1995). Therefore, it appears that the function of $BH_4$ varies in different NOS isoforms, although it is an unconditional requirement for •NO synthesis. $BH_4$ is now a well recognized 1-electron donor to the oxyferrous complex of NOS heme and is also an integral part of heme protonation required for •NO synthesis (Gorren *et al.*, 2006).

### 1.2.3  S-nitrosothiols

S-nitrosothiols (RSNOs) are a physiological cellular source of nitric oxide. Since •NO is a relatively short lived molecule, formation of RSNO has been shown to prolong the half life of •NO (Girard and Potier, 1993). Also, RSNOs may serve as a transport and storage system under physiological conditions, and provide the same biochemical effects as •NO.

### 1.2.3.1 Chemistry and Biology of S-nitrosothiols

In order to understand the physiological properties of RSNO compounds, basic chemical

aspects such as formation and decomposition must be discussed.

i) RSNO formation

RSNO formation *in vitro* generally occurs via reaction between protonated nitrite ($HNO_2$)

and thiols at the pH around 2 since the pKa of $HNO_2$ is 3.37.

$$HONO + RSH \longrightarrow RSNO + H_2O$$
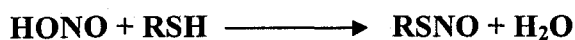
Since these are highly unlikely conditions to occur in the cell, another reaction that takes

place is called transnitrosation.

$$RSNO + R'SH \longrightarrow RSH + R'SNO$$
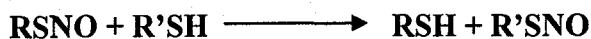
As shown in the above reaction, the RSNO compound is able to transfer its NO moiety to

another thiol (RSH) molecule without releasing •NO. This mechanism is most likely the

way by which various protein thiols become S-nitrosated.

ii) RSNO decomposition

Decomposition of RSNO may occur either by homolytic or by heterolytic cleavage as

shown in the following reactions (Arnelle and Stamler, 1995).

1. Homolytic cleavage

$$RS-N{=}O \longrightarrow RS\bullet + NO\bullet$$

2. Heterolytic cleavage

$$RS \longrightarrow N=O \longrightarrow RS^+ + NO^-$$

$$RS \longrightarrow N=O \longrightarrow RS^- + NO^+$$

Homolytic cleavage occurs when the S-N bond is broken in such a way that one electron remains on sulfur and one on nitrogen generating RS• and •NO, respectively. During heterolytic cleavage, the S-N bond breaks and two electrons are either transferred to nitrogen resulting in $NO^-$ and $RS^+$, or to sulfur thereby producing $NO^+$ and $RS^-$ species. The presence of specific metal ions such as iron, mercury and copper also results in the generation of •NO from RSNO (Williams, 1996; Vanin et al., 1997). Iron and copper decompose RSNO in a similar manner which involves reduction of the cupric ion ($Cu^{2+}$) by thiolate to a cuprous ion ($Cu^+$), followed by the reaction of $Cu^+$ with RSNO via an intermediate formation [I] to generate •NO, RS• and $Cu^{2+}$ which can then initiate the next reaction (Vanin et al., 1997) (Figure 1.16, A). On the contrary, mercury is believed to form a complex with RSNO by coordination with the sulfur atom (Williams, 1996) subsequently producing $HNO_2$, as the product of RSNO decomposition (Figure 1.16, B). Finally, RSNOs can be decomposed via UV radiation resulting in a homolytic cleavage and radical formation (Figure 1.16, C) (Sexton et al., 1994).

**A**

$$Cu^{2+} + RS^- \longrightarrow Cu^+ + RS\bullet$$

$$Cu^+ + RSNO \longrightarrow [I] \longrightarrow Cu^{2+} + RS^- + NO\bullet$$

$$2\,RS\bullet \longrightarrow RSSR$$

**B**

$$RSNO + Hg^{2+} \longleftrightarrow [RS(Hg)NO]^{2+}$$

$$[RS(Hg)NO]^{2+} + H_2O \rightarrow RSHg^+ + HNO_2 + H^+$$

**C**

$$RSNO \xrightarrow{\ hv\ } RS\bullet + \bullet NO$$

$$RS\bullet + RSNO \longrightarrow RSSR + \bullet NO$$
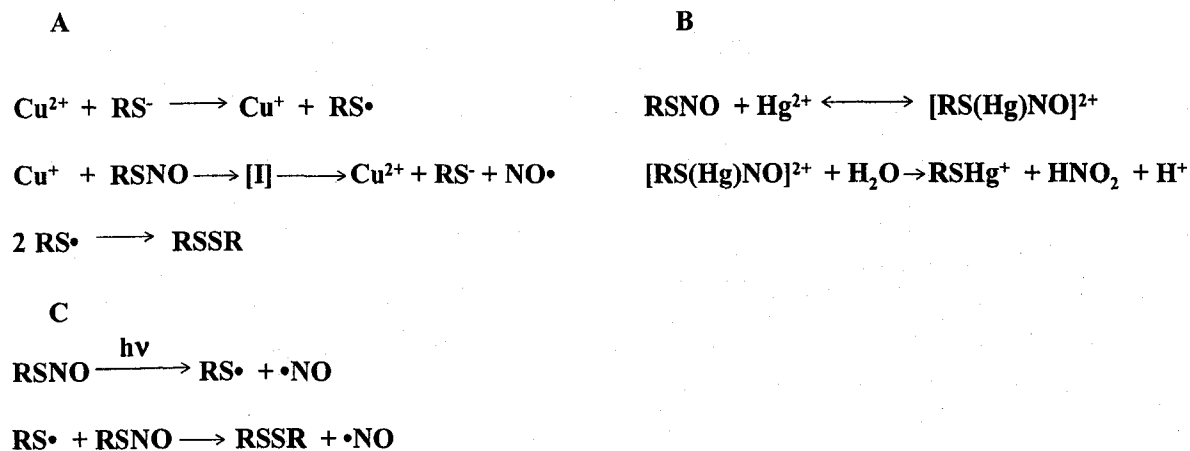
**Figure 1.16: Decomposition of RSNO**

### 1.2.3.2 Proteins and S-nitrosothiols

Since RSNOs are physiologically found throughout the cell, it is not surprising that many proteins and enzymes are involved in either the decomposition of RSNO or are possible targets for transnitrosation reaction.

RSNO consumption/degradation has been demonstrated *in vitro* by various enzymes such as thioredoxin/thioredoxin reductase (Nikitovic and Holmgren, 1996), xanthine/xanthine oxidase (Trujillo *et al.*, 1998), γ glutamyl transpeptidase (Lipton *et al.*, 2001), Cu/Zn superoxide dismutase (Johnson *et al.*, 2001; Romeo *et al.*, 2003), glutathione dependent formaldehyde dehydrogenase (Jensen *et al.*, 1998; Liu *et al.*, 2001), and protein disulfide isomerase (Ramachandran *et al.*, 2001).

The mechanisms describing the formation of S-nitrosated proteins are currently under investigation, although there are a few groups that have proposed several possibilities. For example, Noble and Williams (2001) showed *in vitro* that nitrosated serum albumin (SA) was able to transnitrosate cysteine resulting in cysteine-SNO formation.
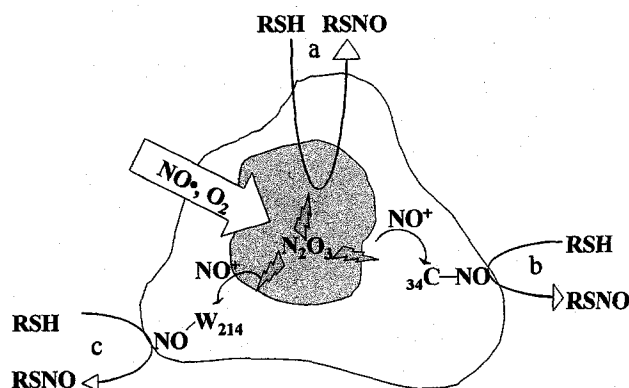


**Figure 1.17: Albumin mediated RSNO formation (Rafikova *et al.*, 2002)**

Rafikova and coworkers (Rafikova *et al.*, 2002) studied S-nitrosation of serum albumin and proposed the mechanism as shown in Figure 1.17. In the presence of •NO and $O_2$, formation of $N_2O_3$, a potent nitrosating agent, may occur in the hydrophobic pockets of serum albumin which results in three possible outcomes. In the presence of small molecular weight thiols, such as GSH, direct transnitrosation may occur resulting in the formation of RSNO (Figure 1.17, a). A second possibility involves transfer of nitrosyl cation ($NO^+$) and subsequent nitrosation of the surface exposed cysteine 34, which can then transnitrosate available RSH molecules (Figure 1.17, b). Similarly, the transfer of

$NO^+$ to the nearby tryptophan 214 yields the same result (Figure 1.17, c). Regardless of the pathway, the ability of proteins to consume $N_2O_3$ in their hydrophobic pockets may serve as the physiological source of •NO which consequently leads to formation of RSNOs or transnitrosation with other protein thiols.

There are numerous enzymes that upon S-nitrosation lose their activity such as alcohol dehydrogenase, aldehyde dehydrogenase, aldolase, calpain, cathepsin B, creatine kinase, cysteine protease, cytochrome P-450, glutathione peroxidase, glutathione reductase, glyceraldehyde-3-phosphate dehydrogenase, methionine synthase, protein kinase C, to name a few (Buga and Ignarro, 2000).

## 1.3    Role in disease

As described above, nitric oxide possesses a unique chemistry and biology, thus it is not surprising that it plays a major role in number of physiological conditions. Some of them will be discussed in the following section.

### 1.3.1    Diabetes

The general cause of diabetes is the inability of insulin to stimulate glucose uptake either by i) the absence or decreased production of insulin by $\beta$-cells in pancreas as in Type I diabetes or ii) inability of insulin to stimulate the insulin signaling pathway as in Type II diabetes, leading to an increase in circulating sugar levels. Previous studies have shown that cytokine IL-1 modulates $\beta$-cell function and islet damage by inhibiting insulin secretion (Mandrup-Poulsen *et al.*, 1985; Bendtzen *et al.*, 1986). Initially, it was

hypothesized that nitric oxide may be involved in mediating cytokine-induced inhibition of insulin secretion by β-cells, since nitric oxide targets and either activates or inhibits iron-sulfur centers in proteins, such as cytokine IL-1 (Corbett and McDaniel, 1992). This hypothesis was confirmed with the use of NOS inhibitors to show prevention in cytokine-induced inhibition of insulin secretion (Corbett et al., 1991). Therefore, nitric oxide is involved in the inhibition of insulin secretion that eventually leads to β-cell death.

## 1.3.2 Cardiovascular disease

The use of nitric oxide donors in treatment of cardiovascular disease dates back in 19th century when William Murrell in 1879 reported that administration of nitroglycerin relieved attacks of angina pectoris (Murrell, 1879). It was not until 1980s when the endothelium-derived relaxing factor was discovered to be indeed nitric oxide (Reviewed in Ignarro, 2000). Nitric oxide mediates the vascular tone of the endothelium by providing vasorelaxation and a number of processes that lead to the development of cardiovascular disease such as inhibition of platelet aggregation (Stamler et al., 1989), leukocyte adhesion (Bath et al., 1991), endothelial generation of reactive oxygen species (Clancy et al., 1992) and proliferation of vascular smooth muscle (Garg and Hassid 1989).

## 1.3.3 Apoptosis

Apoptosis, also known as a programmed cell death, is accompanied by a series of events such as cell shrinkage, chromatin condensation, cellular membrane blebbing and DNA degradation (Wylie et al., 1980; Roy et al., 1992). •NO mediates apoptosis in a dose-,

time- and cell type-dependent process (Ponte and Huot, 1996). Ponte and Huot investigated the effect of nitric oxide on total intracellular thiol concentration and found that at the sublethal concentrations of •NO, glutathione levels were increased (Ponte and Huot, 1998). This observation was explained by the theory that, in response to the nitrosative stress induced by •NO, cells start producing stress proteins that help scavenge reactive oxygen species, as well as mobilize their antioxidant system consisting of increased levels of GSH, superoxide dismutase and catalaze. Therefore, the •NO plays a dual role in apoptosis; it either promotes it, or protects from it.

### 1.3.4 Cancer

The role of •NO in cancer is as variable as in apoptosis. Basal •NO levels are thought to promote tumor progression, while a high dose of •NO leads to tumor regression (Buga and Ignarro, 2000). One of the mechanisms of •NO mediated tumor progression involves regulation of the tumor-suppressor protein p53, which is either mutated or deleted in many human cancers. •NO may modify the p53 DNA-binding domain consisting of a tetrahedrally coordinated Zn atom bound to cysteine residues, by either binding to cysteine residues or coordinating with the Zn atom. Both of these interactions would result in a conformational change in p53, resulting in its inactivation and propagation of cancer (Calmels *et al.*, 1998).

# CHAPTER 2

# Characterization of S-Denitrosation Activity of Protein

# Disulfide Isomerase

## 2.1 Introduction

Although protein disulfide isomerase (PDI) was first isolated and identified in the 1960s (Goldberger *et al.*, 1963) as a resident of the endoplasmic reticulum (ER) where it assists in folding of the newly synthesized proteins by performing its isomerase activity (Noiva and Lennarz, 1992), new roles for PDI are still being discovered. Not too long ago, PDI was found in the secreted form and associated with the surface of the cells via electrostatic interactions (Zai *et al.*, 1999 Terada *et al.*, 1995). The question which arises is what is PDI doing on the cell surface? One potential answer came from the study of Chen and coworkers (1995), who showed that PDI associated with the surface of the platelets plays a role in the integrin mediated platelet aggregation and adhesion as described in Chapter 1, Figure 1.7. The most studied functions of cell surface PDI involve either disulfide reduction, thiol oxidation or disulfide rearrangement (Chapter 1, Figure 1.6, 1.8). However, the study by Ramachandran and coworkers (Ramachandran, 2001) showed that cell surface PDI was also able to denitrosate S-nitrosoglutathione (GSNO) and transport the nitric oxide (•NO) equivalents into the cytosol. Another study performed by Root and coworkers (2004, a part of Chapter 3) showed that platelet surface PDI was also able to denitrosate GSNO and by doing so, platelet aggregation was abolished. Therefore, the role of PDI on the surface of the cells may have a greater role than its usual isomerization activity.

S-nitrosothiols (RSNOs) are known nitric oxide donors (Feelisch, 1998). Physiologically, RSNO may be small molecular weight thiols such as S-nitrosoglutathione, S-nitrosocysteine and S-nitrosohomocysteine, as well as high molecular weight S-nitrosated proteins such as serum albumin. •NO has a very short half

life (2-5 seconds) (Balbatun *et al.*, 2003) and by forming an RSNO, its half life is prolonged up to several hours (Whiteside *et al.*, 2002). The RSNO bound-NO could be transported throughout the cellular environment such as in the case of S-nitrosated serum albumin (Rafikova et al., 2000) and S-nitrosated hemoglobin (Jourd'heuil *et al.*, 2000).

The current study was initiated since the PDI-mediated denitrosation acitivity of RSNOs has not been well characterized. The RSNO used here was S-nitrosoglutathione, as it is the most physiological small RSNO found in the body (Clancy *et al.*, 1994). The RSNO decomposition was monitored using two methods. In the first method, the decrease in absorbance of the S-NO bond at 334 nm was used to detect its cleavage due to PDI (Williams, 1996), while the second method made use of an amperometric device for measuring soluble nitric oxide (Zhang and Broderick, 2000). For detection of thiyl and dithiyl radicals, we used a conjugate of acridine and TEMPO (2,2,6,6-tetramethylpiperidine-1-oxyl), which is a nonfluorescent probe until it reacts with thiyl radicals resulting in acridine-piperidine which is highly fluorescent (Borisenko *et al.*, 2004). We also used a non-specific nitric oxide probe, diaminonaphthalene for measuring the presence of nitric oxide species. We addressed the fate of nitric oxide after it has been released and showed that PDI was able to store nitric oxide in the form of $N_2O_3$ in its hydrophobic pockets. This stored nitric oxide was then able to react with exogenous thiols and transfer its •NO equivalents.

## 2.2 Materials and Equipment

### 2.2.1 Materials

| | |
|---|---|
| Acetone; | Sigma-Aldrich Canada Ltd., Oakville, Ontario |

4-(9-Acridinecarbonyl)-amino)-2,2,6,6-tetramethylpiperidine-1-oxyl (Ac-Tempo);

| | |
|---|---|
| | Molecular Probes, Eugene, OR |
| Ammonium persulfate; | Sigma-Aldrich Canada Ltd., Oakville, Ontario |
| Ammonium sulfamate; | Sigma-Aldrich Canada Ltd., Oakville, Ontario |
| Biorad Bradford Reagent; | Bio-Rad Laboratories Ltd., Mississauga, Ontario |
| Bovine Serum Albumin; | Sigma-Aldrich Canada Ltd., Oakville, Ontario |
| Copper (II) sulfate; | Sigma-Aldrich Canada Ltd., Oakville, Ontario |
| 2,3-diaminonaphthalene (DAN); | Sigma-Aldrich Canada Ltd., Oakville, Ontario |
| Diethylamine NONOate (DEANO); | Sigma-Aldrich Canada Ltd., Oakville, Ontario |
| Dimethyl formamide (DMF); | Sigma-Aldrich Canada Ltd., Oakville, Ontario |
| 5, 5'-dithiobis(2-nitrobenzoic) acid; | Sigma-Aldrich Canada Ltd., Oakville, Ontario |
| Dithiothreitol (DTT); | Sigma-Aldrich Canada Ltd., Oakville, Ontario |
| Ethylene diamine tetraacetic acid; | Sigma-Aldrich Canada Ltd., Oakville, Ontario |
| Hemoglobin; | Sigma-Aldrich Canada Ltd., Oakville, Ontario |

Monoclonal anti-PDI antibody RL90;Abcam USA, Cambridge, MA

| | |
|---|---|
| Imidazole; | Sigma-Aldrich Canada Ltd., Oakville, Ontario |
| Neocuprine; | Sigma-Aldrich Canada Ltd., Oakville, Ontario |
| N-ethylmaleimide (NEM) | Sigma-Aldrich Canada Ltd., Oakville, Ontario |
| Ni-Cam$^{TM}$ Resin; | Sigma-Aldrich Canada Ltd., Oakville, Ontario |

| | |
|---|---|
| Oxidized glutathione; | Sigma-Aldrich Canada Ltd., Oakville, Ontario |
| Potassium ferricyanide; | Sigma-Aldrich Canada Ltd., Oakville, Ontario |
| Potassium phosphate; | Sigma-Aldrich Canada Ltd., Oakville, Ontario |
| Reduced glutathione; | Sigma-Aldrich Canada Ltd., Oakville, Ontario |
| Sephadex G-25; | Sigma-Aldrich Canada Ltd., Oakville, Ontario |
| Sodium chloride; | Sigma-Aldrich Canada Ltd., Oakville, Ontario |
| Sodium dithionate; | Sigma-Aldrich Canada Ltd., Oakville, Ontario |
| Sodium hydroxide; | Sigma-Aldrich Canada Ltd., Oakville, Ontario |
| Sodium nitrite; | Sigma-Aldrich Canada Ltd., Oakville, Ontario |
| Sodium phosphate monobasic: | Sigma-Aldrich Canada Ltd., Oakville, Ontario |
| Sodium phosphate dibasic; | Sigma-Aldrich Canada Ltd., Oakville, Ontario |
| TEMED; | Bio-Rad Laboratories Ltd., Mississauga, Ontario |

## 2.2.2  Equipment

Agilent 8453 UV-VIS spectrophotometer;

   (Agilent Technologies Canada Inc, Mississauga, Ontario)

Beckman J2-HS Centrifuge;

   (Beckman Coulter Canada Inc., Mississauga, Ontario)

BioRad Fraction Collector Model 2110;

   (Bio-Rad Laboratories Ltd., Mississauga, Ontario)

ISO-NO Mark II with WPI MKII Nitric Oxide electrode;

   (World Precision Instruments Inc., Sarasota, Florida)

Jouan CR3i Centrifuge;

(Jouan Inc, Winchester, Virginia)

Labconco FreeZone 4.5 Liter Benchtop Freeze Dry Systems;

(Labconco Corporation, Kansas City, Missouri)

Mettler AJ100 Balance;

(Mettler Toledo Canada, Mississauga, Ontario)

Microtiter 96-well Solid Plate;

(Thermo Electron Corp. Canada, Burlington, Ontario)

Mini-Protein II Gel Electrophoresis System;

(Bio-Rad Laboratories Ltd., Mississauga, Ontario)

Orion Model 420A pH Meter;

(Thermo Electron Corp. Canada, Burlington, Ontario)

Stir Plate 360 Series;

(VWR International, Mississauga, Ontario)

Varian Eclipse Fluorescence Spectrophotometer;

(Varian Canada, Mississauga, Ontario)

## 2.3 Experimental Methods

### 2.3.1 Purification of Protein Disulfide Isomerase

The expression vector pET-28b was prepared by Seslija (Seslija MSc Thesis, 2005) from Dr. Lana Lee's lab and generously donated to our lab. The vector contained the entire human PDI sequence with the N-terminal $His_6$ tag (Pihlajaniemi et al., 1987). The pET-28b vector was transformed to *Escherichia coli* strain BL21 (DE3), and protein expression was induced with 1 mM isopropylthiogalactoside. Following cell lysis, purification of recombinant PDI from the soluble fraction of cell lysate was performed using a high capacity nickel affinity matrix, Ni-CAM™ HC Resin. After several washes with 30 mM imidazole to remove any non specific binding, PDI was eluted using 250 mM imidazole prepared in 50 mM Tris-HCL, pH 8.0 and collected in 2.0 mL fractions using a Bio-Rad fraction collector. The fractions containing PDI were pooled and dialyzed against 100 mM potassium phosphate buffer, pH 7 in order to remove imidazole. Bradford assay was used to quantify protein using bovine serum albumin as a standard (Bradford, 1976). The purity of protein was determined by SDS-PAGE gel electrophoresis and Western blotting.

### 2.3.2 PDI Assay Buffer

Unless otherwise specified, all experiments were performed in the PDI assay buffer containing 100 mM potassium phosphate, pH 7.0, and 2 mM EDTA.

### 2.3.3 Synthesis of S-Nitrosoglutathione

The free thiol concentration in the GSH was determined by DTNB assay (Jiang *et al.*, 1999). A stoichiometric amount of acidified $NaNO_2$ (pH 2) to the free thiol concentration of GSH, was reacted with GSH for 30 minutes at 4°C, followed by the pH adjustment to 7.4 using NaOH (2 M). GSNO was recrystallized by the slow addition of ice-cold acetone and resuspended in the appropriate buffer.

### 2.3.4 Preparation of Oxyhemoglobin and Methemoglobin

Oxyhemoglobin and methemoglobin were prepared as described by Nikitovic and Holgren (1996). Briefly, oxyhemoglobin was prepared by the reduction of human hemoglobin with dithionate in 100 mM potassium phosphate, pH 7.4, followed by the chromatographic separation using Sephadex G-25. Methemoglobin was prepared by oxidizing human hemoglobin with 5% molar excess of potassium ferricyanide in 100 mM potassium phosphate, pH 7.0, followed by chromatographic separation of unreacted species using a Sephadex G-25 column equilibrated with the same buffer. Oxyhemoglobin and methemoglobin were prepared fresh prior to each experiment and conformation of their characteristic heme state was obtained by monitoring specific peak appearance at 542 nm and 580 nm for oxyhemoglobin and 630 nm for methemoglobin by UV-vis spectrophotometry.

### 2.3.5 Hemoglobin Assay

The hemoglobin assay was used to determine the final product of GSNO cleavage by PDI (Arnelle and Stamler, 1995). Detection of •NO can be achieved though the oxidation of

oxyhemoglobin to methemoglobin, which can be monitored as a decrease in absorbance at 542 and 580 nm and an increase at 630 nm (Bazylinski and Hollocher, 1985; Stone and Marletta, 1994). The reaction mixture contained 30 μM oxyhemoglobin, 1.2 mM GSH, 100 μM GSNO (blank), and 2 μM PDI (sample), in 100 mM potassium phosphate buffer, pH 7.4, containing 1 mM EDTA. The possibility of NO⁻ generation was monitored via methemoglobin reduction to oxyhemoglobin which would result in an increase in absorbance peak at 542 nm and 580 nm and a concomitant decrease at 630 nm. The assay solution contained 30 μM methemoglobin, 1.2 mM GSH, 100 μM GSNO (blank) and 2 μM PDI (sample), in 100 mM potassium phosphate buffer, pH 7.0, including 1 mM EDTA. All spectra were recorded from 500-700 nm at specific time intervals. The extinction coefficient for oxyhemoglobin at pH 7.0 is 13900 $M^{-1}cm^{-1}$ and 14000 $M^{-1}cm^{-1}$ at 545 and 580 nm (Bazylinski and Hollocher, 1985), respectively, whereas the GSNO extinction coefficient of 15 $M^{-1}cm^{-1}$ at 545 nm (Hart, 1985) and is therefore considered insignificant.

### 2.3.6 Direct Monitoring of PDI Denitrosation Activity with UV-visible Spectroscopy

The kinetcs of PDI-mediated denitrosation activity of GSNO was monitored as the decrease in absorption at 340 nm as a function of time. The reaction was performed in a PDI assay buffer containing various [GSNO] (10-500 μM) as a substrate, 3 μM PDI and GSH (1.2 mM) to study the kinetic parameters. PDI denitrosation activity was also monitored using a nitric oxide meter (described below) in order to directly detect NO

generation due to GSNO cleavage. All measurements were performed at the room temperature.

### 2.3.7 Detection of PDI Radicals with Ac-Tempo

Previous studies reported that Ac-Tempo, a paramagnetic nonfluorescent conjugate of 2,2,6,6-tetramethylpiperidine-1-oxyl and acridine, interacts with glutathionyl radicals resulting in an increase in fluorescence of acridine-piperidine moiety (Borisenko *et al.*, 2004). The Ac-Tempo concentration was first determined by measuring the absorbance at 359 nm ($\varepsilon=10.4$ mM$^{-1}$cm$^{-1}$), and fluorescence measurements were performed with excitation and emission wavelengths of 360 nm and 440 nm, respectively. PDI radical formation was detected by mixing stoichiometric amounts of PDI and GSNO (2 μM) with Ac-Tempo (10 μM), followed by the time-dependent measurement of fluorescence at 440 nm ($\lambda_{ex}=$ 360 nm). The control reaction was performed using DTT and GSH instead of PDI, to determine whether any compound with vicinal thiols could also generate GS•. As another control, BSA was used in the same amount as PDI to see if there is a possibility of another protein interacting with the Ac-TEMPO probe. The standard plot of thiyl radical formation was constructed using photolysis (355 nm) (Sexton *et al.*, 1994) and employing various concentrations of GSNO (1-20 μM) in the presence of Ac-Tempo followed by florescence measurements. This standard plot was used for quantification of thiyl/dithiyl radicals.

## 2.3.8 Generation of a Standard Curve with DAN

A standard curve was generated by incubating varying concentrations of GSNO (200 nM to 25 $\mu$M) in the presence of DAN (200 $\mu$M) and $HgCl_2$ (100 $\mu$M) for 10 minutes in PBS (100 mM phosphate, pH, 7.4) at room temperature. The fluorescence readings were recorded at 415 nm with an excitation at 375 nm. The amount of $NO_x$ generated experimentally was estimated using this standard curve.

## 2.3.9 Demonstration of the Ability of BSA and PDI to Store NO-equivalents

In order to demonstrate that BSA and PDI are able to store NO-equivalents, 25 $\mu$M GSNO was incubated with 100 $\mu$M $HgCl_2$ for 10 minutes in the presence of 1, 2, and 4 $\mu$M BSA or PDI, followed by the addition of ammonium sulfamate (0.1 %) to remove the excess of $HNO_2$. The increase in fluorescence using DAN (200 $\mu$M) was monitored as a function of time at 415 nm ($\lambda_{ex}$ 375 nm), as an indicative of the presence of $NO_x$. All experiments were performed in 100 mM PBS buffer, pH 7.4, at the room temperature.

## 2.3.10 Preparation of PDI-reduced and S-nitrosated PDI (PDI-SNO)

Reduced PDI was prepared by treatment with 10-fold molar excess of DTT for 30 minutes at room temperature, followed by the overnight dialysis (MW cutoff 5 kDa) in 20 mM phosphate buffer, pH 6.3 at 4°C. The concentration of free thiols was quantified by the DTNB assay. S-nitrosated PDI (PDI-NO) was prepared by incubating reduced PDI with 5-fold molar excess of DEA-NO for 30 minutes at the room temperature. The degree of nitrosation of PDI was assessed using an NO meter with $HgCl_2$ as the NO releasing agent (Borisenko *et al.*, 2004) as described below.

### 2.3.11 Nitric Oxide Determination Using an NO Meter

Soluble nitric oxide was measured using ISO-NO Mark II Nitric Oxide meter equipped with WPI MKII NO electrode. A standard curve for NO was generated by adding GSNO (10-100 $\mu$M) to 100 mM phosphate buffer, pH 7.0, containing 100 $\mu$M $HgCl_2$. In order to test for S-nitrosated PDI, PDI-NO (1 $\mu$M) was placed in the vial containing 100 mM phosphate buffer, pH 7.4, and the electrode was blanked using this mixture. At 20 sec, 100 $\mu$M $HgCl_2$ was added, and the •NO generation was monitored until •NO was no longer detected. In a parallel experiment, 2 $\mu$M reduced PDI was added to PDI-NO to verify whether PDI alone could act upon PDI-NO. In a control experiment, BSA (2 $\mu$M) was used instead of PDI as another possible protein to contribute to PDI-SNO denitrosation.

To test the involvement of the active site thiols, NEM-blocked PDI was incubated with DEA-NO for 30 minutes at the room temperature, to generate •NO saturated PDI. 3 $\mu$M of this NO-saturated PDI was placed in the vial containing 100 mM phosphate buffer, pH 7.4, and the NO signal was measured as a base line for the first 40 seconds. At 40 seconds, 100 $\mu$M $HgCl_2$ was added to remove any S-NO present in the sample. After obtaining a stable signal at 130 seconds, 500 $\mu$M GSH was added to potentially scavenge $N_2O_3$ postulated to be present in the hydrophobic domains of PDI. The control was obtained using NEM-blocked PDI without exposure to DEA-NO. The actual •NO concentration was estimated from the standard curve.

## 2.3.12 Quantification of Thiols in PDI

In order to quantify the stability of PDI thiols, 10 μM PDI was incubated with 10 mM DTT for 1 hour at the room temperature, followed by the chromatographic separation of DTT via Sephadex G-25. 1.2 μM PDI was then incubated with DTNB for 30 minutes at different time intervals and the absorbance was monitored at 412 nm in 100 mM Tris-HCl buffer, pH 8 ($\varepsilon = 13900 \ M^{-1}cm^{-1}$ at 412 nm).

## 2.3.13 Monitoring PDI-SNO Formation by UV-visible Spectroscopy

Freshly reduced PDI (10 μM) was treated with DEA-NO for 30 minutes, followed by separation through a Sephadex G-25 column. The absorption spectra of PDI-SNO were monitored between 300 nm-450 nm. The •NO dissociation from PDI-SNO was initiated by the addition of $HgCl_2$, and the quantification of S-nitrosation was obtained by monitoring a decrease in absorbance at 340 nm using the molar extinction coefficient of $980 \ M^{-1}cm^{-1}$.

## 2.4 Results

The experiments involving spectrophotometric analysis of PDI-mediated GSNO denitrosation and DAN assay were performed by my colleague, Dr. Arun Raturi.

### 2.4.1 Kinetics of PDI mediated GSNO denitrosation

The initial rates of PDI-mediated GSNO denitrosation were obtained using two different methods. In the first method, the initial rates of denitrosation were monitored spectrophotometrically at 340 nm to detect the loss of the S-NO bond absorbance in the presence of PDI (3 $\mu$M), GSH (1.3 $\mu$M) and a range of [GSNO] (0-500 $\mu$M). Initial rates as a function of [GSNO] were accommodated with the Michaelis-Menten equation and the apparent $K_M$ for GSNO was estimated to be 65 ± 5 $\mu$M (Figure 2.1 A). In the second method, PDI (2 $\mu$M) denitrosation activity in the presence of GSNO (10-140 $\mu$M) was monitored by an NO electrode. The apparent $K_M$ was estimated to be 40 ± 10 $\mu$M (Figure 2.1 B). The slightly higher $K_M$ observed spectrophotometrically is probably due to the uncertainty in the initial rates at low GSNO concentration owing to the low extinction coefficient of the S-NO bond at 340 nm ($\varepsilon$=980 $M^{-1}cm^{-1}$).
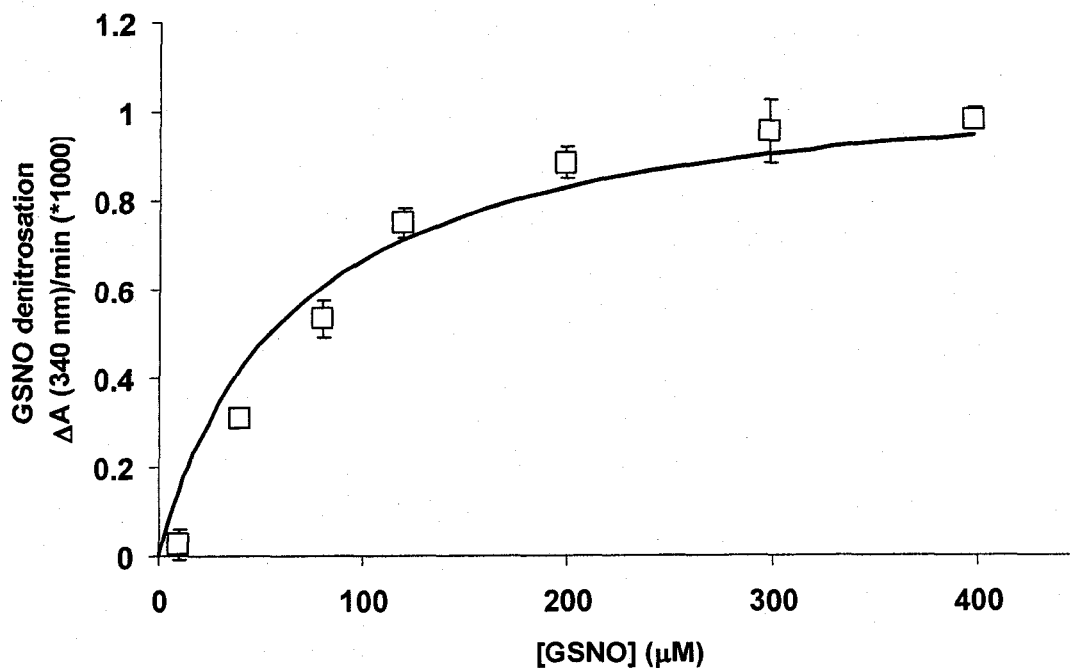
**Figure 2.1 : PDI denitrosation kinetic summary.**

A. Samples containing PDI (3 $\mu$M) were mixed with 1.2 mM GSH, and denitrosation was monitored at 343 nm as a function of time. The rates were corrected by subtracting the blank rates (without PDI) and plotted against increasing GSNO concentrations. The solid line represents the best fit of the calculated data based on the experimentally determined kinetic parameters using the Michaelis-Menten equation.
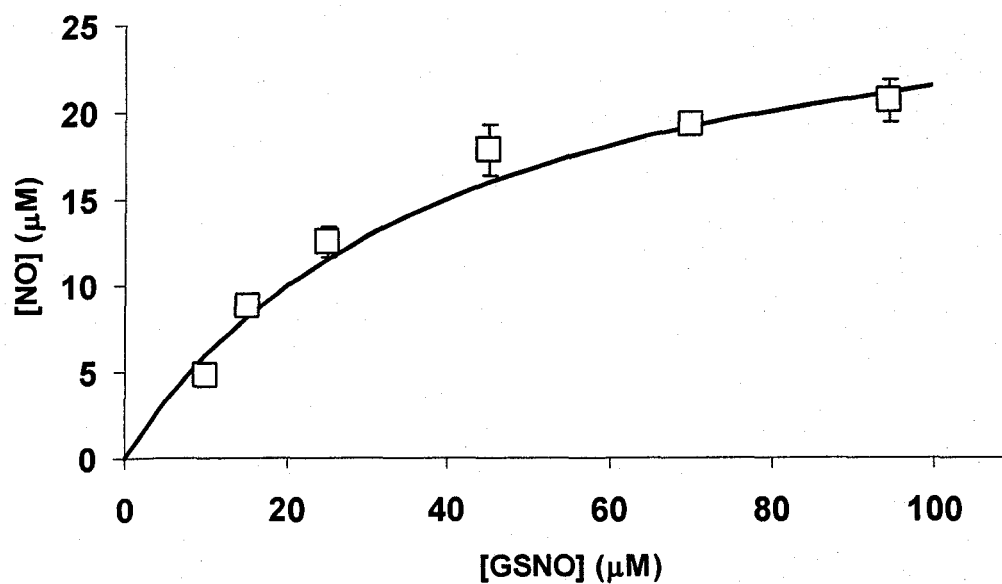
B. Sample containing PDI ($3\mu$M) was mixed with 1.2 mM GSH and an NO electrode was placed in the mixture. PDI denitrosation activity was initiated by the addition of increasing GSNO concentrations. •NO generated by PDI was obtained after correcting for release by 1.2 mM GSH, using an •NO standard curve.

The end product of PDI-mediated GSNO denitrosation could be either NO$^•$ or NO$^-$.  In order to identify the actual product of PDI denitrosation activity, a hemoglobin assay was performed (Arnelle and Stamler, 1995).  Oxyhemoglobin was incubated with GSNO, GSH and without (blank) or with PDI (sample), and a time dependent decrease at 542 nm and 580 nm and in increase at 630 nm indicated the formation of methemoglobin, suggesting that the major product of PDI-mediated GSNO denitrosation was indeed NO$^•$ (Figure 2.2 A).  In order to test for the second possibility of NO$^-$ generation, a methemoglobin assay was performed using the same experimental set up as for the oxyhemoglobin assay.  If NO$^-$ were produced, it would reduce methemoglobin that could be monitored by an increase in absorbance at 540 and 580 nm accompanied by a decrease at 630 nm.  As Figure 2.2 B shows, methemoglobin spectra in the presence of PDI and GSNO was stable over 20 minutes, suggesting that if any NO$^-$ was being produced, it was below the detection limit of this assay.
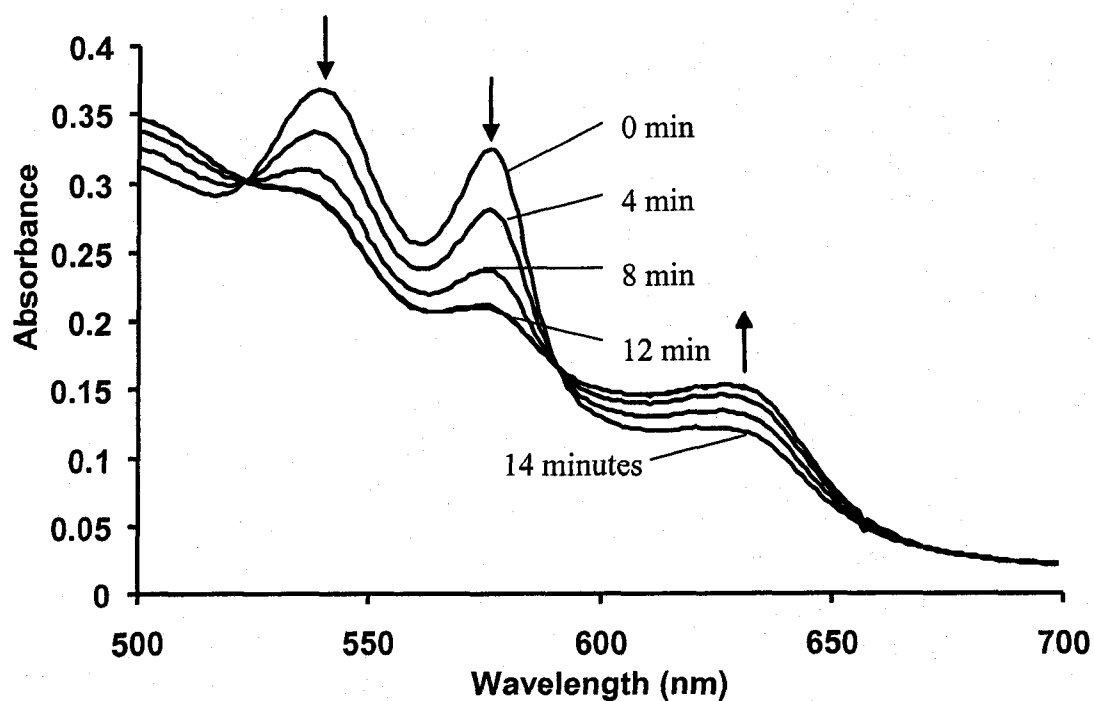
**Figure 2.2: Monitoring NO˙/NO⁻ release by hemoglobin assay.**

A. Oxyhemoglobin assay contained 30 $\mu$M oxyhemoglobin, 1.2 mM GSH, 100 $\mu$M

GSNO and 2 $\mu$M PDI in 100 mM potassium phosphate, 1.0 mM EDTA, pH 7.4. A

decrease at 542 and 580 nm, and consequential increase at 630 nm was an indicative of

NO˙ production. The reaction was over in approximately 12 minutes.
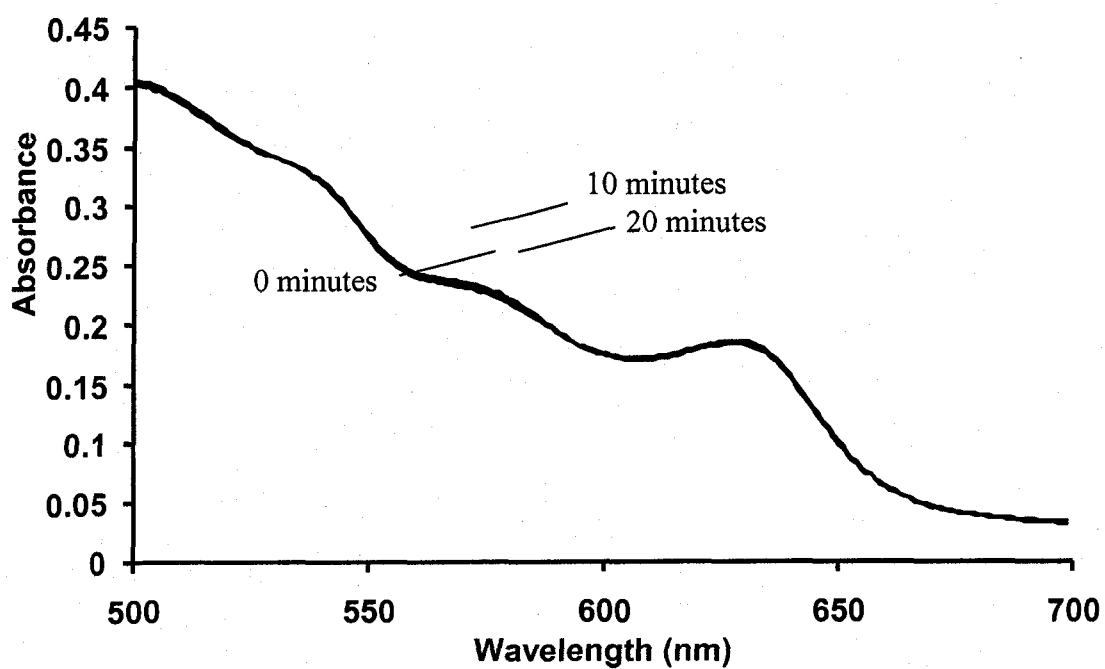
B. Methemoglobin assay contained 30 $\mu$M methemoglobin, 1.2 mM GSH, 100 $\mu$M

GSNO and 2 $\mu$M PDI in 100 mM potassium phosphate, 1 mM EDTA, pH 7.4. There was

no change in spectrum observed over 20 minutes of incubation indicating the lack of NO⁻

production during GSNO denitrosation by PDI.

## 2.4.2 PDI Thiyl/dithiyl Radical Formation as a Result of GSNO Denitrosation

A previous computational study by Houk and coworkers (Houk *et al.*, 2003) suggested a novel mechanism for transnitrosation reaction involving the formation of a nitroxyl disulfide intermediate, given that the interacting thiols are in a close proximity to each other as in PDI active site. Therefore, if PDI active site thiols were part of such a mechanism, then beside •NO generation, there should also be a consequent thiyl/dithiyl radical formation. For this purpose, a thiyl radical probe, Ac-Tempo, was used. Previous studies have shown that Ac-Tempo, upon interacting with thiyl radicals gives off a fluorescent signal. Therefore, we set to determine whether PDI could form a thiyl radical in its active site as a result of GSNO denitrosation. In a control trial, GSNO was added to the cuvette containing Ac-Tempo alone and the lack of fluorescence suggested that there is no spontaneous interaction between GSNO and Ac-Tempo (Figure 2.3 A, triangles). However, upon addition of equimolar (2 µM) PDI and GSNO to Ac-Tempo (10 µM), a continuous, time-dependent increase in fluorescence was observed (Figure 2.3 A, squares). As a control, the experiment was performed in the presence of BSA instead of PDI and no fluorescent signal was observed upon addition of GSNO (Figure 2.3 B asterisk). Also, to eliminate the possibility that the signal comes from the second product of GSNO denitrosation (GS), the same experiment was performed in the presence of GSH and PDI, and no detectable fluorescent signal was observed (Figure 2.3 B, filled circles). By converting the fluorescent signal obtained by Ac-Tempo experiments to the actual thiyl radical formation (Figure 2.4, squares) and the generation of •NO from oxyhemoglobin experiments (Figure 2.4 diamonds), we were able to quantify that 0.8 ± 1.2 mol of NO was produced per 3 ± 0.43 mol of thiyl/dithiyl radical formed.
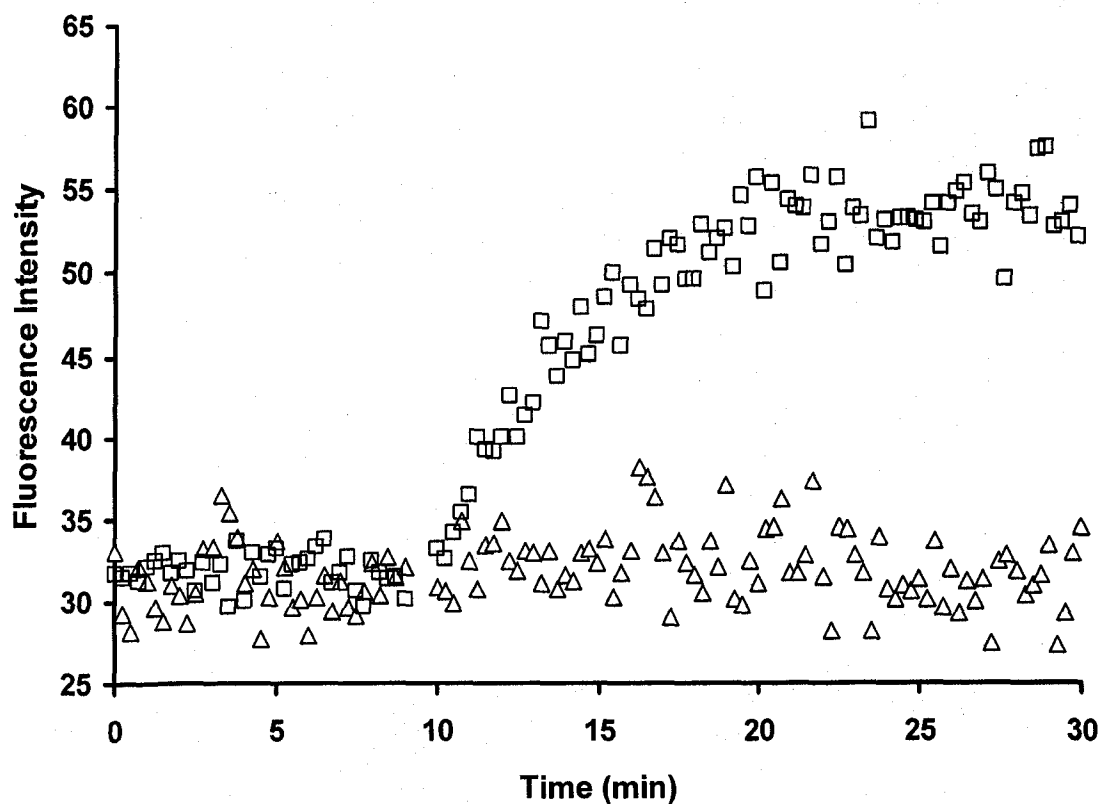
**Figure 2.3: Thiyl/dithiyl radical generation due to PDI mediated GSNO denitrosation.**

A. Ac-Tempo (10 μM) was placed in a cuvette containing buffer only (triangles) or PDI (2 μM; squares). After a stable signal was obtained by monitoring fluorescence at 440 nm (excitation 360 nm), GSNO (2 μM) was added and the generation of thiyl/dithiyl radical was observed.
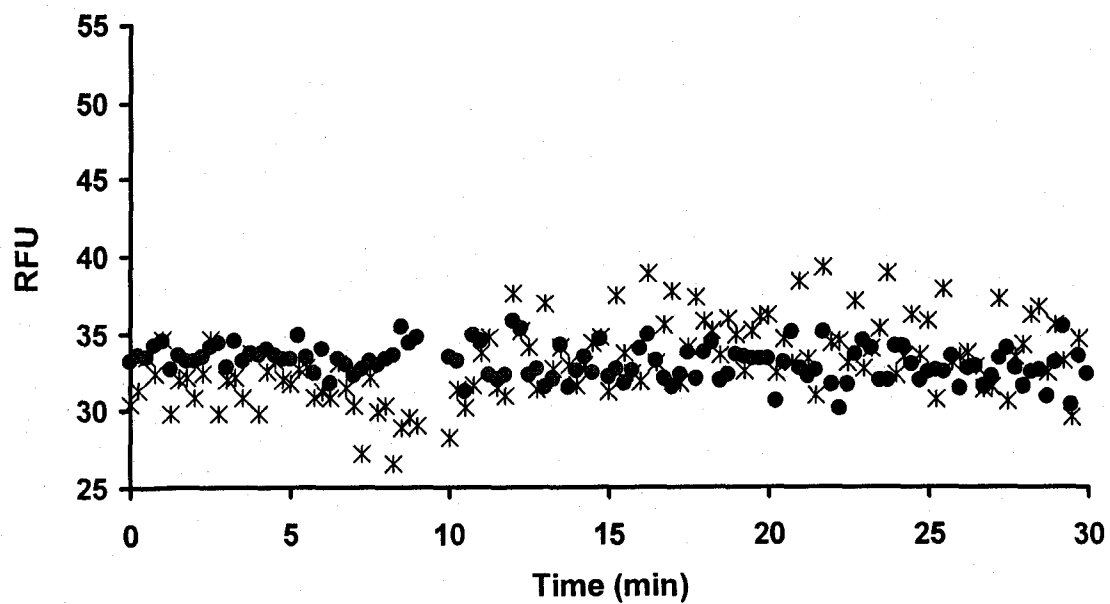
B. Ac-Tempo (10 μM) was placed in a cuvette containing BSA (2 μM; asterisk) or PDI

(2 μM; filled circles). After a stable signal was obtained by monitoring fluorescence at

440 nm (excitation 360 nm), GSNO (2 μM) was added to the sample containing BSA and

GSH was added to the sample containing PDI. The generation of thiyl/dithiyl radical was

monitored over 30 minutes.
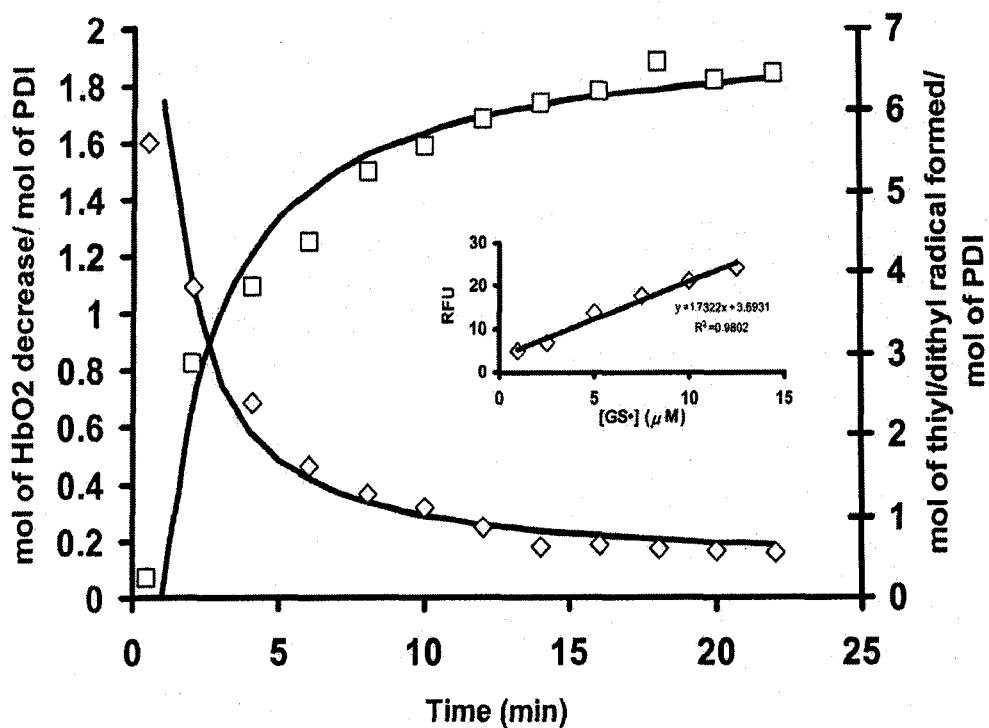
**Figure 2.4: Quantification of •NO and thiyl/dithiyl radical generation during PDI-medaited GSNO denitrosation.**

Ac-Tempo (10 μM) was mixed with 2 μM PDI and 2 μM GSNO, and the fluorescent signal was measured over time (*squares*). In parallel experiments, 40 μM oxyhemoglobin ($HbO_2$) was mixed with 2 μM PDI and 2 μM GSNO, and the decrease at 542 nm (indicative of NO-induced methemoglobin formation) was monitored over time (*diamonds*). The rates of NO formation and thiyl/dithiyl radical formation were nearly superimposable. The yields were 0.8 ± 0.12 mol NO produced/ 3.0 ±0.43 mol thiyl/dithiyl radical (*n* =3). *Inset*, standard plot of Ac-Tempo fluorescence (in relative fluorescence units (*RFU*)) as a function of [GS•] generated by flash photolysis (355 nm) of varying concentrations of GSNO.

### 2.4.3 PDI and BSA Act as a NO Sink

Previous studies (Rafikova *et al.*, 2002) have shown that proteins containing hydrophobic domains, such as serum albumin, are able to accumulate •NO and $O_2$ in the form of the potent nitrosating agent $N_2O_3$. Here, we used the DAN assay to test if PDI could also behave in the same manner. DAN works on the basis of N-nitrosation of the amino group by •NO as well as other reactive nitrogen species such as $NO_2^-$ and $N_2O_3$ (Kleinhenz *et al.*, 2003; Wink *et al.*, 1999). The second amino group of DAN then reacts with the nitrosated intermediate, resulting in the highly fluorescent naphthotriazole derivative. In this experiment, the NO was generated by incubating GSNO (50 μM) with $HgCl_2$ (Williams, 1996) in the presence of 1, 2 and 4 μM of BSA (Figure 2.5 A) or PDI (Figure 2.5 B). As seen in Figure 2.5 A and B, the amount of naphthotriazole decreased with increasing concentration of each protein, suggesting that there was a decrease in soluble $NO_x$ available to react with DAN.

Nudler and coworkers (Rafikova *et al.*, 2002) have shown that the accumulated $N_2O_3$ inside the hydrophobic pockets of BSA could potentially nitrosate protein thiols. In this study, the most likely target for S-nitrosation would be the active site thiols of PDI. Based on this proposal, the following experiments were performed.
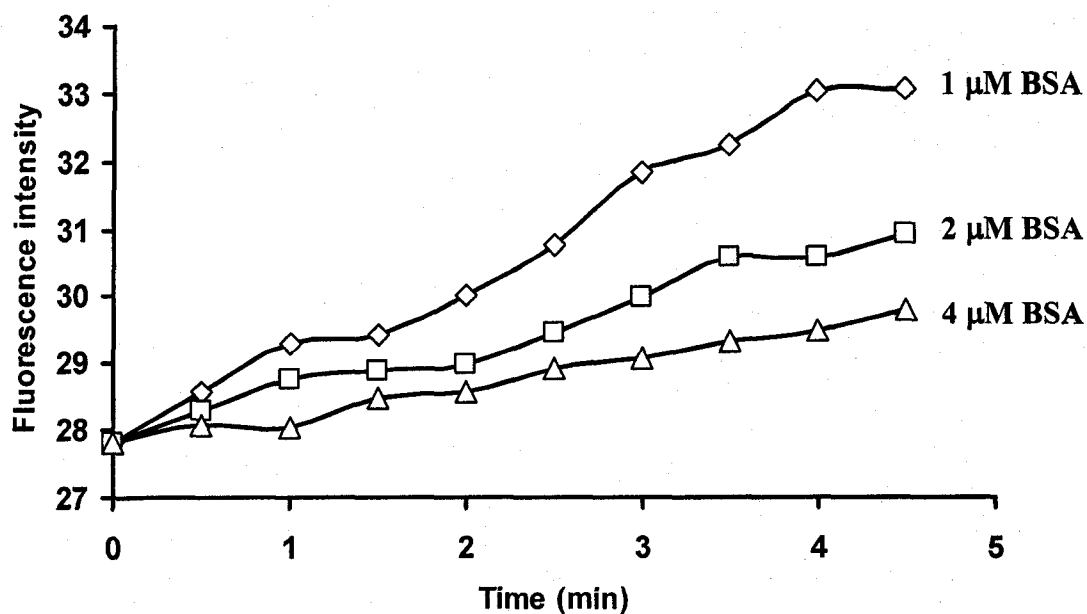
**Figure 2.5: Monitoring denitrosation rate using the DAN assay**

A. Denitrosation of GSNO with $HgCl_2$ in the presence of BSA: 25 $\mu$M of GSNO was incubated with 100 $\mu$M copper sulphate for 10 min in the presence of varying concentration of BSA followed by the addition of ammonium sulfamate (0.1%) to remove excess of $HNO_2$. DAN (200 $\mu$M) was added and the denitrosation rate was monitored as a function of time. The experiment was performed in 0.1 mM PBS buffer, pH 7.4 at room temperature.
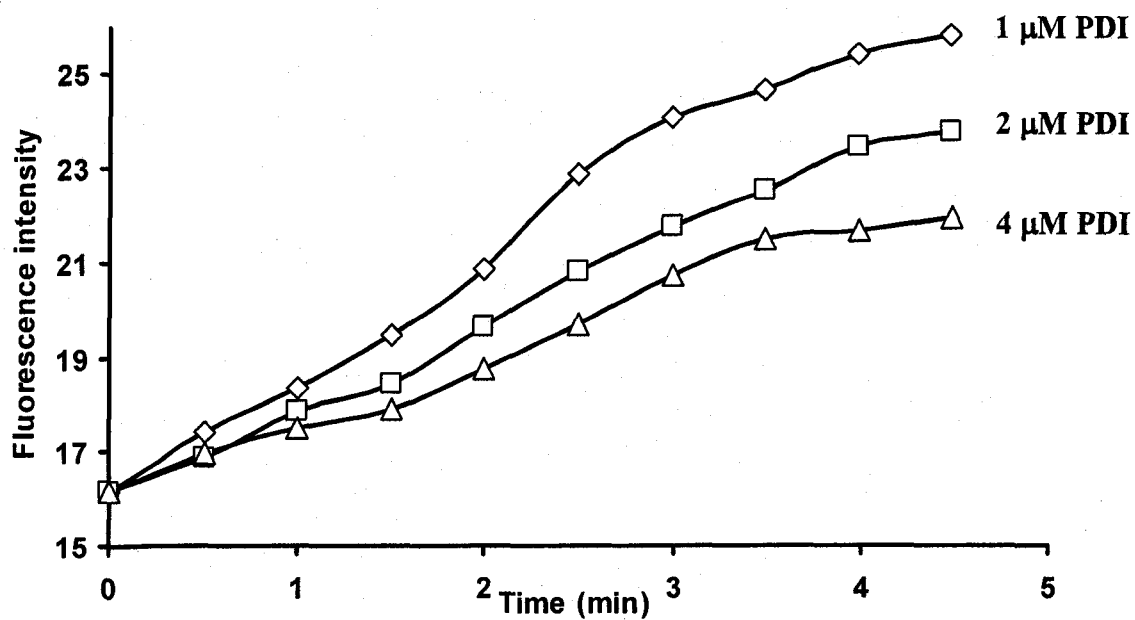
B. Denitrosation of GSNO with $HgCl_2$ in the presence of PDI: 25 $\mu$M of GSNO was incubated with 100 $\mu$M copper sulphate for 5 min in the presence of varying concentration of PDI followed by the addition of 200 $\mu$M DAN. Ammonium sulfamate (0.1%) was added to remove excess $HNO_2$. The experiment was performed in 0.1 mM PBS buffer, pH 7.4 at room temperature.

### 2.4.4 PDI Can Release NO from PDI-SNO

The ability of PDI to be nitrosated was tested by the DTNB assay. Reduced PDI was prepared by incubating native PDI with 10-fold molar excess DTT, followed by chromatographic separation on a Sephadex G-25 column. Freshly reduced PDI was incubated with DTNB and the total thiol concentration was found to be ~4 ± 0.25 mol per mole of PDI (Figure 2.6). However, freshly reduced PDI incubated with an excess of DEA-NO, and then subjected to the DTNB assay, showed a significant decrease in thiol concentration (0.25 ± 0.05 mol per mole of PDI) (Figure 2.6).

In order to further validate that PDI is being S-nitrosated at its cysteine residues, the absorption spectrum of PDI-SNO formed by incubating freshly reduced PDI with DEA-NO was obtained. As seen in Figure 2.7, PDI-SNO spectrum gave a peak at 340 nm, an indicative of S-NO bond formation.
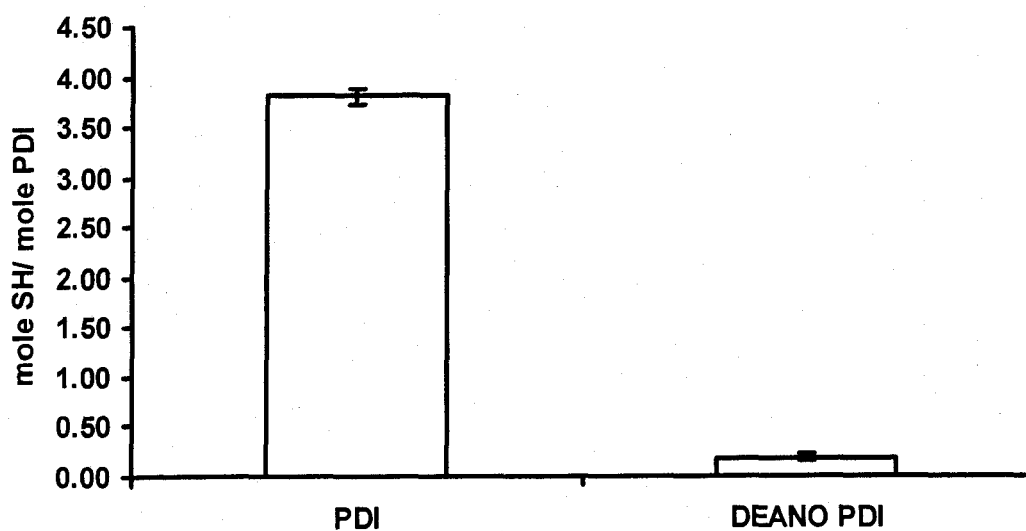
**Figure 2.6: Thiol quantification by DTNB of PDI and PDI-SNO**

Monitoring total thiols of PDI and PDI-SNO was performed by incubating PDI (10 μM) with 10 mM DTT for 1 hour at the room temperature, followed by chromatographic separation using a Sephadex G-25 column. 2 μM PDI was then incubated with excess DTBN in 100 mM Tris-HCl buffer, pH 8.0 and the absorbance at 412 nm was obtained. PDI-SNO was prepared by incubating freshly reduced PDI with excess DEA-NO followed by the removal of unreacted species using Sephadex G-25. Immediately after obtaining PDI-SNO, the sample was incubated with DTNB and the absorbance at 412 nm was measured.
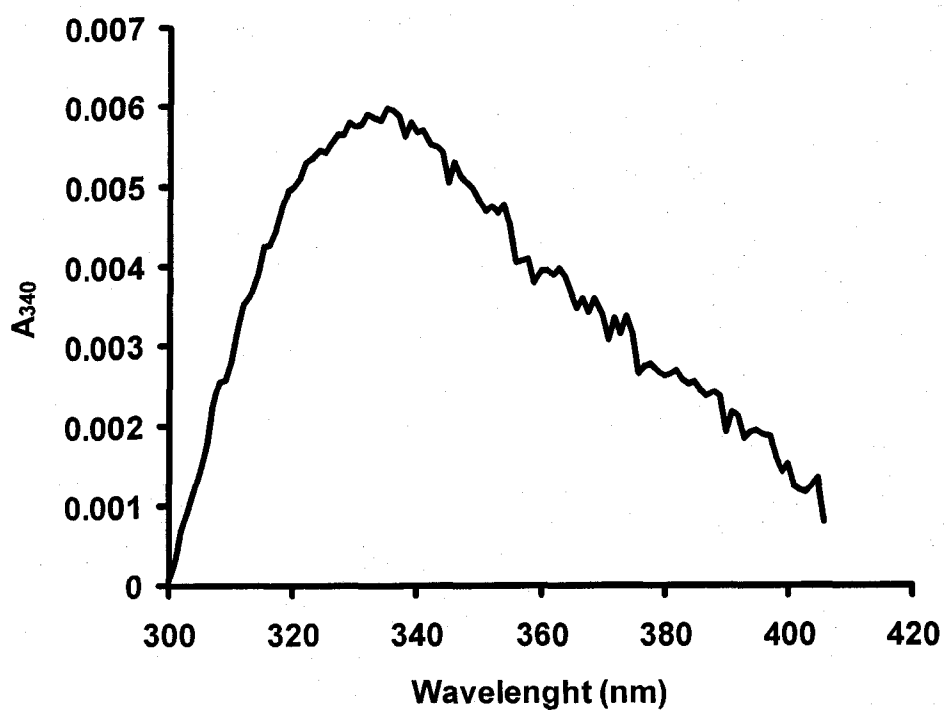
**Figure 2.7: Validation of S-nitrosated PDI**

Freshly reduced PDI (10 µM) was incubated with excess DEA-NO for 30 minutes at room temperature, followed by the chromatographic separation using Sephadex G-25 column and PDI assay buffer. The absorption spectra from freshly reduced PDI and PDI-SNO in the range from 300-400 nm were obtained and the difference spectrum was obtained and plotted as shown above.

Next, we used the NO-meter approach to detect the release of •NO from PDI-SNO. In these experiments, an •NO electrode was placed in the buffer containing NO-saturated PDI (1.0 µM) and the •NO signal was monitored for 20 seconds to ensure there is no spontaneous •NO generation (Figure 2.8 A and B). At that time, $HgCl_2$ (100 µM) was added and the increase in signal due to the release of •NO from PDI-SNO was monitored and corresponded to 4 ± 0.5 µM of •NO/µM of PDI (Figure 2.8 A). In a similar experiment, freshly reduced PDI (2 µM) was used instead of $HgCl_2$ and this also resulted in the increase in signal corresponding to 4 ± 0.5 µM •NO/µM of PDI (Figure 2.8 B). Therefore, the •NO released form PDI-SNO was determined to be ~4.5 µM/ µM of PDI, under these experimental conditions.
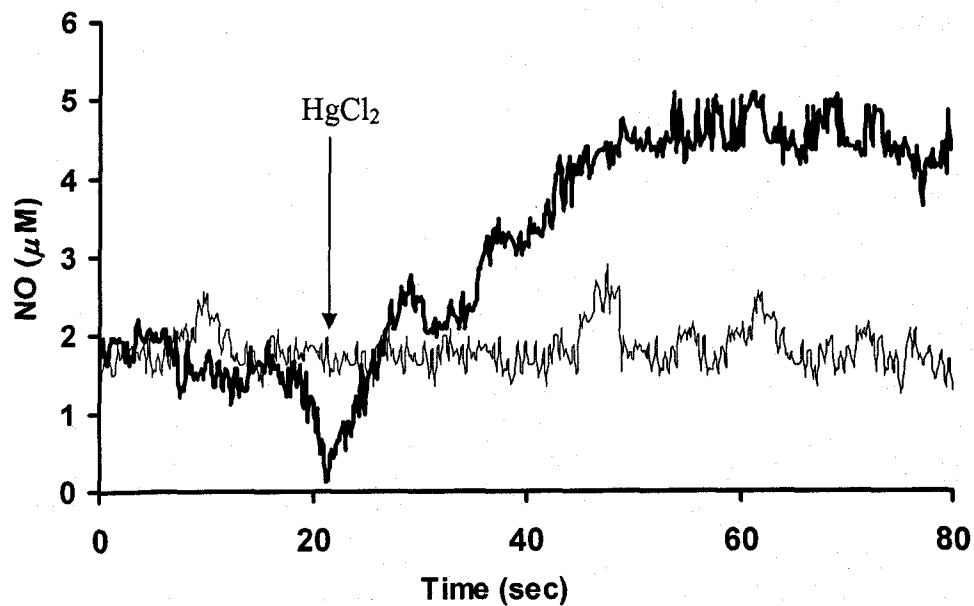
**Figure 2.8: PDI-SNO denitrosation with Hg and PDI**

A. PDI-SNO (1 μM) was placed in the vial and the NO meter was blanked using this solution. After a stable signal was obtained at about 20 seconds, 100 μM HgCl₂ was added and the •NO generation was monitored until saturation was obtained.
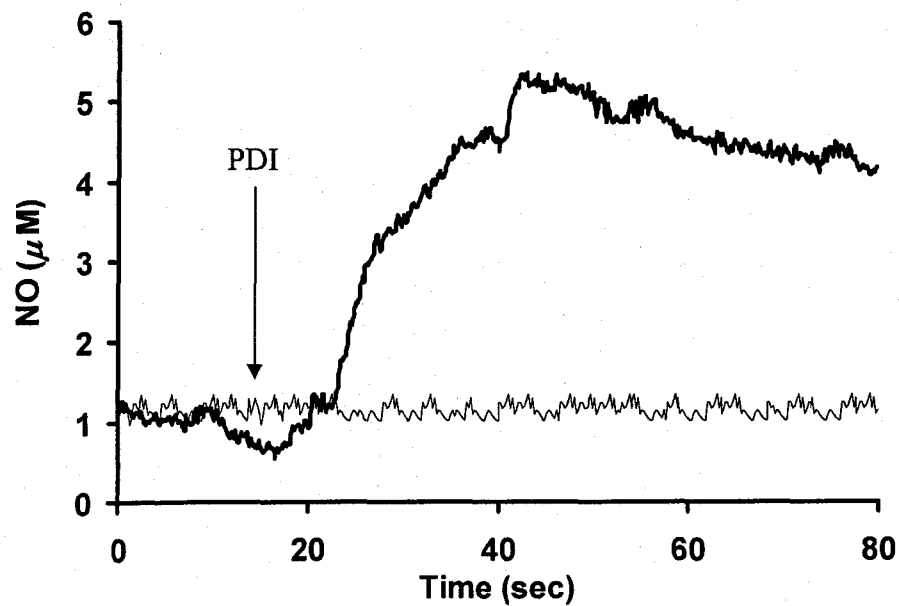
B. PDI-SNO and PDI reduced was prepared as described in the "Experimental section".

A solution containing PDI-SNO was placed in the vial and the NO signal was monitored

for 20 seconds to establish the baseline. At that time, reduced PDI was added to the

sample and the •NO generation was monitored until saturation.

Lastly, we wanted to explore the possibility of PDI storage of NO in the form of $N_2O_3$ in its hydrophobic pockets. For this purpose, freshly reduced PDI was incubated with NEM, in order to block free thiols, followed by the incubation with DEA-NO. This method ensured that there is no PDI-SNO formation.

When $HgCl_2$ (100 μM) was added to the NEM-blocked NO-saturated PDI, no change in signal was observed. However, upon addition of GSH, a slow increase in signal was observed and the concentration of NO generated was found to be ~10 ± 1 μM/ μM of PDI (Figure 2.9, dashed line). When the experiment was performed in the reverse order of addition of GSH and $HgCl_2$, the same trend was obtained. These results were interpreted in the following way: the generation of NO observed was likely due to the GSNO formation in the presence of GSH, which was then released by the addition of $HgCl_2$. These experiments suggested that PDI is able to store NO in the form of $N_2O_3$ under our experimental set up.
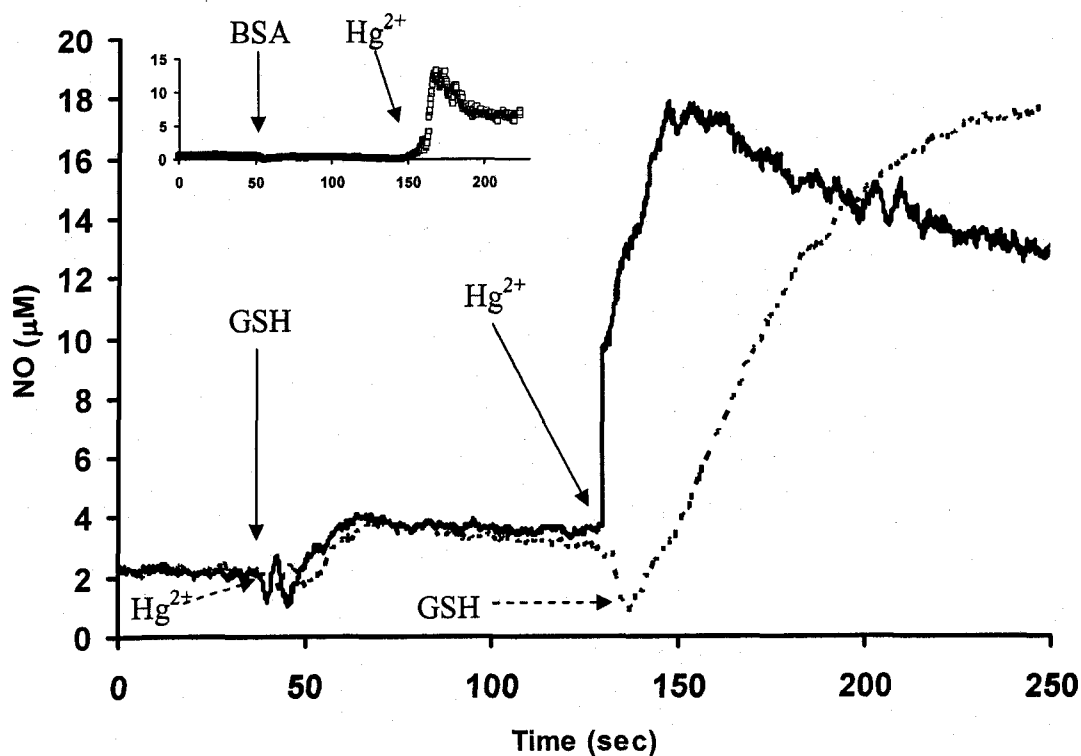
**Figure 2.9:** •NO storage by PDI

The ability of PDI to store •NO was tested by using NEM-blocked PDI (3 μM) saturated

with •NO, as described under "Experimental methods". After a stable signal was

obtained, at 50 seconds, 100 μM $HgCl_2$ (thick line) or 500 μM GSH (dashed line) was

added and no signal change was observed. Addition of either 500 μM GSH (thick line)

or 100 μM $HgCl_2$ (dashed line) at 120 seconds resulted in a steady increase in current

until saturation was obtained. *Inset*, control experiment obtained by the addition of BSA

instead of reduced PDI to PDI-SNO, followed by the addition of $HgCl_2$.

## 2.5 Discussion

S-denitrosation activity of PDI was shown in several different studies (Zai *et al.*, 1999; Ramachandran *et al.*, 2001) but the actual mechanism is still unknown. In this study, we set to establish the kinetic parameters for PDI-mediated GSNO denitrosation using recombinant human PDI. The PDI-dependent denitrosation activity as a function of varying GSNO concentrations was studied using two different methods. The first one employed a spectrophotometric method taking advantage of absorbance of S-NO bond at 340 nm, and the second one used a NO-meter to directly monitor •NO generation as a result of GSNO decomposition due to PDI activity. The $K_M$ using the spectrophotometric method was estimated to be $65 \pm 5$ $\mu M$ (Figure 2.1 A), while the NO-meter experiments gave a value of $40 \pm 10$ $\mu M$ (Figure 2.1 B).

Next we wanted to find out what was the end product of PDI-mediated GSNO denitrosation. For this purpose, the hemoglobin assay was employed and the results obtained showed that it is •NO and not NO⁻ being formed during the GSNO denitrosation by PDI (Figure 2.2 A and B). This finding was in agreement with the previous study by Nikitovic and Holmgren that showed the same product as a result of reaction of GSNO and thioredoxin (Nikitovic and Holmgren, 1996). In the light of these results, a PDI denitrosation mechanism is proposed in Scheme 2.1. This mechanism involves an initial transnitrosation reaction of one of the cysteines in the PDI active site consisting of the CXXC sequence, with the RSNO substrate (Scheme 1, I and II). Next step involves the attack on nitrogen of S-N=O with the second active site cysteine resulting a nitroxyl disulfide intermediate (Scheme 1. III).
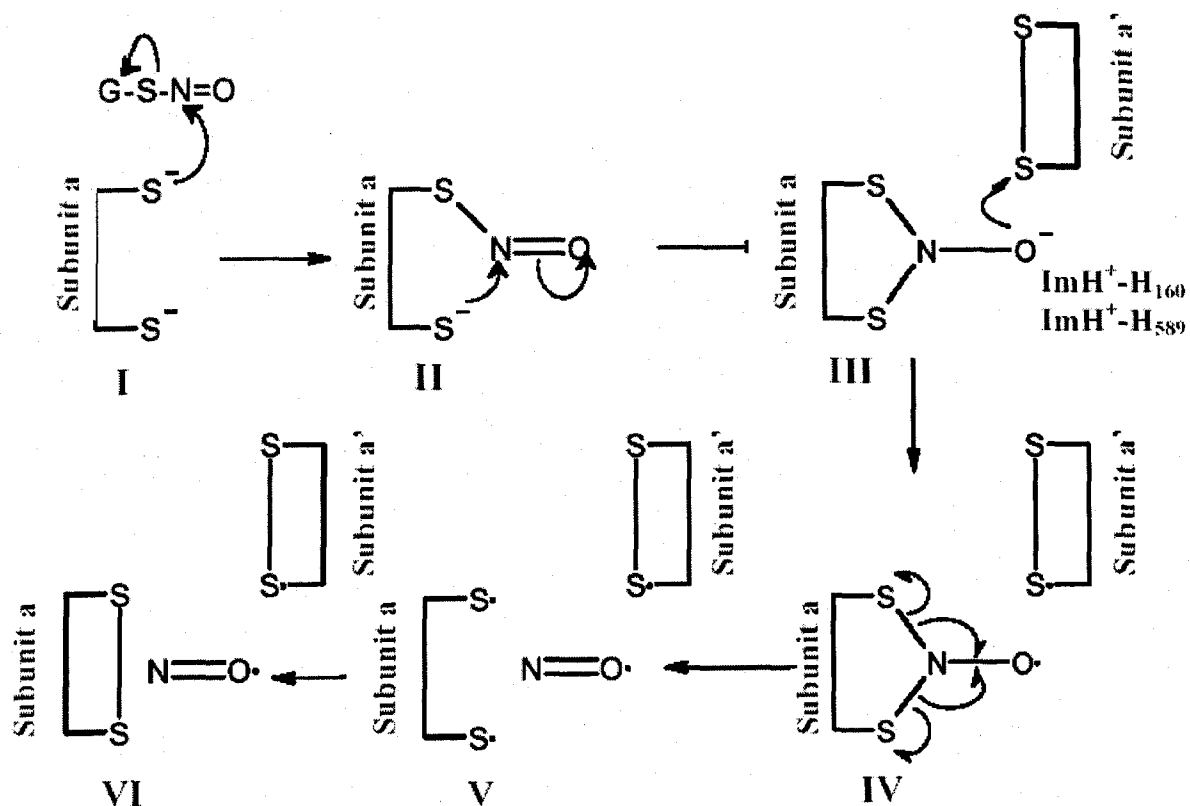
**Scheme 2.1. PDI denitrosation mechanism.**

One of the vicinal thiols of PDI active site *subunit a*, undergoes transnitrosation reaction

(*I*) in the presence of RSNO, followed by the attack of the second cysteine (*II*) at N of the

S–N=O resulting in formation of a nitroxyl disulfide intermediate (*III*), which could be

stabilized by the nearby imidazole (*ImH$^+$*) of His589. One-electron reduction by the

second active site of PDI (*subunit a'*) leads to a formation of an unstable radical

intermediate and dithiyl radical in *subunit a'*(*IV*). The final product after one enzymatic

turnover is an oxidized protein active site of *subunit a* and •NO (*V* and *VI*) (Nikitovic and

Holmgren, 1996).

This formation is most likely due to the translocation of the electrons from the N=O

double bond to N-O, which could then be stabilized by the positively charged side chain

in the vicinity of the active site, such as $His_{160}$ in the a-domain or His 589 in the a' domain (GenBank$^{TM}$ accession number AK027647). The next step involves a one electron oxidation leading to the formation of nitroxyl disulfide radical (Scheme 1, IV), which undergoes rearrangement to form oxidized S-S PDI active site plus •NO (Scheme 1, V and VI). The mechanism proposed is based on the recent study by Houk and coworkers (Houk et al., 2003) which showed by using a computational approach that the formation of such nitroxyl disulfide intermediate was possible. For this mechanism to work there is the requirement for an electron acceptor which could be either the second active site, based on the recent crystal structure of yeast PDI (Tian et al., 2006) the oxidized active site thiols of PDI dimer in the antiparallel arrangement (Solovyov and Gilbert, 2004). This hypothesis is also supported by the fact that PDI active site is the most oxidative (-180 mV) (Wilkinson and Gilbert, 2004) of all other members of thioredoxin-like family of proteins. In support of this, it has been reported that the oxidized active site thiols of DsbD, which is a prokaryotic PDI-like protein, can serve as the electron transporter via succession of disulfide exchange reactions (Rietsch et al., 1997; Collet et al., 2002).

Additional evidence supporting this mechanism was obtained with the experiments using Ac-Tempo thiyl/dithiyl radical probe. By mixing equimolar concentrations of PDI and GSNO, thyil/dithyl radicals were generated (Figure 2.3 A) while GSNO alone was unsuccessful in reacting with the probe. In order to ensure that the radical formation observed was purely due to the PDI denitrosation activity, the experiments were performed using BSA and no detectable radical formation was observed (Figure 2.3 B).

To further support our mechanism, the rate of thiyl/dithiyl radical formation was compared with •NO generation from oxyhemoglobin studies. The estimated stoichiometries of two independent experiments indicate that there are 3 moles of thiyl/dithiyl radical formed per 1 mole of NO produced (Figure 2.4). This experimental evidence is well accommodated by the proposed mechanism in Scheme 1, which suggests that the two active site S˙ plus the S-S˙ plus NO˙ (Scheme 1, IV and V) are formed in a concerted manner rather than sequential.

Next, we wanted to find out what is the fate of •NO once released by PDI from GSNO. Previous studies (Rafikova et al., 2002) suggested that serum albumin was able to store NO in the form of $N_2O_3$ in its hydrophobic pockets and potentially auto S-nitrosate its own cysteine resides. Our findings suggest that PDI behaved in the same manner, since the experiments using DAN and NO generated by GSNO and $HgCl_2$ demonstrated a decrease in NO availability in the presence of increasing protein (BSA or PDI) concentrations (Figure 2.5 A and B).

In order to show that PDI thiols were able to undergo S-nitrosation in the presence of NO donor, the thiols of freshly reduced PDI or freshly reduced PDI exposed to DEA-NO was monitored with DTNB assay. As shown in Figure 2.6, freshly prepared PDI contained ~4 moles of thiol per mole of PDI, while PDI exposed to DEA-NO essentially did not have any thiols available to react with DTNB. To ensure that this was due to S-nitrosation rather than oxidation of thiols, the absorption spectrum of S-nitrosated PDI was obtained. As seen in Figure 2.7, PDI-SNO showed a characteristic S-NO peak at 340 nm,

supporting our hypothesis. Further, the NO-meter was used as an unambiguous method to detect NO released from PDI-SNO. When the sample containing PDI-SNO was exposed to either $HgCl_2$ (Figure 2.8 A) or freshly reduced PDI (Figure 2.7 B), 4 μM of •NO were rapidly released per μM of PDI. In order to support the proposal that PDI could act as a sink for $N_2O_3$, PDI was treated with NEM to ensure unavailability of active site thiols to undergo S-nitrosation, followed by the exposure to DEA-NO, to saturate PDI with $N_2O_3$. Upon addition of GSH followed by the addition of $HgCl_2$, this NEM-blocked NO-saturated PDI was able to generate ~10 μM of NO per μM of PDI (Figure 2.9). It is interesting to note that while the addition of $HgCl_2$ followed by the addition of GSH resulted in the slower rate of •NO generation (Figure 2.9, dashed line), the reversed order caused a rapid liberation of •NO (Figure 2.9, solid line). This was probably due to the fact that when GSH was introduced first, it already started forming and accumulating GSNO, which was then readily available for cleavage by $HgCl_2$.

In summary, the results obtained in the course of this study have very important implications with respect to the role of PDI in the transport of •NO. Our result show that at low concentrations of •NO, PDI was able to denitrosate GSNO, while at the higher concentrations, PDI itself may be the target for S-nitrosation and •NO storage. The importance of our study becomes evident in the recent study by Uehara and coworkers (Uehara *et al.*, 2006) which showed that PDI-SNO loses its isomerase activity which leads to the disregulated protein folding in the ER that promotes neuronal cell death, resulting in the development of neurodegenerative disease.

# CHAPTER 3

# The role of redox state active site thiols of platelet surface PDI

# in S-nitrosothiol consumption

## 3.1 Introduction

PDI-mediated RSNO denitrosation activity was established in the previous chapter. Here, we will apply these findings to determine the physiological role of PDI denitrosation activity under different physiological conditions. This chapter will investigate the role of platelet surface PDI in RSNO denitrosation, platelet ROS production, platelet aggregation and detection of the dynamic state of PDI active site thiols using ICAT-MALDI technology.

### 3.1.1 Platelet physiology

Platelets were discovered in 1860's by Max Schultze as blood constituents, and characterized in 1880's by Bizzozero as the first component of the blood to respond and adhere to damaged blood vessels (Brewer, 2006). Since then, many discoveries have been made about platelet structure and function.

Platelets are derived from the bone marrow cells called megakaryocytes through a process of thrombopoiesis regulated by a glycoprotein hormone thrombopoietin. They are 1-3 $\mu$M in size and during the resting state, platelets are smooth and disc shaped. However, upon activation, platelets undergo shape change and develop into a spiny spherical form. Platelets are composed of a phospholipid bilayer membrane which contains various glycoproteins that serve as receptors for factors that cause platelet activation and aggregation (Shapiro, 2000). Platelet cytoskeleton and the microtubular system are responsible for maintaining the discoid shape of resting platelets, while the nearby dense tubular system, which serves as calcium storage, contains the open

canalicular system through which secretion of granules occur (Fuse, 1996). Platelet cytosol contains dense and alpha granules, mitochondria and lysozymes. The dense granules contain ATP and ADP, serotonin and calcium, while alpha granules contain adhesive proteins such as fibrinogen, thrombospondin, von Willebrand factor, to name a few (Packham, 1994). Upon platelet activation, the granular contents are released into the peri-platelet environment thus initiating interactions with other platelets and cells.


### 3.1.2 Platelet Function

Platelets play a crucial role in vascular hemostasis. Upon vascular injury, platelets rapidly aggregate and form a plug which is stabilized by fibrin filaments. Platelet activation is caused by the release of granular contents such as collagen, ADP, thrombin, fibrinogen, von Willebrand factor (vWF), all of which act synergistically to potentiate platelet aggregation (Ware *et al.*, 1987). This results in the interaction between platelet glycoprotein (GP) complexes and its ligands, GPIIb/IIIa which bind to vWF and GPIa/IIa ($\alpha2\beta1$) and collagen. The aggregation of platelets is mediated through the fibrinogen receptor GPIIb/IIIa which undergoes a conformational change essential for aggregation (Tsuji *et al.*, 1999). The binding of collagen or fibrinogen to their respective receptors involves disulfide bond reduction and oxidation (Essex *et al.*, 1999; Lahav *et al.*, 2002). The outcome of platelet stimulation with agonists such as collagen or thrombin results in hydrolysis of the membrane phospholipids accompanied with the increase in inositol 1,4,5,-biphosphate (IP$_3$). IP$_3$ accumulation stimulates an increase in intracellular calcium levels which essentially modify actin filaments responsible for conformational change of platelets (Leopold and Loscalzo, 1995).

### 3.1.3 Platelet Surface Protein Disulfide Isomerase

The first report of platelet-surface associated PDI (psPDI) came from the study of Chen and coworkers (Chen *et al.*, 1992). Their hypothesis was based on the previous observations that intra- and intermolecular thiol-disulfide exchange of thrombospondin occurs during the platelet activation. Their findings suggested that there is a PDI-like protein activity released upon platelet activation. A few years later, Chen and coworkers successfully purified PDI from activated platelets. Their study showed that PDI was localized to the platelet plasma membrane, where it can contribute to the modification of proteins through its reduction or isomerization activity resulting in cross-linking of proteins within the extracellular matrix or cell membranes. A later study by Essex and Li (Essex and Li, 1999) showed that psPDI contributes to the activation of fibrinogen receptor GPIIb/IIIa through the disulfide bond exchange resulting in platelet aggregation. The extension of this study showed that platelet aggregation is mediated though the redox state of platelet surface vicinal thiols, such as PDI, with respect to the GPIIb/IIIa activation (Essex and Li, 2003).

Concurrently, the role of •NO in mediating platelet activation and aggregation was studied. •NO was found to inhibit platelet activation and aggregation though the activation of soluble guanylate cyclase (sGC), resulting in an increase in cGMP levels. Consequently, platelets exhibited a reduction in cytosolic calcium levels, inhibition of cAMP phosphodiesterase and activation of protein kinase G. These events contribute to the decrease in platelet aggregation and adhesion and even disaggregation of platelet aggregates (Alonso and Radomski, 2003).

Previous studies have shown that PDI is involved in consumption of S-nitrosothiols (RSNO) and disulfide exchange. Therefore, it was only a matter of time to correlate these two activities of PDI in elucidating its role in platelet aggregation with respect to the presence of RSNO.

### 3.1.4 Type 2 Diabetes and Platelets

Type 2 diabetes (T2D) is often accompanied with insulin resistance. Insulin resistance simply means that cells do not respond to insulin signaling responsible for glucose uptake by cells. Therefore, hepatic glucose produced by the body is not successfully internalized by skeletal muscle resulting in an increase in circulating glucose levels leading to hyperglycemia and hyperinsulinemia. These abnormal physiological conditions affect many cellular systems including platelets. As previously described, platelets circulate throughout vasculature without adhering to the endothelium unless there is a vascular injury. However, diabetic platelets are known to exhibit higher levels of adhesiveness and aggregation either spontaneously or by agonist stimulus *in vitro*. Previous studies have shown that T2D platelets are more prone to adhesion to the endothelial cells, leukocytes and other platelets resulting in the thrombus formation and atherosclerosis (Vinik *et al.*, 2001).

The presence of reactive oxygen species (ROS) has been shown to promote hyperaggregability in diabetic platelets resulting in the development of cardiovascular disease (Spitaler and Graier., 2002; Sonta *et al.*, 2004). Previous findings from our lab

(Root PhD Thesis, 2004) showed that upon exposure of platelets to exogenous ROS, a decrease in RSNO metabolism was observed as well as enhanced platelet aggregation. The main factor of these events is psPDI. Therefore, the observed loss in platelet RSNO metabolism was attributed to the oxidation of psPDI active-site thiols due to the increased oxidant load.

T2D is accompanied by increased levels of cholesterol, and the current treatment of hypercholesteronemia makes use of statins which act as the inhibitors of 3-hydroxy-3-methylglutaryl coenzyme A reductase (HMG-CoA reductase), an enzyme that catalyzes the rate limiting step of cholesterol biosynthesis (Maron *et al.*, 2000). Recently, it has been observed that statins may have additional vasculoprotective benefits other than cholesterol lowering (Collins *et al.*, 2004). The current hypothesis is that statins may contain antioxidant properties through inhibition of assembly of NADPH oxidase (NOX). NOX is a multimeric protein composed of plasma membrane catalytic subunits $p22^{phox}$ and $p91^{phox}$, cytosolic regulatory subunits $p47^{phox}$, $p40^{phox}$, $p67^{phox}$ and the small G-protein Rac1 or Rac2. Assembly of NOX subunits requires association of Rac GTPase which is regulated through its carboxy-terminal geranylgeranylation (Ando *et al.*, 1992). Therefore, it was of great interest to establish the relationship between platelets ROS levels and the PDI activity with respect to RSNO denitrosation and aggregation.

The Syrian Golden hamster was the animal of choice for development of pre-diabetic state. Upon fructose feeding for 7 days, animals develop hyperinsulinemia and

hyperlipidemia thus representing a viable model for prediabetic, insulin-resistant state (Taghibiglou *et al.*, 2002).

### 3.1.5 ICAT-MALDI TOF Technology

PDI active site thiols direct its activity. Common approaches to analyze thiol redox state include spectrophotometric and fluorescence assays (Wright and Viola, 1998) which provide quantitative information about average number of modified thiols, but not their exact identity. The new approach of quantitative proteomics involves the use of isotope coded affinity tag (ICAT) reagents in combination with mass spectrometric analysis to detect protein labeling in a complex mixture and accurately quantify the difference in protein redox state (Smolka *et al.*, 2001). The ICAT reagent is comprised of three functional components. The first one is a thiol-reactive group, followed by the ethylene glycol linker that differentiates labeled peptides based on its isotope mass and the biotin group which provides an easy purification of tagged peptides by affinity chromatography. Therefore, the ICAT approach may be the most suitable way to detect dynamic changes in PDI active site thiol status under different conditions.

Therefore, the objectives of this study were to: 1- Determine the kinetic parameters of psPDI-mediated GSNO denitrosation; 2- Establish the link between the psPDI denitrosation activity, ROS production and platelet aggregation in normal and fructose-fed animal model and study the effects of rosuvastatin on normalizing these activities; 4- Detect the dynamic redox state of PDI active site thiols using MALDI-TOF technology.

## 3.2 Materials and Equipment

### 3.2.1   Materials

| | |
|---|---|
| Adenosine diphosphate; | Sigma-Aldrich Canada Ltd., Oakville, Ontario |
| Acetone; | Sigma-Aldrich Canada Ltd., Oakville, Ontario |
| Ammonium persulfate; | Sigma-Aldrich Canada Ltd., Oakville, Ontario |
| Ammonium sulfate; | Sigma-Aldrich Canada Ltd., Oakville, Ontario |
| Amplex Red assay; | Molecular Probes ,Eugene, Oregon |
| Apyrase; | Sigma-Aldrich Canada Ltd., Oakville, Ontario |
| Biorad Bradford Reagent; | Bio-Rad Laboratories Ltd., Mississauga, Ontario |
| Bovine serum albumin; | Sigma-Aldrich Canada Ltd., Oakville, Ontario |
| Citric Acid Monohydrate; | Sigma-Aldrich Canada Ltd., Oakville, Ontario |
| Copper sulfate; | Sigma-Aldrich Canada Ltd., Oakville, Ontario |
| cGMP Enzymeimmunoassay; | Amersham Biosciences, Piscataway, New Jersey |
| 5, 5'-dithiobis(2-nitrobenzoic) acid; | Sigma-Aldrich Canada Ltd., Oakville, Ontario |
| Dithiothreitol (DTT); | Sigma-Aldrich Canada Ltd., Oakville, Ontario |
| Diphenyleneiodonium chloride (DPI); | Sigma-Aldrich Canada Ltd., Oakville, Ontario |
| Ethylene diamine tetraacetic acid; | Sigma-Aldrich Canada Ltd., Oakville, Ontario |
| Fructose; | Sigma-Aldrich Canada Ltd., Oakville, Ontario |

Goat anti-mouse polyclonal antibody, horseradish peroxidase conjugate;

| | |
|---|---|
| | Stressgen Bioreagents, British Columbia |
| Heparin; | Sigma-Aldrich Canada Ltd., Oakville, Ontario |
| Imidazole; | Sigma-Aldrich Canada Ltd., Oakville, Ontario |

| | |
|---|---|
| Insulin; | Sigma-Aldrich Canada Ltd., Oakville, Ontario |
| Isofluorane; | Leamington Animal Clinic, Leamington, Ontario |
| Monoclonal anti-PDI antibody RL90; | Abcam USA, Cambridge, MA |
| N-1-Napthylethylenediamine dihydrochloride; | |
| | Sigma-Aldrich Canada Ltd., Oakville, Ontario |
| Ni-Cam™ Resin; | Sigma-Aldrich Canada Ltd., Oakville, Ontario |
| Oxygen gas; | BOC gases, Windsor, Ontario |
| Phosphoric acid; | Sigma-Aldrich Canada Ltd., Oakville, Ontario |
| Potassium phosphate; | Sigma-Aldrich Canada Ltd., Oakville, Ontario |
| Reduced glutathione; | Sigma-Aldrich Canada Ltd., Oakville, Ontario |
| Rosuvastatin; | Astra-Zeneca, London, England |
| Sodium chloride; | Sigma-Aldrich Canada Ltd., Oakville, Ontario |
| Sodium hydroxide; | Sigma-Aldrich Canada Ltd., Oakville, Ontario |
| Sodium nitrite; | Sigma-Aldrich Canada Ltd., Oakville, Ontario |
| Sodium phosphate monobasic: | Sigma-Aldrich Canada Ltd., Oakville, Ontario |
| Sodium phosphate dibasic; | Sigma-Aldrich Canada Ltd., Oakville, Ontario |
| Sulfanilamide; | Sigma-Aldrich Canada Ltd., Oakville, Ontario |
| Syrian Golden Hamster; | Charles River, Montreal, Quebec |
| TEMED; | Bio-Rad Laboratories Ltd., Mississauga, Ontario |
| Tetrazolium 4-([3-(4-iodophenyl)-2-(4-nitrophenyl)-2H-5-tetrazolio]-1,3-benzene | |
| disulfonate sodium salt); | Roche Diagnostics, Indianapolis, Indiana |
| Trizma®; | Sigma-Aldrich Canada Ltd., Oakville, Ontario |

### 3.2.2 Equipment

Agilent 8453 UV-VIS spectrophotometer;

(Agilent Technologie Canada Inc, Mississauga, Ontario)

Beckman J2-HS Centrifuge;

(Beckman Coulter Canada Inc., Mississauga, Ontario)

BioRad Biologic Work Station;

(Bio-Rad Laboratories Ltd., Mississauga, Ontario)

BioRad Fraction Collector Model 2110;

(Bio-Rad Laboratories Ltd., Mississauga, Ontario)

Hemocytometer;

(Reichert Co, Buffalo, NY)

ISO-NO Mark II with WPI MKII Nitric Oxide electrode;

(World Precision Instruments Inc., Sarasota, Florida)

Jouan CR3i Centrifuge;

(Jouan Inc, Winchester, Virginia)

Labconco FreeZone 4.5 Liter Benchtop Freeze Dry Systems;

(Labconco Corporation, Kansas City, Missouri)

MALDI-TOF MS

(DE-pro Voyager, Applied Biosystems, Foster City, California)

MALDI-TOF MS/MS

(4700 Proteomics Analyzer, Applied Biosystems, Foster City, California)

Mettler AJ100 Balance;

(Mettler Toledo Canada, Mississauga, Ontario)

Microtiter 96-well Solid Plate;

(Thermo Electron Corp. Canada, Burlington, Ontario)

Orion Model 420A pH Meter;

(Thermo Electron Corp. Canada, Burlington, Ontario)

Stir Plate 360 Series;

(VWR International, Mississauga, Ontario)

Vacutainer Blood Collection Needles;

(Becton Dickinson, Mississauga, Ontario)

Vacutainer Blood Collection Tubes, ACD, 2.5 mL draw;

(Becton Dickinson, Mississauga, Ontario)

## 3.3 Experimental Methods

### 3.3.1 Preparation of S-nitrosoglutathione

GSNO was prepared as described elsewhere (Sliskovic *et al.*, 2005). Briefly, after determining free thiol concentration in GSH, a stoichiometric amount of acidified $NaNO_2$ was added and the reaction was allowed to proceed for 30 minutes at 4°C. After this, the pH of the solution was adjusted to 7.4. The $NO_2^-$ contamination was considered negligible as detected by the Griess reagent (Munoz-Fuentes *et al.*, 2003). GSNO was recrystallized by the slow addition of ice-cold acetone, which removed $NO_2^-$ levels below the detection limit of the Griess reagent.

### 3.3.2 Purification of Protein disulfide isomerase

Recombinant PDI was expressed using pET-28b vector and *Escherichia coli* BL21 (DE3) strain. This plasmid was prepared by Seslija (2005) and was generously donated to our lab. pET 28 plasmid encodes for the full human PDI sequence and contains an N-terminal $His_6$ tag. Purification of the recombinant PDI was performed using a high capacity nickel column, and PDI was eluted using 250 mM imidazole prepared freshly in 50 mM Tris-HCl, pH 8.0, and collected in 2 mL fractions. The fractions containing PDI were pooled together and dialyzed to remove imidazole, followed by the protein quantification by the Bradford assay (Bradford, 1976).

### 3.3.3 Animal Feeding and Monitoring Protocols

Experiments performed using Golden Syrian Hamsters in the course of this study were approved by the University of Windsor Research Ethics and Animal Care Committees and in accordance with the CCAC *Guide to the Care and Use of Experimental Animals*. Hamsters were housed one per cage and given free access to food and water. Initially, animals were divided into two groups one of which received water feeding (control) and the second one was given 10% fructose. After two weeks of fructose feeding, animals were further divided into four groups: i) control with no rosuvastatin, ii) control with 10mg/kg of rosuvastatin, iii) fructose fed with no rosuvastatin and iv) fructose fed with 10mg/kg of rosuvastatin. Rosuvastatin was daily prepared in water and administered to the animals by oral gavage for 7 days.

### 3.3.4 Pharamcokinetics of Rosuvastatin in the Syrian Golden Hamster

Rosuvastatin present in the plasma was determined by collecting 200 μL of blood at 1 hour intervals after the initial administration for 24 hours. These samples were analyzed for rosuvastatin content by the reverse-phase high performance liquid chromatography with electrospray ionization tandem mass spectrometric detection at AstraZeneca (Wilmington, Denver).

### 3.3.5 Collection of Blood and Platelet preparation

Isofluorane delivered with 1% oxygen was used to anaesthetize hamsters in an induction chamber. Hamsters were then transferred to a heating pad in the supine position and fitted with a rodent circuit. After washing the thorax and abdomen with 70%

isopropanol, hamsters were put to death by exsanguination. Blood was removed from the inferior vena cava with 25 3/8 gauge syringe needle and mixed with ACD (acid citrate dextrose: 25 g/L trisodium citrate dehydrate, 15 g/L citric acid monohydrate and 20 g/L dextrose) at 9:1 ratio.

Platelet suspension was obtained by the method described by Mustard (Mustard *et al.*, 1989). Platelet rich plasma was obtained by centrifuging the whole blood for 15 minutes at 190 x g at 37°C. Platelets were isolated by further centrifugation for 15 minutes at 2000 x g and 37°C, and washed three times in Tyrode-albumin solution (pH 7.4). The first wash contained heparin (2 U/mL) and apyrase (1 U/mL), the second wash contained apyrase only, while the third wash contained Tyrode's solution without apyrase and heparin. Platelets were counted using a hemocytometer.

### 3.3.6 Platelet surface NADPH oxidase Activity

Platelets (100 µL, $10^8$) in Tyrode-albumin solution, obtained from four study groups of hamsters were placed in 96 well plates. The reaction mixture contained 25 µM NADPH, 25 µM ADP and 10 µL of stock tetrazolium 4-([3-(4-iodophenyl)-2-(4-nitrophenyl)-2H-5-tetrazolio]-1,3-benzene disulfonate sodium salt) (WST-1) colorimetric probe. The blank mixture did not contain platelets. NOX activity was monitored as the increase in absorbance at 430 nm, as the result of formazan formation, species indicative of superoxide presence.

### 3.3.7 GSNO consumption by platelets

Consumption of GSNO by washed human platelets was accomplished by directly monitoring NO accumulation using the Apollo 400 free radical analyzer equipped with a Clark type NO electrode. A standard curve was obtained with various GSNO concentrations ranging from 0-250 μM and 500 μM $CuSO_4$ (Pfeiffer *et al.*, 1998). Washed human platelets were prepared as previously described and the solution containing $2 \times 10^6$ platelets/mL was added to ACD buffer containing a range of GSNO concentration (0-250 μM), followed by time dependant monitoring of PDI-mediated NO release.

The role of ps PDI was assessed by preincubating platelets for 30 minutes with 20 μg/mL of anti-PDI antibodies and monitoring the release of NO by the addition of 40 μM GSNO.

### 3.3.8 Platelet aggregation studies

A stock solution of washed human platelets was prepared in Tyrode's buffer at the concentration of $10 \times 10^8$ platelets/mL. Aggregation of platelets was initiated with 2.5 μM ADP and monitored at 630 nm for the loss of turbidity using a 96-well plate spectrophotometer (Krause *et al.*, 2001).

### 3.3.9 Platelet cGMP measurements

Standard curve for cGMP detection was prepared as per manufacturer's instruction. Briefy, varying cGMP concentrations (2 fmol-512 fmol) were placed in the 96-well plate and incubated with reaction mixture containing cGMP conjugated to horseradish

peroxidase. Addition of TMB substrate results in a color development which can be monitored by measuring absorbance at 630 nm. Similarly, platelet samples ($10^8$) previously exposed to L-NMMA, an inhibitor of endogenous NO generation, were exposed to a known NO donor (Wang *et al.*, 1999) S-nitroso-N-acetlypenicillamine (SNAP) (100 μM), for 1 hour at 37°C followed by cGMP measurements as the standards.

### 3.3.10 Platelet cholesterol measurements

Platelets from healthy volunteers and diabetic patients were prepared as described above. Cholesterol standard curve was obtained by incubating varying cholesterol concentrations (0-10 μM) with the Amplex Red solutions as per manufacturer's instructions. Platelets (100 μL, $10^8$) were placed in the 96 well plate and the reaction was initiated by the addition of Amplex Red (300 μM), HRP (2 U/mL), cholesterol oxidase (2 U/mL) and cholesterol esterase (0.2 U/mL). The mixture was incubated for 1 hour at 37°C and the end point determination was performed in 96-well fluorescence spectrometer with 530 nm excitation and 590 nm emission wavelengths. The increase in fluorescence as a result of Amplex Red conversion to resorufin due to the presence of $H_2O_2$ that is generated as the result of cholesterol oxidation, was used to estimate the amount of cholesterol present in each sample, using the cholesterol standard curve.

### 3.3.11 PDI reduction and spontaneous auto-oxidation

Recombinant PDI (100 μg) was fully reduced by incubation with 5 x molar excess of DTT for 2 hours at the room temperature, followed by the chromatographic separation of DTT over Sephadex G-25 column in 100 mM phosphate buffer, pH 7.0. Following the

separation, PDI was immediately acetone precipitated and labeled with light $^{12}$C-ICAT reagent. For auto-oxidation experiments, freshly reduced PDI was incubated for 1 and 3 hours at the room temperature, acetone precipitated and labeled with heavy $^{13}$C-ICAT reagent.

### 3.3.12 ICAT labeling of PDI

Following the labeling of reduced and auto-oxidized PDI with $^{12}$C- and $^{13}$C- ICAT reagent for 2 hours at 37°C, two samples were mixed together and subjected to digestion with *Glu-C* for 12 hours at room temperature. Desalting was done using a cation exchange cartridge and biotin-labeled peptides were purified using an avidin affinity cartridge. After drying of the isolated peptides, the acid cleavable linker was released by incubation in the cleavage reagent for 2 hours at 37°C, followed by drying and resuspending in 1% formic acid. Prior to MALDI MS analysis, all samples were desalted using micro-C18 ZipTips.

### 3.3.13 Mass spectrometry analysis

Purified peptides were analyzed by MALDI-TOF MS and MALDI-TOF MS/MS. Samples were mixed with matrix in 1:1 ratio (α-cyano-4-hydroxycinnamic acid), spotted onto a MALDI target plate and analyzed in reflector mode. Reverse-phase nanoflow HPLC system was used for MS/MS analysis thus providing identification of the amino acid sequence within the human PDI active site.

## 3.4 Results

The animal treatment and blood isolation was performed in collaboration with my colleague Shane Miersch. The ICAT-MALDI TOF experiments were performed by Anna Kozarova under the supervision of Dr. Otis Vacratsis, Department of Chemistry and Biochemistry, University of Windsor.

### 3.4.1 Kinetic parameters of platelet surface PDI mediated GSNO consumption

Platelet surface PDI-mediated GSNO denitrosation was monitored using an NO-electrode. Initially, the electrode was placed in the ACD buffer containing a range of GSNO concentrations (10-250 µM) in order to obtain a blank signal. Then, a suspension of platelets ($10^8$) was added and the release of nitric oxide was monitored over time (Figure 3.1 A). The initial rate of NO generation with respect to time, as a function of increasing GSNO concentrations displayed saturation kinetics with an apparent $K_M$ of ~22.5 ± 1.2 µM (Figure 3.1 B). In order to establish the contribution of PDI to GSNO denitrosation, platelets were preincubated with anti-PDI antibodies for 30 minutes and placed in the vial containing GSNO (40 µM). The NO generated with platelets with anti-PDI antibodies was ~85% lower than platelets alone (Figure 3.2).
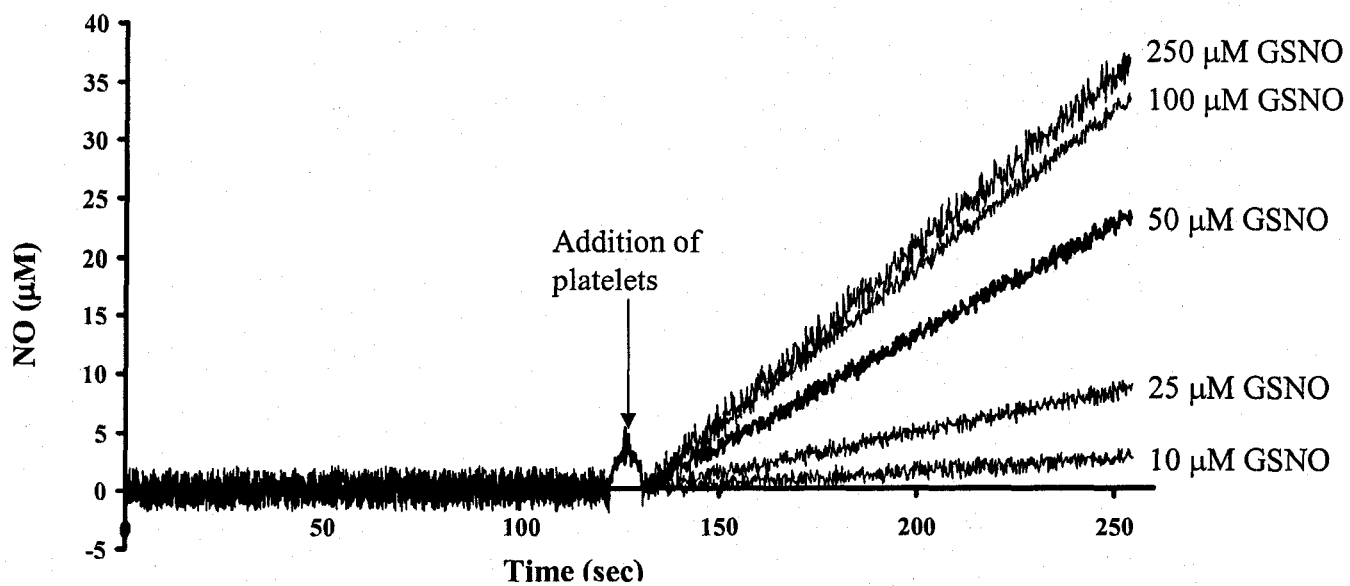
**Figure 3.1 Platelet surface PDI mediated GSNO denitrosation.**

A. The rate of spontaneous NO generation from GSNO concentrations ranging from 10-250 µM was monitored for 120 seconds. At that time platelets ($10^8$) in ACD buffer were added and the initial rates of NO release were monitored for the kinetic determination.
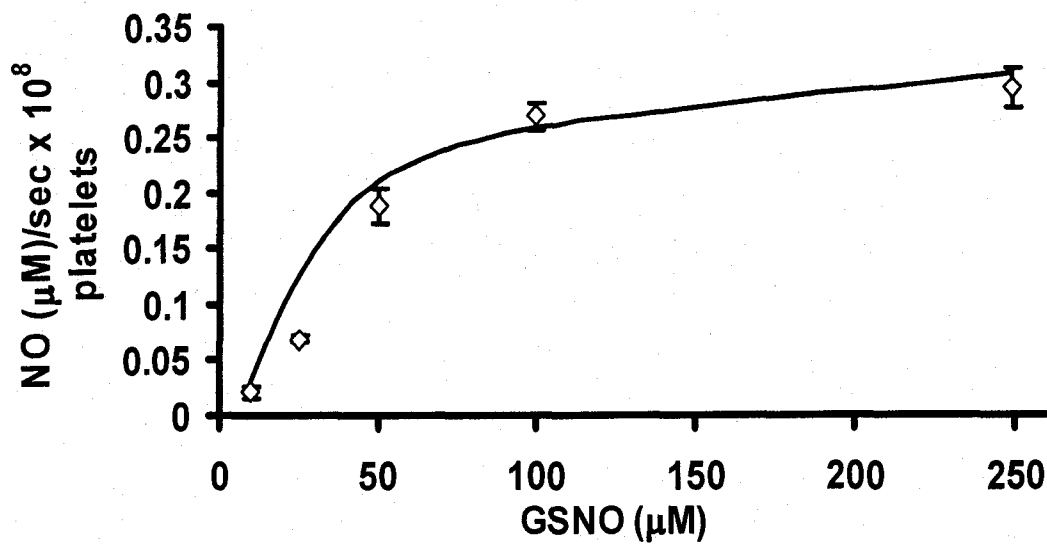
B. The consumption of GSNO by platelets as shown in the above figure followed Michaelis-Menten kinetics as shown by plotting initial rates of •NO release over a range of GSNO concentrations (25-250 μM).
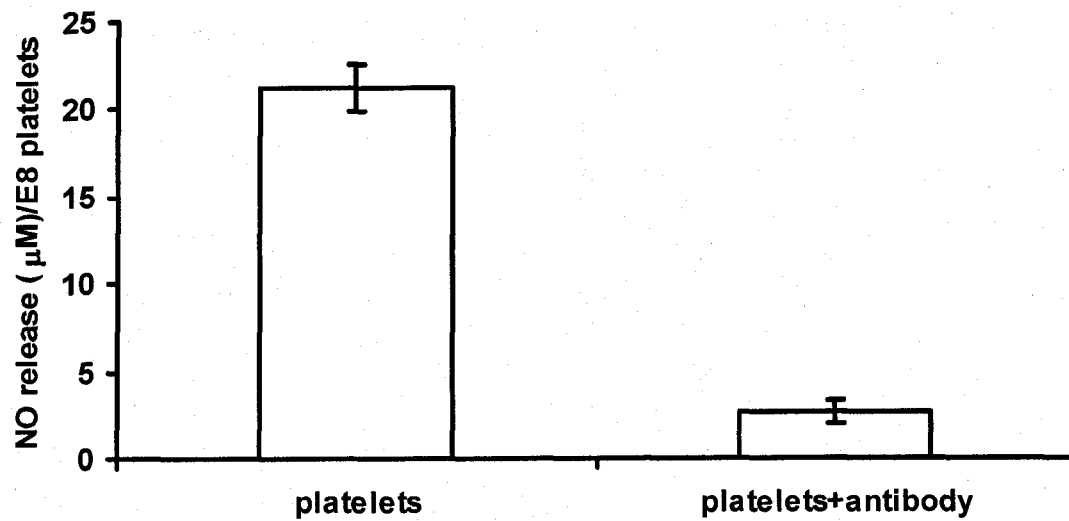
**Figure 3.2 Inhibition of GSNO denitrosation by PDI antibodies.**

Platelet suspension was preincubated with specific PDI antibodies for 30 minutes. Denitrosation of GSNO (40 μM) was monitored using an NO-meter in the absence or presence of anti-PDI antibodies and represented as the concentration of •NO generated over time (n=4).

### 3.4.2 The role of PDI in pre-diabetic platelets of Syrian hamster model

A time course study of plasma rosuvastatin concentration was determined and showed a maximum of 20 nM rosuvastatin at about 4-6 hours following drug administration. The increase in rosuvastatin levels at the end of 24 hours was probably due to re-ingestion of the drug by coprophagia (Figure 3.3).

Next, we wanted to establish the relationship between four different groups of hamsters including i) control (no fructose, no rosuvastatin), ii) drug control (no fructose, rosuvastatin), iii) fructose-fed (fructose, no rosuvastatin) and iv) fructose-fed with treatment (fructose and rosuvastatin), with respect to PDI denitrosation activity, reactive oxygen species generation and platelet aggregation.
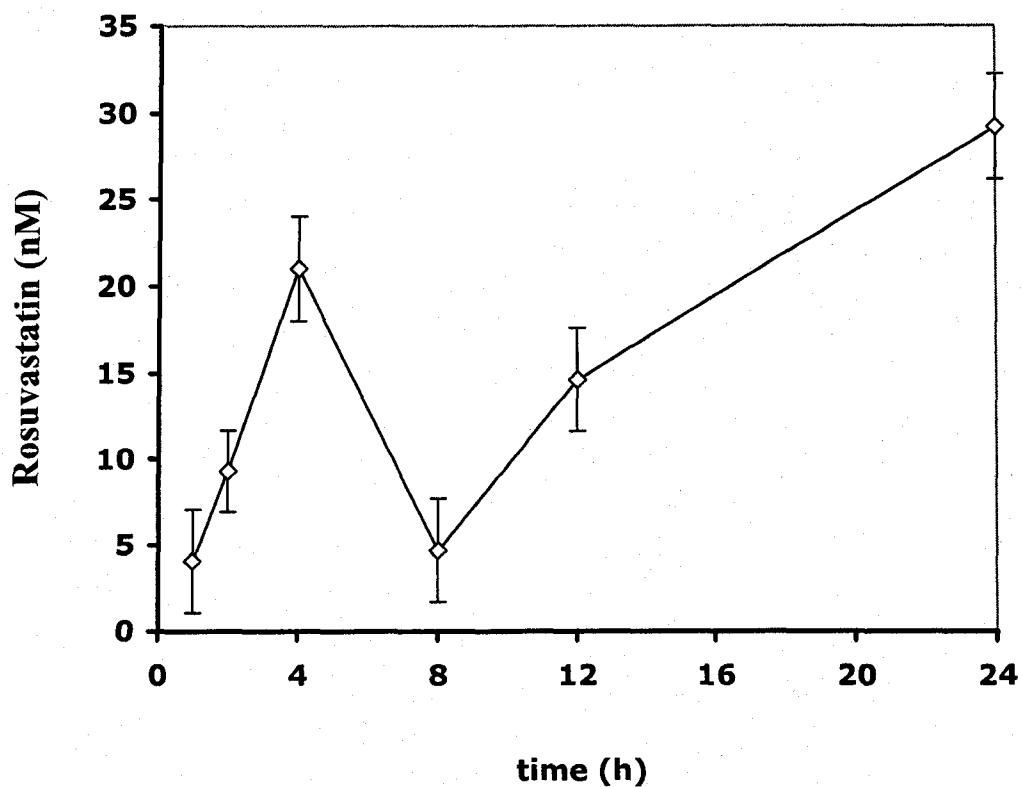
**Figure 3.3: Monitoring pharmacokinetics of rosuvastatin in Syrian hamster.**

Determination of rosuvastatin levels in plasma was obtained by collection of 200 μL of blood at different time intervals over 24 hours from the initial drug administration. Plasma concentrations of rosuvastain were analyzed and quantified by the reverse-phase HPLC with electrospray ionization tandem mass spectrometric detection.

Upon fructose feeding, PDI-dependent GSNO denitrosation decreased by ~42% as compared to the control group. Administration of rosuvastatin to a control group that did not receive fructose resulted in a 20% decrease in the denitrosation activity as compared to the control. Interestingly, the fructose fed group that received rosuvastatin treatment successfully recovered PDI denitrosation activity almost to the level of control group (Figure 3.4 A).

Conversely, while ROS production was relatively low in the control group, the animals fed with fructose showed a 60% increase in ROS levels relative to the control. Rosuvastatin administration to the control group did not change the ROS levels, while the treatment of the fructose fed group decreased and normalized the levels of ROS (Figure 3.4 B)
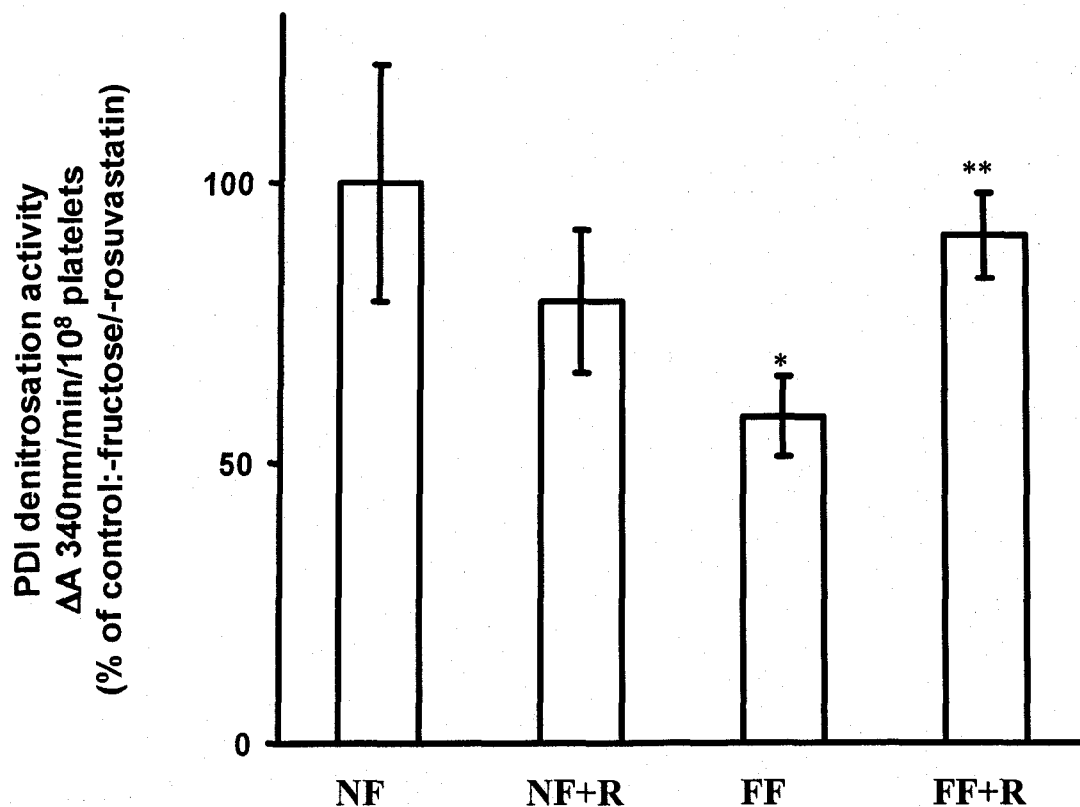
**Figure 3.4: Monitoring Platelet-surface PDI activity and ROS generation in Fructose and Rosuvastatin fed Syrian hamsters**

A. Platelets from both control and fructose fed hamsters, with and without 10mg/kg of Rosuvastatin were collected and prepared as described in Materials and Methods. PDI activity was monitored in the presence of 250 μM GSNO over a 15 minutes time period, as a decrease in absorbance at 340 nm, an indicative of S-NO bond cleavage from GSNO. Data shown represents the percent difference in rates of •NO release with respect to control, with n=13 study samples. $P < 0.005$, * with respect to control, ** fructose fed plus Rosuvastatin with respect to fructose fed.

NOX activity
($\Delta$A 430 nm)/min/10$^8$ platelets
(% of control: -fructose/-rosuvastatin)

150

100

50

0

NF    NF+R    FF    FF+R

*  **
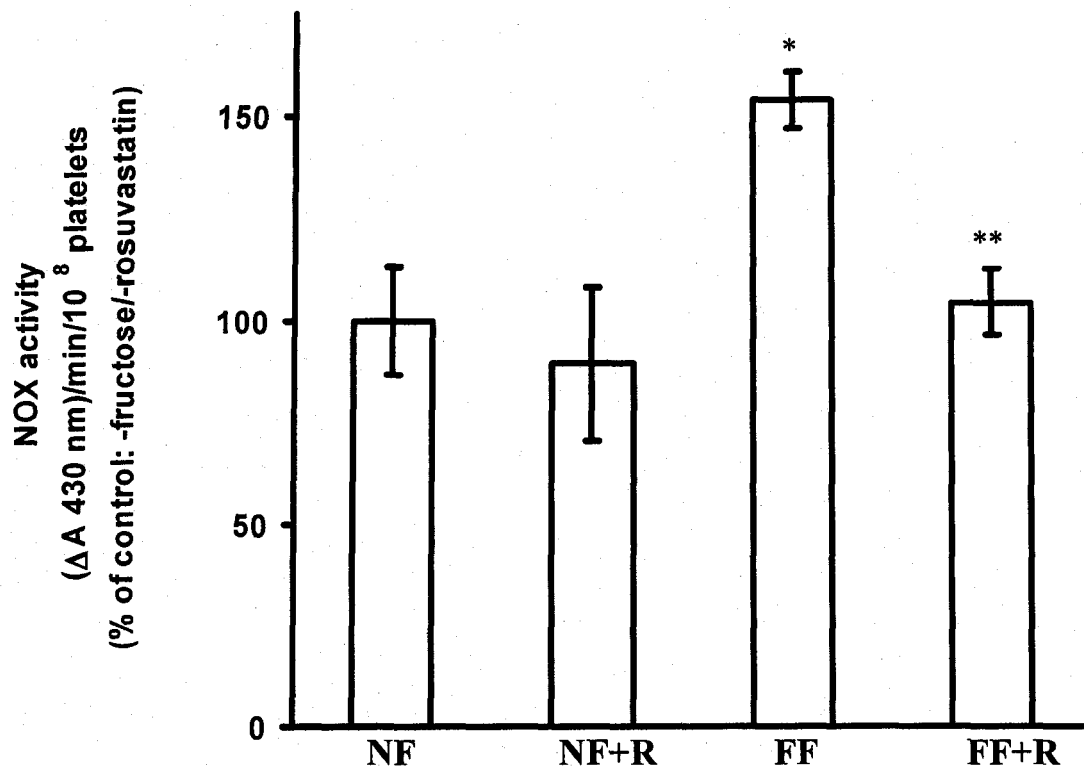
B. Platelets from both control and fructose fed hamsters, with and without 10 mg/kg of Rosuvastatin were collected and prepared as described in Materials and Methods. NOX activity was monitored in the presence of 10 $\mu$L of WST-1 (stock solution) over a period of time. The formation of formazine, indicative of superoxide production was monitored as the increase in absorbance at 430 nm. Data shown represents the percent difference in rates of formazine formation with respect to control, with n=13 study samples. P<0.005, * with respect to control, ** fructose fed plus Rosuvastatin with respect to fructose fed.

Next, we wanted to correlate the amount of ROS production and PDI-denitrosation activity with the ability of platelets to aggregate. Platelet aggregation favors the oxidized state of active site thiols of PDI, which are required for integrin-ligand interactions (Chapter 1, 1.1.4 b). Upon induction of platelet aggregation with 2.5 µM ADP, the fructose-fed group showed an increase of about 90% in aggregation rates (Figures 3.5 A and B). This observation was in accordance with diminished PDI denitrosation activity and an increase in ROS production. Administration of rosuvastatin to a control group showed an increase in aggregation rates of about ~20% while fructose fed group that received rosuvastatin demonstrated aggregation rates comparable to the control group with the rosuvastatin treatment alone.
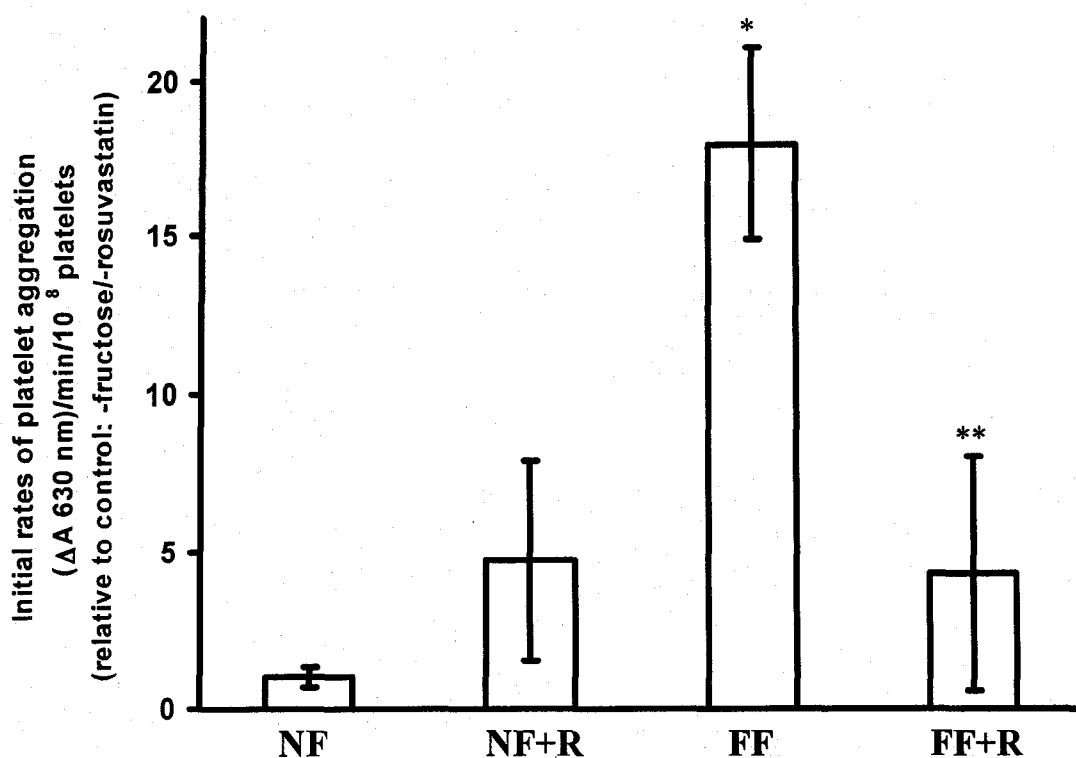
**Figure 3.5: Effects of Fructose feeding and Rosuvastatin administration on Aggregation rates of Syrian hamster platelets**

A. Platelets from four study groups of hamsters were collected and prepared as outlined in Materials and Methods. Aggregation of platelets in Tyrode-albumin solution ($10^8$), was monitored in the absence or presence of 2.5 $\mu$M ADP at 630 nm, over 10 minutes time period. Data shown represents percent difference in aggregation rates with respect to control. n=13 study samples, P<0.005, * with respect to control, ** fructose-fed plus Rosuvastatin with respect to fructose-fed.
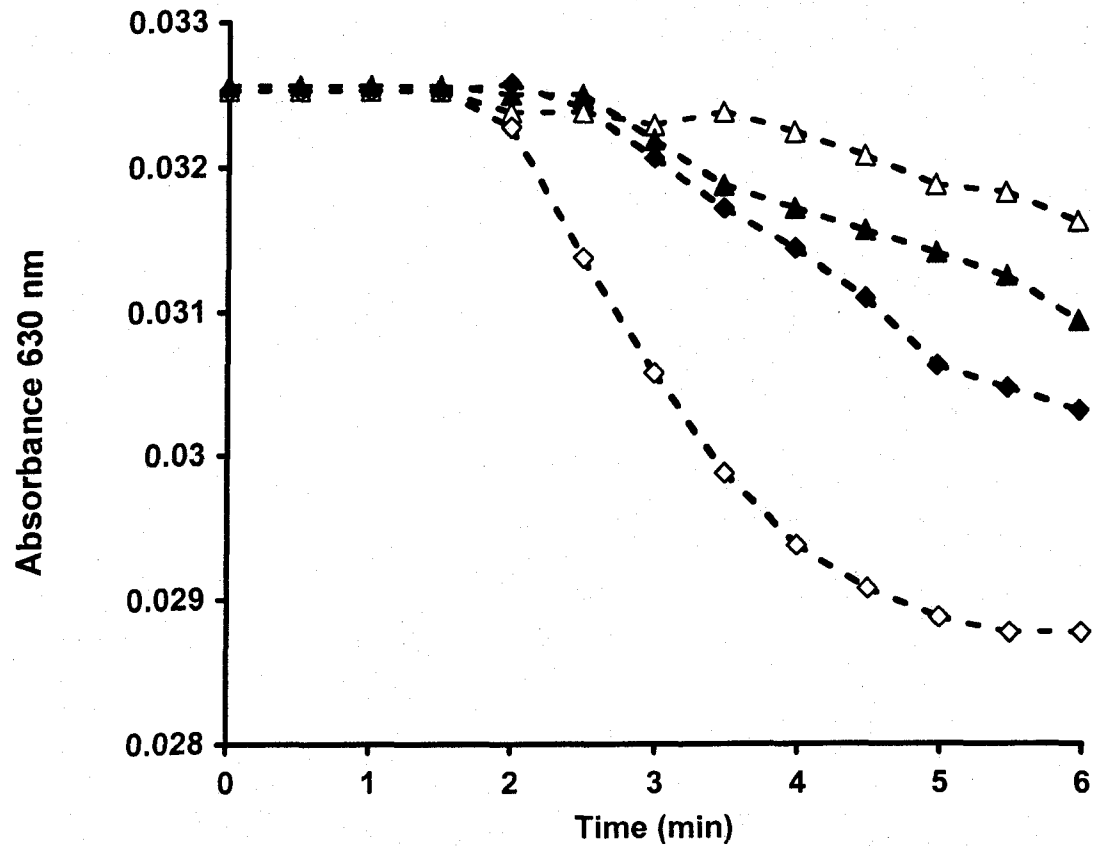
B. Actual traces of the above figure. Water-fed, no Rosuvastatin (white triangles); water fed, 10mg/kg Rosuvastatin (black triangles); fructose-fed, no Rosuvastatin (white diamonds); fructose-fed, 10mg/kg Rosuvastatin (black diamonds).

### 3.4.3 Characteristics of diabetic versus normal human platelets

Cholesterol assay and cGMP assay were used to evaluate the levels of cholesterol and cGMP in diabetic and normal platelets. Cholesterol assay sensitivity was found to range from 1 to 10 $\mu$M (Figure 3.6 A), while the cGMP assay was able to detect levels of 2-512 fmol of cGMP (Figure 3.6 B). Diabetes is often accompanied by increased cholesterol levels, which usually result in a variety of complications.

For this purpose, we used platelets from patients with Type 2 diabetes and from healthy individuals. First, the platelet samples used for membrane cholesterol estimation were exposed to L-NMMA, the inhibitor of nitric oxide synthase, for 5 hours in order to block endogenous NO biosynthesis. Next, these platelets were exposed to SNAP (100 $\mu$M) for 1 hour at 37°C and their intracellular cGMP production was measured. Plasma membrane cholesterol levels of platelets obtained from healthy subjects were ~2 fold lower than T2D (Figure 3.6 C, yellow square). Consequently, the cGMP production yielded ~4-fold decrease in T2D platelets as compared to control (Figure 3.6 C, blue squares).

The chart shows a cholesterol standard curve plotting RFU versus Cholesterol (μM). The linear regression equation is:

$$y = 1.9058x + 1.4581$$
$$R^2 = 0.9957$$
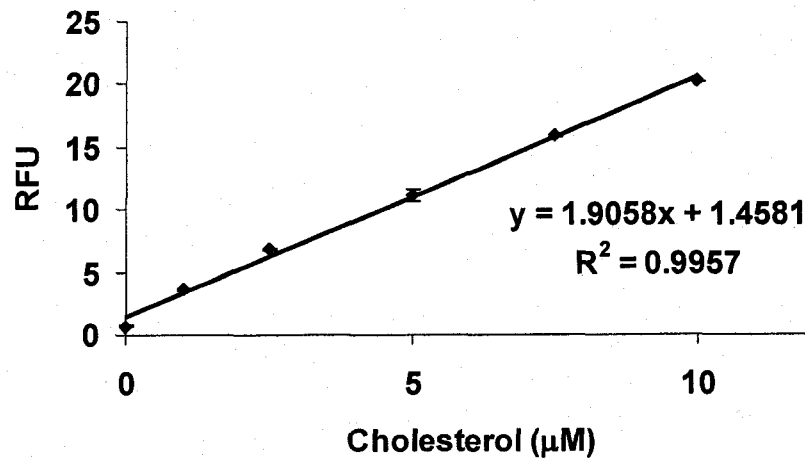
**Figure 3.6: cGMP and cholesterol levels of normal and diabetic patients.**

A. Cholesterol strandard curve with Amplex Red assay. Varying cholesterol concentrations (0-10 μM) were used in order to obtain the cholesterol standard curve as described in "Experimental Methods", which was employed for the estimation of cholesterol levels in normal and diabetic platelets.

$$y = -34.625x + 105.38$$
$$R^2 = 0.9809$$
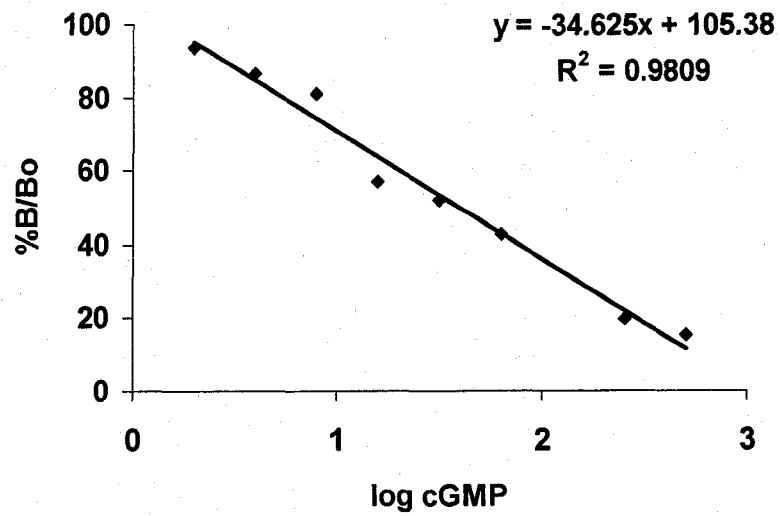
B. cGMP standard curve. cGMP standard curve was obtained using an increasing concentrations of cGMP (2 fmol-512 fmol) as described under "Experimental Methods". The levels of cGMP in diabetic and control platelets were estimated using this curve.
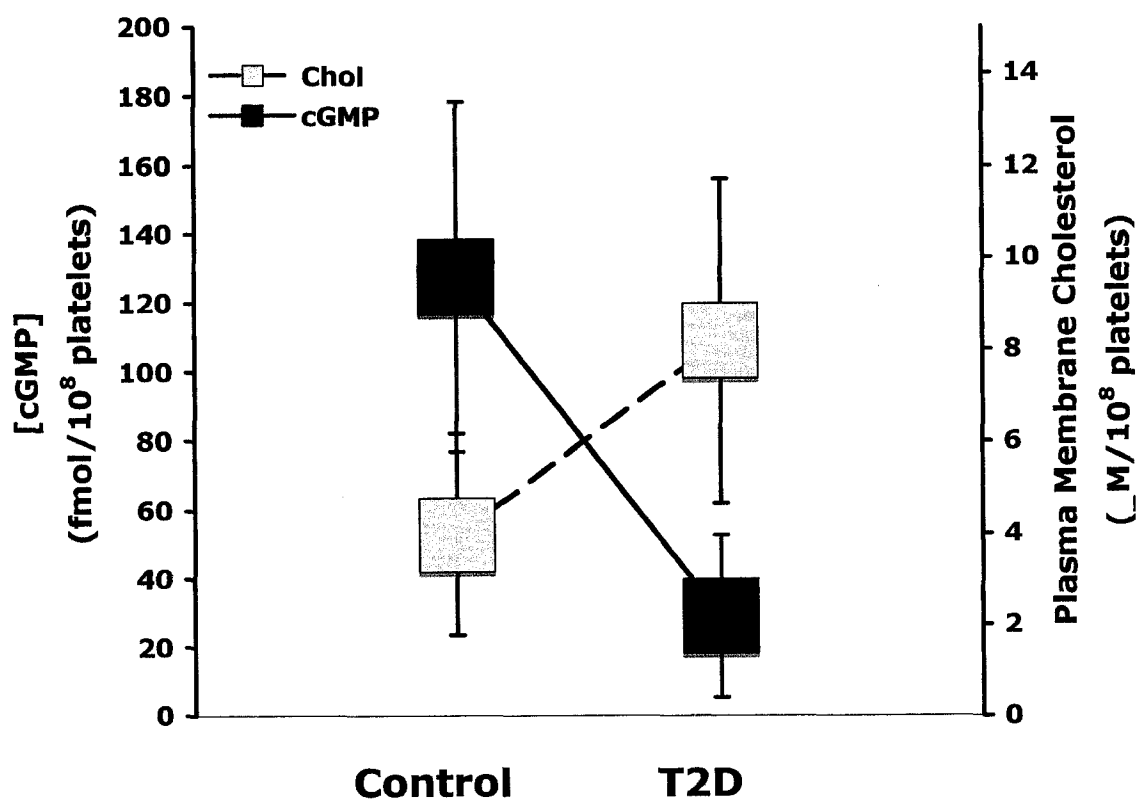
C. cGMP and cholesterol levels from normal and diabetic patients.

Platelets from normal and diabetic patients (n=13) were isolated as described under "Experimental Methods". cGMP assay and cholesterol assay were performed as per manufacturer's instructions. (n=13)

### 3.4.4 Determination of PDI active site redox state

The redox state of PDI active site thiols directs its activity. As seen from the above studies, under different conditions PDI appears to favor denitrosation, where it requires active site to be in its reduced state, or it favors aggregation which involves disulfide exchange and consequently oxidized form of PDI active site thiols, as seen with the pre-diabetic model. Therefore, by monitoring the redox state of PDI active site, it would be possible to establish the parameters for an early detection of a disturbed physiological state. For that purpose, we used the ICAT thiol labeling approach (Figure 3.7 C) coupled to MALDI-TOF to determine different oxidation states of PDI under spontaneous auto-oxidation. We have observed that fully reduced PDI undergoes a self auto-oxidation in a time dependent manner (Figure 3.8). There was a 60% decrease in total thiol concentration observed upon 3 hour incubation of fully reduced PDI at room temperature. In order to determine which of the PDI active site thiols are susceptible to oxidation, a more sensitive approach was utilized.
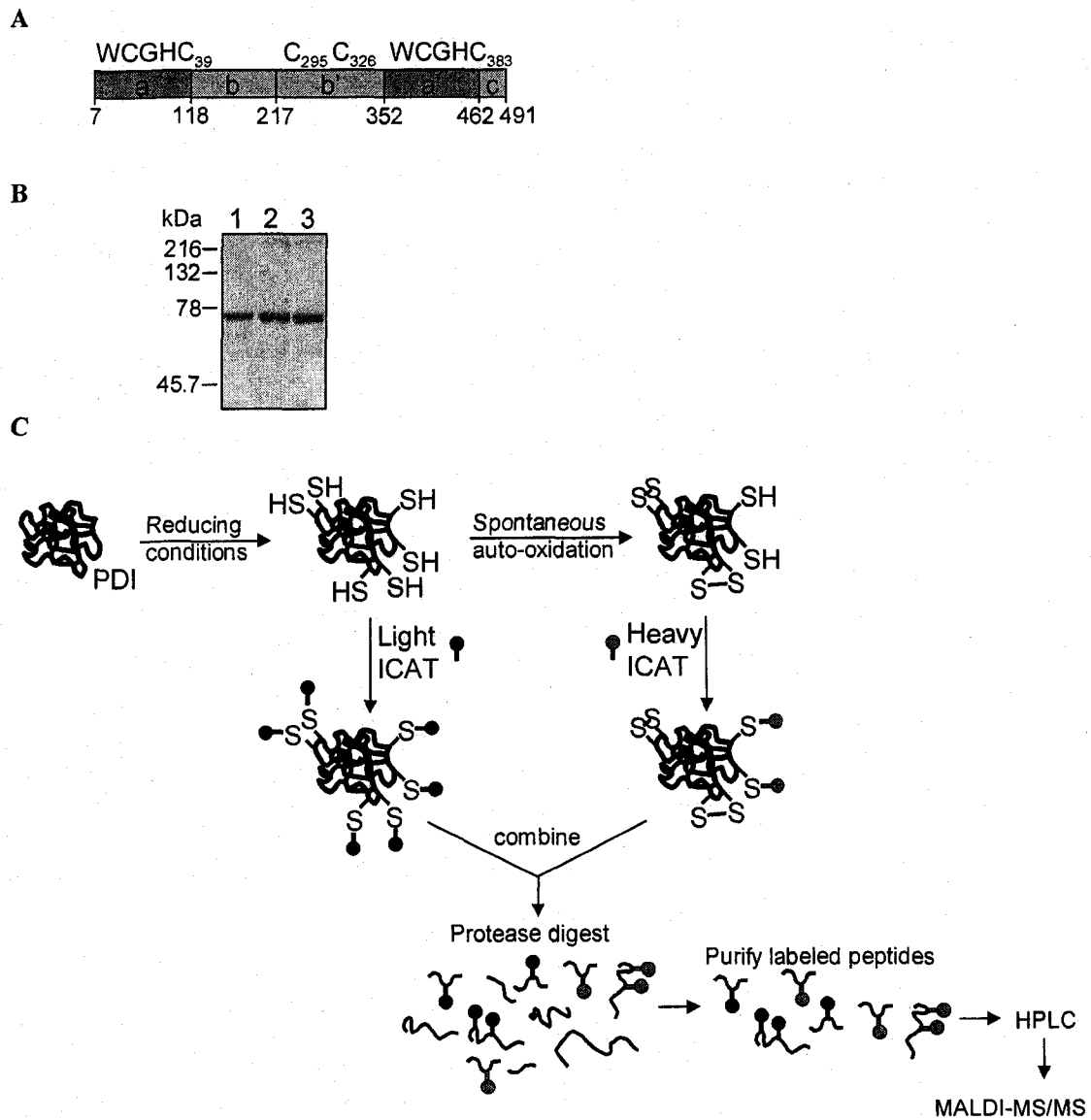
Figure 3.7: Schematic of ICAT strategy. A. A schematic model of domain architecture of human PDI. Position of all six cysteine residues within the human PDI is highlighted. B. PDI was separated using SDS-PAGE (10%) and visualized by Coomassie blue stain. Lane 1 PDI control purchased from Sigma, lane 2 reduced His-PDI, lane 3 auto-oxidized His-PDI. C. Schematic presentation of ICAT labelling protocol.
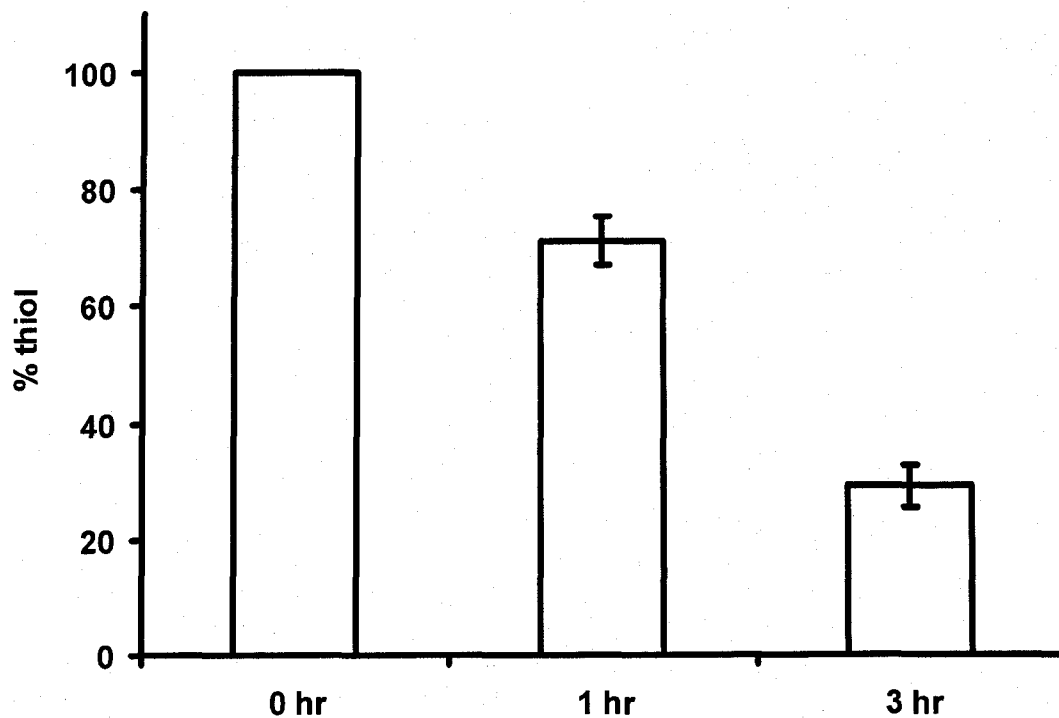
**Figure 3.8: Auto-oxidation of PDI thiols.**

Freshly reduced PDI (1 µM) was incubated with DTNB (1 mM) at zero, 1 and 3 hour

times. After 3 hour incubation, 60% reduction in thiol concentration was observed.

Results are presented as % decrease in thiol concentration with respect to fully reduced

PDI. (n=3)

The ICAT labeling approach was successful in detecting both PDI active site thiols in **a** and **a'** domain (Figure 3.9). Upon labeling the freshly reduced PDI with $^{12}$C-ICAT label, the peak at 2147 m/z was detected which represents the labeling of both cysteines in the active site **a** domain FYAPWC$_{36}$GHC$_{39}$KALAPE. Accordingly, the two cysteines within **a'** domain comprising of sequence FYAPWC$_{380}$GHC$_{383}$KQLAPIWDKLGE were also detected at 2916 m/z (Figure 3.9 A).

Once the labeling parameters were obtained, we sought to determine if this approach could be used for detecting the redox state of PDI under oxidative conditions. As shown in Figure 3.8, PDI undergoes 60% oxidation in 3 hours during the incubation at the room temperature. For that purpose, freshly reduced PDI and auto-oxidized PDI were incubated with $^{12}$C and $^{13}$C- ICAT label respectively, and the oxidation state of active site thiols in **a** domain was analyzed. As seen in Figure 3.9 B, there was a 5 fold decrease in active site thiols observed in the sample that contained auto-oxidized PDI as calculated from the relative intensities of $^{12}$C- and $^{13}$C- labeled peptides which occurred at 2147 and 2165 m/z respectively.

ICAT
FC$_{326}$HRFLE

ICAT
EC$_{295}$PAVRLITLEEE

100
90
80
70
60
50
40
30
20
10
0

% Intensity

1178.82

ICAT
EC$_{295}$PAVRLITLE

1728.99

ICAT
FFLKKEEC$_{295}$PAVRLITLEEE

ICAT  ICAT
FYAPWC$_{36}$GHC$_{39}$KALAPE

2579.25

1470.98

2163.02

ICAT  ICAT
FYAPWC$_{380}$GHC$_{383}$KQLAPIWDKLGE

2147.03
2178.99

2932.22
2916.23
2948.23

1100    1500    1900    2300    2700    3100
Mass (m/z)
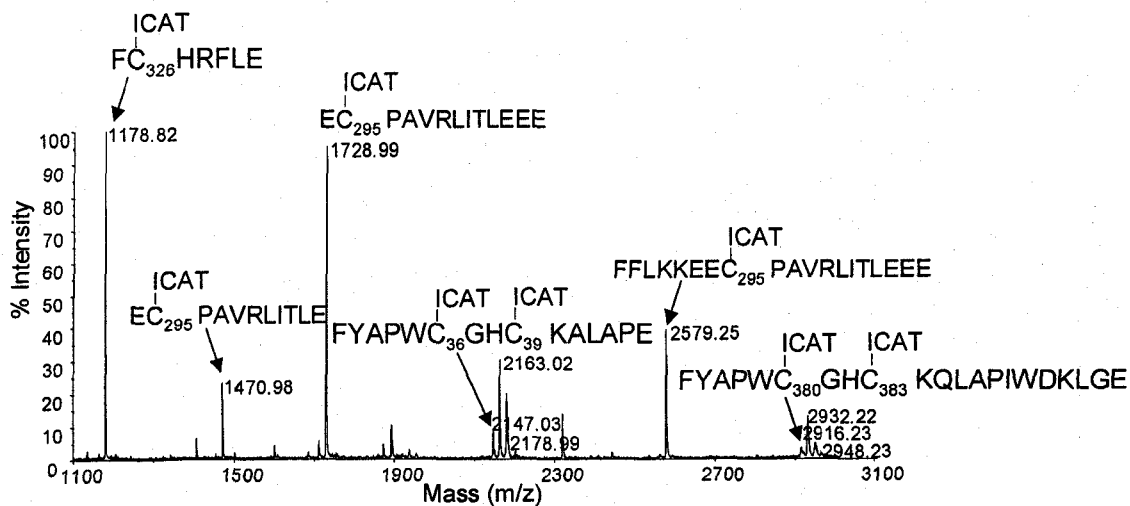
**Figure 3.9: Reduced PDI labelled with light $^{12}$C-ICAT reagent.**

A. Full scan MALDI-TOF spectrum of ICAT-labelled *Glu-C* digested peptides from PDI. All six cysteine residues of PDI were ICAT labelled and detected, the 2147 m/z fragment corresponds to the *a* domain active site with both Cys residues ICAT labelled, 2916 m/z fragment corresponds to the *a'* domain active site with both Cys residues ICAT labelled, fragment at 1178 m/z corresponds to the Cys326 present in the *b'* domain and fragments at 1470 m/z, 1728 m/z and 2579 m/z present various mis-cleavages of the sequence containing Cys295.
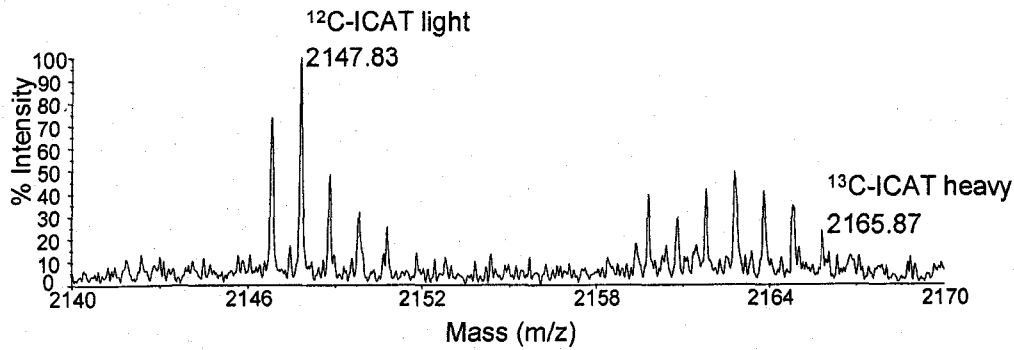
B. MALDI-TOF quantification of reduced (light ^{12}C-ICAT-labelled) and auto-oxidized (heavy ^{13}C-ICAT-labelled) PDI following the reverse-phase nano-LC separation. Modified peptides corresponding to the **a** domain active site were detected for reduced PDI at L (light ICAT label): 2147 m/z and auto-oxidized PDI at H (heavy ICAT label): 2165 m/z.

## 3.5 Discussion

The initial results of this study are in agreement previous findings that platelets are able to metabolize GSNO (Shah *et al.*, 2003). However, we have shown that platelet ability of GSNO consumption is due to psPDI. The kinetic study demonstrated that the denitrosation activity of platelets follows the saturation kinetics which is indicative of an enzyme-mediated process (Figure 3.1 A and B). The participation of PDI was established with the use of anti-PDI antibodies and it was observed that platelet denitrosation activity was diminished by 80% as compared to the sample without anti-PDI antibodies (Figure 3.2). It was previously established the product of RSNO denitrosation, nitric oxide, prevents platelet aggregation through a GC/G kinase dependent process (Wang *et al.*, 1998). In this pathway, •NO stimulates soluble guanylate cyclase resulting in an increase in cGMP that activates G kinase (GK). Activation of GK leads to the phosphorylation of thromboxane $A_2$ receptor preventing the coupling of the receptor to GTP-binding protein thus inhibiting the activation of phospholiapse C, which results in prevention of cellular activation.

Our study suggests another possibility for •NO-mediated inhibition of platelet activation. PDI active site thiols are required for ligand-integrin interaction which leads to the platelet aggregation. Therefore, by altering the availability of PDI active site thiols, platelet aggregation could be prevented. We are proposing that in the presence of RSNO, platelet surface PDI has its active site thiols occupied by performing its denitrosation activity thus inhibiting platelet aggregation (Root *et al.*, 2004).

After the initial parameters for platelet surface PDI-mediated GSNO denitrosation were obtained, the next step was to establish the relationship of platelet surface PDI under diseased conditions, such as Type 2 Diabetes (T2D). Previous studies have shown that platelets of T2D patients contain elevated levels of ROS thus promoting their hyperaggregability (Gregg et al., 2004; Redondo et al., 2005). The present study was initiated due to previous observations in our lab that diabetics and an animal model of pre-diabetes show a decrease in platelet surface PDI denitrosation activity and concomitant increase in the generation of reactive ROS (Root PhD Thesis, 2004). Therefore, the hypothesis derived from these independent studies is that the high levels of ROS in diabetic platelets could contribute to the oxidation of PDI active site thiols thus diminishing its RSNO reductase activity and promoting platelet aggregation.

Rosuvastatin belongs to a group of drugs that inhibit the rate-limiting conversion of hydroxymethylglutaryl CoA to mevalonate which is required for the biosynthesis of isoprenoids that in turn play a role in assembly of NADPH oxidase subunits responsible for ROS production. It was of a great interest to determine the effects of rosuvastatin administration to a pre-diabetic animal model in terms of PDI denitrosation activity and levels of ROS. Pre-diabetic animal model of T2D using the Syrian Golden hamster was previously shown to develop insulin resistance upon fructose feeding of hamsters for 2-3 weeks (Taghibiglou et al., 2002).

In agreement with previous observations, our data demonstrated a significant decrease in PDI denitrosation activity by ~42% upon fructose feeding as compared to the control

(Figure 3.4 A), and a concomitant increase of 60% in ROS production (Figure 3.4 B). Also, the aggregation rates of fructose fed animals displayed a 90% increase relative to the control. Therefore, our results suggest that increased ROS levels could potentially be responsible for the oxidation of PDI active site thiols resulting in diminished GSNO denitrosation accompanied by a concomitant increase in platelet aggregation rates.

The next aim of this study was to establish the effects of short-term rosuvastatin treatment on the platelet parameters tested in this study. As shown in Figure 3.4 B, rosuvastatin did not affect the levels of ROS when administered to the control group. Interestingly, the fructose fed group that received a drug treatment attenuated the generation of ROS to the control levels. As for the platelet surface PDI, rosuvastatin treatment to the control group of hamsters decreased PDI denitrosation activity by ~20% (Figure 3.4 A). Previous studies from our lab provided evidence that the interaction of PDI with the platelet plasma membrane is likely mediated by hydrophobic interactions, rather than electrostatic interactions as previously reported (Raturi PhD Thesis, 2007). Therefore, it could be possible that the lowering of cholesterol by rosuvastatin alters the hydrophobic character of the platelet plasma membrane in control animals, thus diminishing the abundance of the bound enzyme which would account for this ~20% loss in denitrosation activity. However, treatment of fructose-fed animals with rosuvastatin resulted in restoration of psPDI denitrosation activity. Therefore, these results suggest that rosuvastatin at nM $C_p$ is effective in decreasing the levels of ROS in platelets, resulting in improved psPDI-catalyzed release of sufficient •NO from GSNO to inhibit platelet aggregation. This can be observed from aggregation studies (Figure 3.5 A and B)

in which rosuvastatin treatment slightly decreased aggregation rates of control animals (~20%) and significantly decreased the initial rates of fructose fed animals (~50%). Therefore, the overall significance of this study is that rosuvastatin treatment of pre-diabetic animal model not only contributes to the normalization of platelet ROS production and psPDI activities but also improves normal platelet aggregability.

As an extension of the above study, we wanted to determine if the platelet plasma membrane cholesterol affects the NO-signaling. T2D is often accompanied with hypercholesterolemia (Smith, 2007). The recent observations from our lab suggested that NO-diffusion in platelets is blocked by the presence of increased levels of plasma membrane cholesterol. We sought to establish the relationship of plasma membrane cholesterol and NO-signaling via cGMP pathway in T2D and healthy subjects. As previously observed, T2D platelets had ~2-fold higher membrane cholesterol levels as the control. Upon probing the same platelet sample for exogenous NO-induced cGMP production, T2D platelets displayed a ~4-fold decrease relative to the healthy platelets. The data obtained in the course of this study support the proposed hypothesis that increased levels of membrane cholesterol may affect the intracellular NO-signaling.

The results obtained in the course of this study emphasize the importance of redox state of PDI active site thiols in mediating different enzymatic activities. For example, we have shown that in the presence of highly oxidizing conditions such as high ROS, PDI favors platelet aggregation and consequently shows a decrease in metabolizing GSNO. Therefore, it was of great interest to establish a method for detecting the dynamic state of

PDI active site thiols, which could potentially be used as a tool to monitor changes of individual cysteine residues under various conditions such as T2D. This study was initiated by our previous observations that fully reduced PDI undergoes auto-oxidation by incubation at the room temperature (Figure 3.8). In order to find out which cysteines undergo oxidation, ICAT-MALDI technology was employed. First of all, we wanted to determine both active site cysteines could be labeled with ICAT. Incubation of freshly reduced PDI with $^{12}$C ICAT label and peaks at 2147 m/z and 2916 m/z were detected representing the labeling of the active site thiols in a and a' domain respectively (Figure 3.9 A). Next, in order to determine the auto-oxidation of PDI active site thiols, freshly reduced PDI and auto-oxidized PDI were labeled with $^{12}$C and $^{13}$C ICAT respectively, as shown in Figure 3.7 C. Under our experimental conditions, we were able to detect a 5-fold decrease upon auto-oxidation of active site thiols of PDI a domain. On the contrary, detection of a' domain active site thiols under auto-oxidation conditions was unsuccessful. This could be due to the fact that the active site in a' domain is more prone to oxidation than a domain active site (Lyles and Gilbert, 1994). Overall, this approach could still be used for determining the specific redox states of PDI in response to different environmental stimuli as well as specific physiological conditions such as T2D.

# CHAPTER 4

# The Role of Protein Disulfide Isomerase in Nitric Oxide

# Transport in Red Blood Cells

## 4.1 Introduction

Nitric oxide (•NO) is the potent regulator of the vascular tone through the induction of vasodilation that enhances blood flow. Previous studies by Stamler and coworkers (Stamler *et al.*, 1992) suggested that S-nitroso albumin is the major carrier of •NO in blood that in turn can stimulate vasodilation transduced by the small mass S-nitrosothiols such as S-nitrosoglutathione (GSNO) with which it exists in equilibrium (Gaston *et al.*, 1993). Supporting this hypothesis, S-nitrosated form of hemoglobin (Jia *et al.*, 1996) and membrane-associated band 3 protein (AE1) (Pawloski *et al.*, 2001) have been detected. Therefore, the S-nitrosation mechanism of red blood cell proteins and pathways of •NO influx and efflux therein are of great interest to current research.

### 4.1.1 Red Blood Cells

Human red blood cells (RBCs) are produced by the red bone marrow by the process called erythropoiesis and are anucleated cells when mature. The formation of RBCs is regulated by the glycoprotein hormone erythropoietin. RBCs resemble biconcave disks with a flattened region in the center and dumb-bell shaped cross section, with an average size of 6-8 μm.

The main function of RBCs is to carry oxygen throughout the body from the lungs. This is achieved with the help of protein hemoglobin (Hb). Hb exists as a tetramer formed from two α and two β subunits and contains four heme groups responsible for oxygen binding. The iron(II)-dioxygen bond is an essential component of transport and storage

of molecular oxygen by Hb. The oxygen is bound by the ferrous form of heme through the following functional cycle (Shikama and Matsuoka, 2003).

$$\text{Deoxy-Fe(II)} + O_2 \xrightleftharpoons{\text{oxygenation}} \text{Fe(II)}O_2$$

reduction (arrow) autoxidation

$$\text{Met-Fe(III)} + O_2^-$$
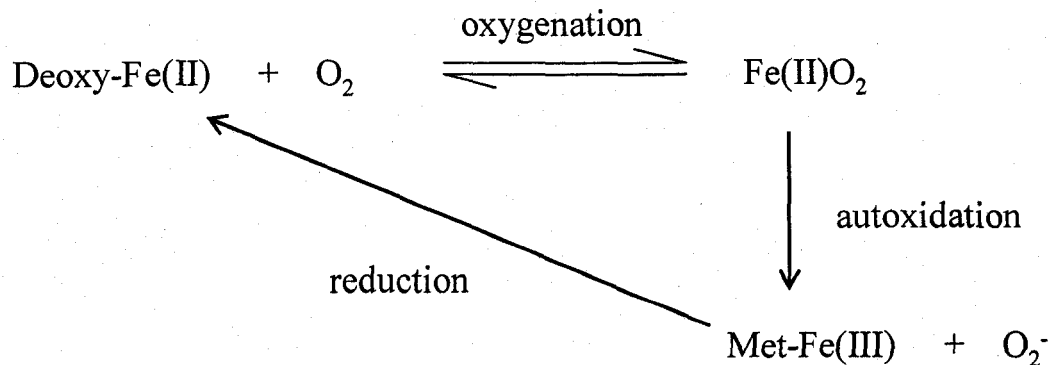
**Scheme 4.1: Oxygen binding in hemoglobin**

Basically, the autoxidation reaction takes place during reversible oxygen binding to deoxy-iron(II) to form oxygenated form of Hb $Fe(II)O_2$ resulting in the generation of met-Hb and superoxide anion. Ferric iron in met-Hb can not bind molecular oxygen and is physiologically inactive. However, RBCs contain an NADH-cytochrome $b_5$ oxidoreductase known as methemoglobin reductase (Yubisui *et al.*, 1986) which is responsible for met-hemoglobin reduction to the ferrous deoxy form. A recent study by Shikama and Matsuoka showed that the interaction of different subunits of Hb result in different oxygen binding functions (Shikama and Matsouka, 2003). The $\alpha1\beta2$ or $\alpha2\beta1$ interaction results in the cooperative oxygen binding, while the $\alpha1\beta1$ or $\alpha2\beta2$ interaction leads to the stable binding of oxygen with iron(II).

### 4.1.2 Ghosts

RBC ghosts are post-hemolytic residues that lack the intracellular elements and are mainly made up of the cell membrane. Depending on the hemolysis method used, there are two types of hypotonic ghosts, resealed ghosts and white ghosts. Resealed ghosts are generally used for incorporation of the solution of interest inside ghosts by a special resealing process. This enables studying the transport processes from the extracellular medium to the cell interior and structural organization of RBC membranes. Resealed ghosts generally have high hemoglobin content since the emphasis is placed on the restoration of the original membrane structure, rather than the purity. White ghosts are usually free from the visible hemoglobin contamination and lack the intracellular content and are widely used for studying the enzymatic properties of the cell membrane (Schwoch and Passow, 1973).

The first report of the presence of protein disulfide isomerase (PDI) in ghosts came from the study of Alloisio and coworkers (Alloisio *et al.*, 1994). They used western blot studies in combination with microscopic studies to identify several residents of the endoplasmic reticulum-resident (ER) proteins amongst which were glucose-regulated protein GRP78, calreticulin and PDI.

### 4.1.3 Nitric oxide in Blood

•NO is the important regulator of various physiological conditions (Chapter 1, 1.3). Interaction of •NO with specific proteins is essential for the regulation of platelet aggregation and vascular smooth muscle relaxation (Hobbs and Ignarro, 1996). The best

characterized example is the interaction of •NO with the heme moiety of soluble guanylate cyclase resulting in its activation and subsequent generation of cGMP (Hobbs, 1997). In blood, the most physiological example of •NO interaction with a metal containing protein is the NO-hemoglobin interaction. •NO can react with ferrous heme or with oxy-hemoglobin as follows (Xu *et al.*, 2003):

$$Fe(II) + NO \rightarrow Fe(II)NO \qquad (1)$$

$$Fe(II)O_2 + NO \rightarrow Fe(III) + NO_3^- \qquad (2)$$

Equation 1 represents the interaction between ferrous iron and •NO that results in the formation of nitrosyl-heme with the rate constant of 2.6 x $10^7$ $M^{-1}s^{-1}$ (Cassoly and Gibson, 1975). Equation 2 shows interaction of oxy-Hb with •NO resulting in the generation of ferric heme and nitrate with the rate constant of 6-9 x $10^7$ $M^{-1}s^{-1}$ (Eich *et al.*, 1996; Herold *et al.*, 2001). For NO to function, it must be in its free form, meaning not bound as it is in nitrosyl-heme. Considering very high hemoglobin concentration (~20 mM) it is very difficult to understand how NO can be available to initiate the vascular smooth muscle relaxation (Lancaster, 1994), since Hb present in the blood would act as a sink for NO available in the environment.

One possibility for solving the puzzle of NO availability in RBCs came from the study of Jia and coworkers (Jia *et al.*, 1996) which identified the existence of S-nitrosated Hb at its β-93 cysteine residue. They proposed that Hb could participate in NO transport along with oxygen transport. The main reason for this hypothesis came from the observations

that S-nitrosation of Hb favors the R-state (high oxygen affinity form), while iron nitrosylation favors T-state (low oxygen affinity). It has been also observed that the intramolecular transfer between HbSNO and HbFe(II)NO is mediated through the oxygen saturation-dependent conformational changes (Jia *et al.*, 1996; Stamler *et al.*, 1997; McMahon *et al.*, 2002). Therefore, this model allows the NO captured by the heme as in equation 1, to be preserved through the formation of HbSNO, by the reaction involving intracellular glutathione (McMahon *et al.*, 2000). The delivery of Hb-bound NO is believed to occur through the allosteric regulation by decreasing oxygen saturation, which would favor transnitrosation reaction from Hb-SNO to other intracellular thiol proteins such as anion exchange protein AE1 (Pawloski et al., 2001).

However, study by Xu and coworkers (Xu *et al.*, 2003) used the whole blood, washed RBCs and Hb to investigate the intramolecular transfer to NO from heme to $\beta$-93 cys and vice versa, under various oxygen tensions and found no evidence to support the proposed mechanism. Therefore, the question of NO transport and availability in RBCs still remains unsolved.

Here we investigated the possibility of ghost membrane-associated PDI playing a role in NO-efflux from RBCs.

## 4.2 Materials and Equipment

### 4.2.1 Materials

Acetone;                                   Sigma-Aldrich Canada Ltd., Oakville, Ontario

Ammonium persulfate;                       Sigma-Aldrich Canada Ltd., Oakville, Ontario

Ammonium sulfamate;                        Sigma-Aldrich Canada Ltd., Oakville, Ontario

Biorad Bradford Reagent;                   Bio-Rad Laboratories Ltd., Mississauga, Ontario

Bovine Serum Albumin;                      Sigma-Aldrich Canada Ltd., Oakville, Ontario

DEAE-Sephacel;                             Sigma-Aldrich Canada Ltd., Oakville, Ontario

Diethylamine NONOate (DEANO);             Sigma-Aldrich Canada Ltd., Oakville, Ontario

Dimethyl formamide (DMF);                  Sigma-Aldrich Canada Ltd., Oakville, Ontario

5, 5'-dithiobis(2-nitrobenzoic) acid;      Sigma-Aldrich Canada Ltd., Oakville, Ontario

Dithiothreitol (DTT);                      Sigma-Aldrich Canada Ltd., Oakville, Ontario

Eosin isothiocyanate;                      Sigma-Aldrich Canada Ltd., Oakville, Ontario

Ethylene diamine tetraacetic acid;         Sigma-Aldrich Canada Ltd., Oakville, Ontario

Hemoglobin;                                Sigma-Aldrich Canada Ltd., Oakville, Ontario

Monoclonal anti-PDI antibody RL90;         Abcam USA, Cambridge, MA

Oxidized glutathione;                      Sigma-Aldrich Canada Ltd., Oakville, Ontario

Phenylarsine oxide;                        Sigma-Aldrich Canada Ltd., Oakville, Ontario

Potassium phosphate;                       Sigma-Aldrich Canada Ltd., Oakville, Ontario

Reduced glutathione;                       Sigma-Aldrich Canada Ltd., Oakville, Ontario

Sephadex G-25;                             Sigma-Aldrich Canada Ltd., Oakville, Ontario

Sodium chloride;                           Sigma-Aldrich Canada Ltd., Oakville, Ontario

Sodium hydroxide;                    Sigma-Aldrich Canada Ltd., Oakville, Ontario

Sodium nitrite;                      Sigma-Aldrich Canada Ltd., Oakville, Ontario

Sodium phosphate monobasic:          Sigma-Aldrich Canada Ltd., Oakville, Ontario

Sodium phosphate dibasic;            Sigma-Aldrich Canada Ltd., Oakville, Ontario

TEMED;                               Bio-Rad Laboratories Ltd., Mississauga, Ontario


## 4.2.2  Equipment

Agilent 8453 UV-VIS spectrophotometer;

> (Agilent Technologie Canada Inc, Mississauga, Ontario)

Beckman J2-HS Centrifuge;

> (Beckman Coulter Canada Inc., Mississauga, Ontario)

BioRad Fraction Collector Model 2110;

> (Bio-Rad Laboratories Ltd., Mississauga, Ontario)

ISO-NO Mark II with WPI MKII Nitric Oxide electrode;

> (World Precision Instruments Inc., Sarasota, Florida)

Jouan CR3i Centrifuge;

> (Jouan Inc, Winchester, Virginia)

Labconco FreeZone 4.5 Liter Benchtop Freeze Dry Systems;

> (Labconco Corporation, Kansas City, Missouri)

Mettler AJ100 Balance;

> (Mettler Toledo Canada, Mississauga, Ontario)

Microtiter 96-well Solid Plate;

> (Thermo Electron Corp. Canada, Burlington, Ontario)

Mini-Protein II Gel Electrophoresis System;

(Bio-Rad Laboratories Ltd., Mississauga, Ontario)

Orion Model 420A pH Meter;

(Thermo Electron Corp. Canada, Burlington, Ontario)

Stir Plate 360 Series;

(VWR International, Mississauga, Ontario)

Varian Eclipse Fluorescence Spectrophotometer;

(Varian Canada, Mississauga, Ontario)

## 4.3 Experimental Methods

### 4.3.1 Preparation of Washed Ghosts

Washed ghost were prepared as described by Dodge and coworkers (Dodge *et al.*, 1963). Briefly, the whole blood was drawn into ACD buffer at 6:1 ratio and centrifuged at 190 x g for 15 minutes in order to separate RBCs from plasma and the buffy coat. RBC were subsequently washed 3 times in isotonic phosphate buffer (155 mM $NaH_2PO_4$ and 100 mM $Na_2HPO_4$, pH 7.4), and made up as a 50% cell suspension. This 50% cell suspension is further diluted 1:10 with isotonic phosphate buffer and stored on ice for 20 minutes. Sedimentation of RBCs was performed by centrifugation at 4000 x g for 20 minutes at 4°C, after which a supernatant was removed and sedimented RBCs were hemolysed by resuspending the cells 1:15 in hypotonic phosphate buffer (10 mM $NaH_2PO_4$ and 6 mM $Na_2HPO_4$, pH 7.4). Lysed RBCs were left on ice for 30 minutes and the ghosts were sedimented by centrifugation at 20 000 x g for 40 minutes at 4°C. Hemoglobin was removed by excessive washes in hypotonic buffer. Once prepared, ghosts were stored at 4°C and used within two days.

The presence of PDI in ghosts was determined by western blotting using RL90 PDI antibodies raised in mouse, and goat anti-mouse-HRP secondary antibodies. The visualization was performed using a chemiluminescent HRP substrate.

## 4.3.2 Purification of PDI from RBC lysates

PDI was purified from the whole blood using a modified protocol by Hillson (Hillson *et al.*, 1984). Whole blood was centrifuged at 190 x g for 15 minutes in order to remove plasma and the buffy coat, and subsequently washed 3 times using isotonic phosphate buffer. Following the last centrifugation, RBCs were lysed in an ice cold hypotonic buffer and centrifuged at 17 000 x g for 45 minutes at 4°C. The resulting supernatant was placed in a water bath and the temperature of the lysate was allowed to reach 54°C, where it was maintained for 15 minutes. The heat treated lysate was placed on ice to cool and centrifuged at 17 000 x g for 45 minutes at 4°C. PDI was further purified by two ammonium sulfate precipitations of 55% (35 g ammonium sulfate/100 mL) and 85% (23 g ammonium sulfate/100 mL). The final pellet obtained after centrifugation at 17 000 x g for 30 minutes was dissolved in ~20 mL of 20 mM sodium phosphate buffer, pH 6.3, and subsequently dialysed overnight against the same buffer. The dialysed sample was loaded onto DEAE-Sephacel column (35 cm x 2 cm) equilibrated with 20 mM sodium phosphate buffer, pH 6.3. Bound proteins were eluted using a linear gradient of 0 to 0.7 M NaCl with a flow rate of 2 mL/min created using a BioRad Biologic Work Station, and collected in 2 mL fractions. Collected fractions were tested for PDI activity using a modified insulin turbidity assay (Holmgren, 1979). 20 µL of each fraction was placed in the 96 well plate with 100 µM insulin and 200 µM DTT in the PDI assay buffer, and the increase in turbidity, due to the enzymatic cleavage of insulin, was monitored at 630 nm. The purity of the enzyme was assessed by SDS-PAGE and western blotting.

### 4.3.3 Synthesis of S-nitroglutathione

S-nitrosoglutathione was prepared as described in Chapter 2.

### 4.3.4 Synthesis of Dieosin-GSSG

Synthesis of dieosin-GSSG was performed as described in Raturi and Mutus (Raturi and Mutus, 2007). Briefly, synthesis was carried out by incubating GSSG with 10-fold molar excess of eosin isothiocyanate in phosphate buffer (100 mM sodium phosphate and 2 mM EDTA, pH 8.5) at the room temperature for 6 hours. Unreacted eosin was separated by Sephadex G-25 column chromatography. The collected aliquots were tested for the maximum increase in fluorescence at 545 nm ($\lambda_{ex}$ 525 nm) by the addition of DTT (10 mM), which cleaves the disulfide bond of GSSG thus releasing two GSH molecules with eosin attached at the amino terminus resulting in fluorescence increase. Aliquots showing a maximum fold increase were pooled together and stored at -80°C. The purity of the product was determined by the thin layer chromatography (TLC) in a methanol-acetone solvent system (30:70).

### 4.3.5 Kinetics of Ghost-Dependent Disulfide Reduction

Ghosts (20 μL from 4 mg/mL of protein) were added to the hypotonic phosphate buffer containing 2 μM DTT and varying concentrations of dieosin-GSSG (0-2000 nM). Increase in fluorescence at 545 nm ($\lambda_{ex}$ 525 nm), as a result of disulfide bond cleavage of GSSG due to the presence of ghosts was monitored as a function of time. Control experiment was performed in the absence of ghosts. The actual rate of dieosin-GSSG cleavage by ghosts was obtained by subtracting the samples containing ghosts from their

corresponding controls. All experiments involving disulfide reductase activity were performed using 96-well fluorescent plate reader.

### 4.3.6 Inhibition of Ghost Disulfide Reductase Activity

Inhibition of the ghosts-dependent disulfide reduction was performed with the use of phenylarsine oxide (PAO), which specifically binds to the vicinal thiols (Donoghue *et al.*, 2000). PAO (200 $\mu$M) was incubated with ghosts for 30 minutes at the room temperature, and the disulfide reductase assay was performed as described in 4.3.5.

The ghost-mediated disulfide-reductase activity was also monitored in the presence of NO donors, GSNO and DEA-NO (25-1000 $\mu$M). Previous studies have shown that GSNO may S-nitrosate protein thiols through transnitrosation, while DEA-NO spontaneously releases NO with a half life of about 2 minutes (Keefer *et al.*, 1996). The control did not contain any ghosts. The final rates of disulfide reductase activity were obtained by correcting for the corresponding control and are represented as the relative fluorescence units with respect to time.

### 4.3.7 Quantification of Thiols

The total thiol concentration of the ghost suspension was determined with DTNB assay. Briefly, the ghost aliquot was incubated with DTNB (1 mM) for 15 minutes at the room temperature, followed by the spectrophotometric analysis of characteristic peak which develops at 412 nm, due to the formation of nitrothiobenzoate which occurs during cleavage of DTNB by thiols. Thiol concentration of ghosts was measured in the presence

of increasing GSNO or DEA-NO concentration (25-2500 μM), with corresponding control which did not contain ghost suspension.

### 4.3.8 Monitoring Nitric Oxide Release

Ghosts in 1 mL suspension (4 mg/mL of protein) were incubated with DEA-NO (1 mM) for 1 hour at the room temperature. The ghost suspension was then centrifuged at 15 000 x g for 10 minutes, followed by 2 washes in hypotonic phosphate buffer to remove degradation products of DEA-NO. The pellet obtained after the last centrifugation was resuspended in hypotonic phosphate buffer, placed in the vial containing a Clark type NO electrode operated though the Apollo 4000 free radical analyzer, and the current was monitored for 60 seconds in order to obtain a stable signal. At this time, $HgCl_2$ (100 μM) was added to initiate NO release, and the signal was monitored until saturation was established. Control sample of ghosts did not receive DEA-NO treatment.

### 4.3.9 Biotin Switch Assay

The biotin switch assay was performed as described by Zhang and coworkers (Zhang *et al.*, 2005), with minor modifications. Ghosts (4 mg/mL of protein) were incubated with GSNO or DEA-NO (1 mM) for 1 hour at the room temperature. Next, N-ethyl maleimide (NEM, 50 mM) was added in order to block any free thiols and incubated at 50°C for 30 minutes. To remove NEM, the ghosts were washed with pre-chilled (-20°C) ethanol, incubated at -20°C for 1 hour and centrifuged at 10 000 x g for 10 minutes. The supernatant was removed and the pellet was resuspended in the hypotonic phosphate buffer. Ascorbate (1 mM) and biotin-NEM (1 mM) were added to the suspension and

further incubated for 2 hours at the room temperature in dark. Following the incubation, the ghosts were precipitated with pre-chilled ethanol to remove excess ascorbate and biotin-NEM and resuspended in hypotonic phosphate buffer.

After biotinylation, the samples were mixed with native loading dye and proteins were separated by SDS-PAGE (10%) and transferred to a nitrocellulose membrane. Blots were developed with strepavidin-HRP (1/100 000 dilution) and with monoclonal RL90 anti-PDI antibodies (1/10 000 dilution) using goat-anti mouse HRP as the secondary antibody.

**4.4 Results**

**4.4.1   Protein Disulfide Isomerase Associated with RBC ghosts**

First, we wanted to detect the presence of PDI in RBC ghosts. Prepared ghosts were subjected to extensive washing in hypotonic phosphate buffer, followed by centrifugation in order to separate soluble proteins from membrane fraction. As seen from Figure 4.1, PDI was detected by western blotting in the supernatant and membrane fraction of ghosts (lane 1 and 2). Next, we wanted to determine if PDI was also present in RBC lysates and for that purpose, the purification procedure was performed as described in "Experimental Methods". Western blot showed a PDI-reactive band corresponding to the band observed with recombinant human PDI (Figure 4.1, lane 4 and 5 respectively).

Once the presence of PDI was established, PDI activity assays were performed as described below.
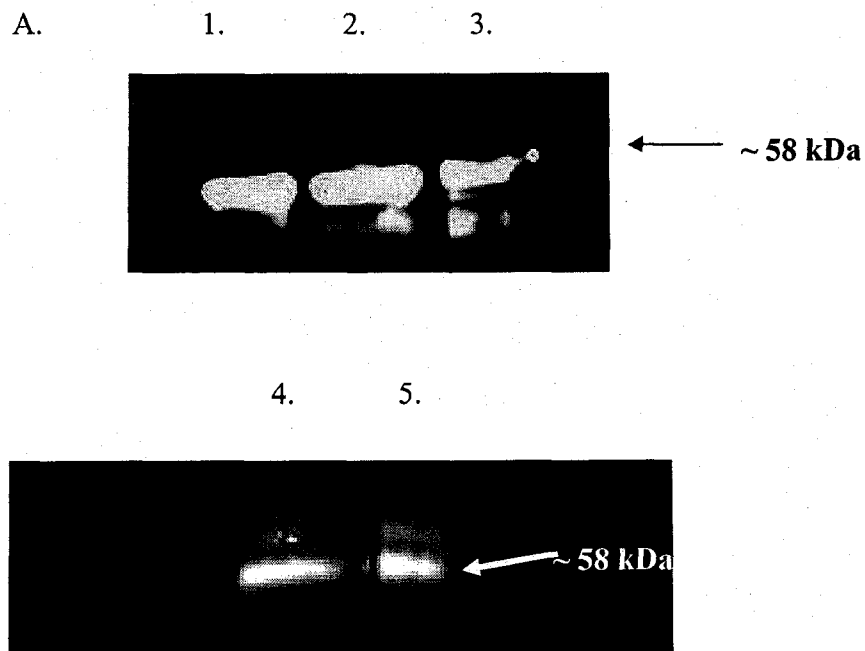
**Figure 4.1: Detection of ghost associated PDI by western blotting**

Western blot of 20 μL of ghosts shows an anti-PDI reactive band at ~58 kDa. Lane assignment: 1. 20 μL of ghost pellet; 2. 20 μL of ghost supernatant; 3. recombinant human PDI (50 ng); 4. 20 μL of purified PDI from RBC lysates. 5. recombinant human PDI (50 ng) (n=3).

### 4.4.2  Disulfide Reductase Activity of Ghosts

The assay used for studying disulfide reductase activity of ghosts employed dieosin-GSSG. Dieosin-GSSG has fluorescent moieties covalently attached to the two N-terminal GSSG residues that results in fluorescence self-quenching and relatively low initial fluorescence. However, upon addition of reducing agent such as DTT or in the presence of PDI, the disulfide bond of GSSG is cleaved thus resulting in an increase in fluorescence (Raturi and Mutus, 2007).

Due to its high sensitivity, this assay was used here for monitoring ghost-associated PDI disulfide reductase activity. To this end, increasing concentrations of dieosin-GSSG (25-2000 nM) were added to 96-well plate containing 20 μL of ghost suspension with 2 μM DTT to a final volume of 100 μL. As Figure 4.2 A shows, there was a continuous increase in fluorescence observed with increasing concentration of substrate over time. Tha initial rates, subtracted for the corresponding blanks which did not contain ghosts, were plotted over increasing dieosin-GSSG concentrations (Figure 4.2 B) and the saturation curve reflected the enzyme mediated disulfide reductase activity with a estimated $K_M$ of ~550 nM.
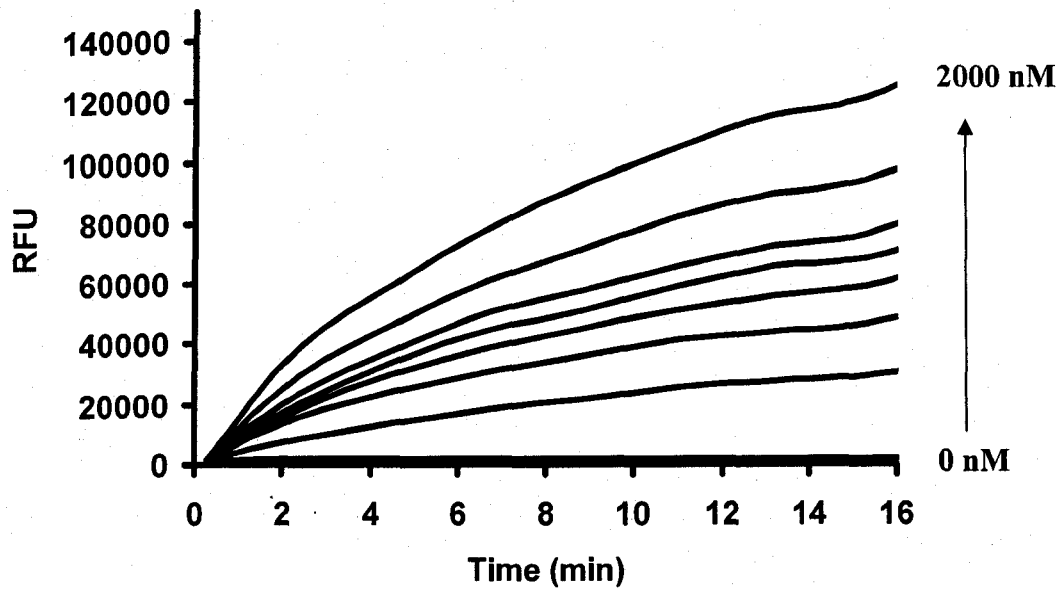
**Figure 4.2: Ghost-mediated disulfide reductase activity**

A.  Concentration dependent increase in disulfide reductase activity.  Increasing concentrations of Dieosin-GSSG (25-2000 nM) were added to ghosts (20 μL) in the presence of 2 μM DTT, and the time dependent increase in fluorescence was monitored over time.  Traces presented here are corrected for the corresponding control which did not contain any ghosts (n=4).
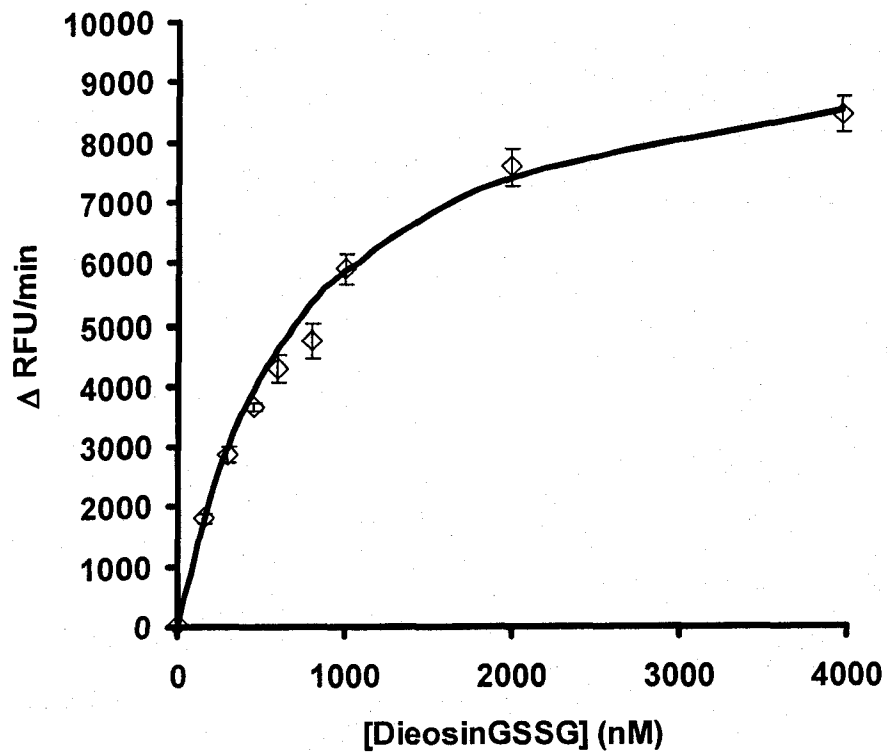
B. Initial rates of disulfide reduction from the above figure as a function of dieosin-GSSG concentration (n=4).

### 4.4.3 Inhibition of Ghost Disulfide Reductase Activity

The ghost membrane contains various proteins with vicinal thiols that can participate in its disulfide reductase activity. The contribution of ghost membrane-associated PDI was assessed with the use of known PDI inhibitors, PAO and RL90 PDI-antibody.

PAO is trivalent arsenical that specifically binds to the vicinal thiols. Upon incubation of the ghosts with PAO (200 $\mu$M, Figure 4.3 black squares) there was a ~80% decrease in disulfide exchange activity of as compared to ghosts that did not contain PAO (Figure 4.3 black diamonds). However, ghosts preincubated with RL90 PDI-specific antibodies showed a ~15% decrease in disulfide exchange activity as determined by dieosin-GSSG assay (Figure 4.4), suggesting that there is a significant contribution of other proteins containing vicinal thiols that are present within the ghost membrane that also contribute to the disulfide reductase activity observed.
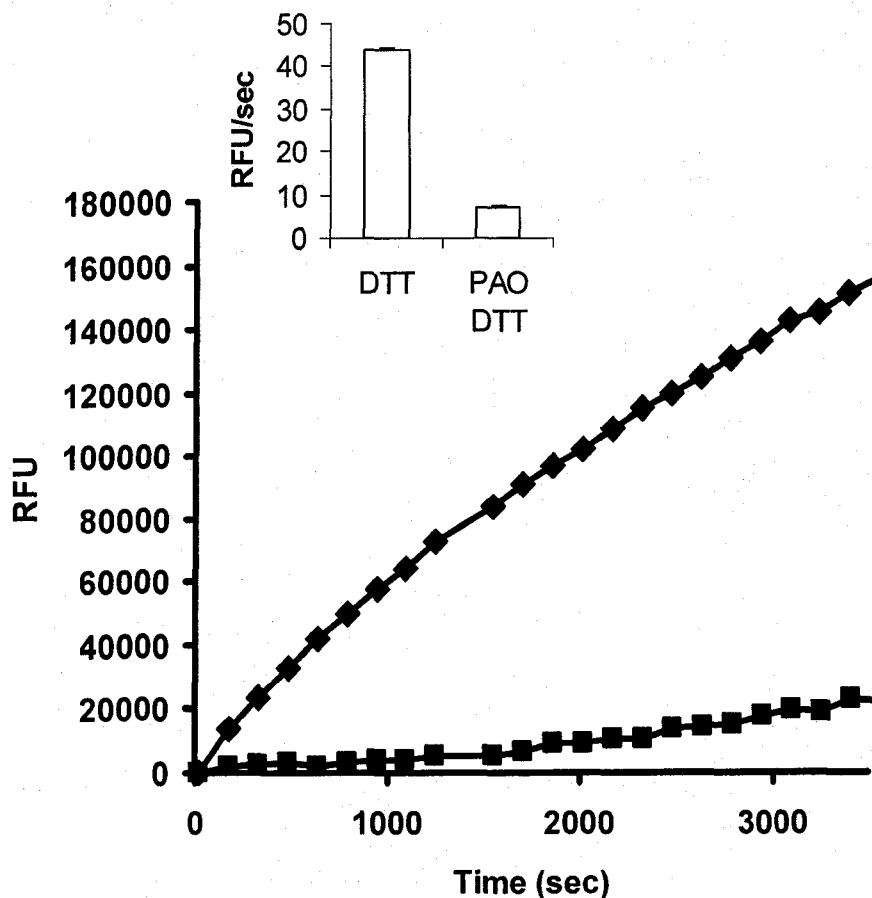
**Figure 4.3: Inhibition of ghost mediated disulfide reductase activity with PAO**

The ghosts were incubated in the presence of PAO (200 μM) for 30 minutes at room temperature. Dieosin-GSSG (500 nM) was added to the sample without (black diamonds) or with PAO (black squares) and the disulfide reductase activity was monitored in the presence of DTT (2 μM, n=4).
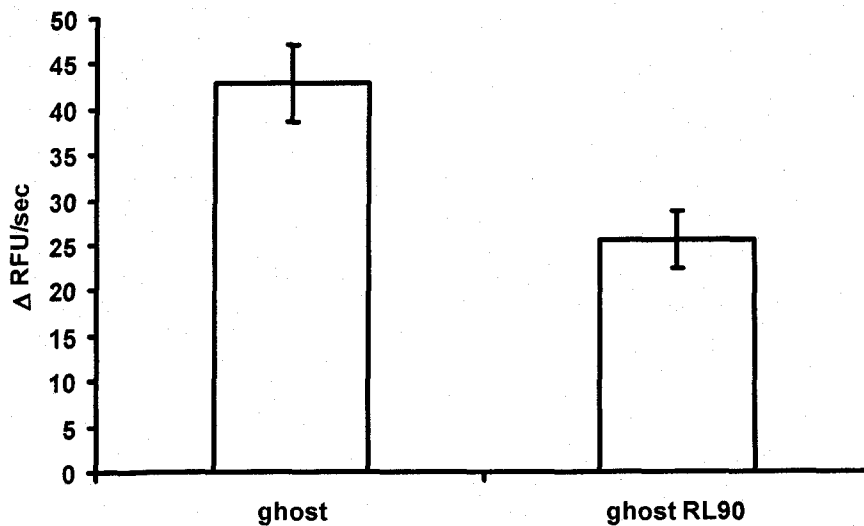
**Figure 4.4: Inhibition of ghost disulfide exchange activity with RL90**

The ghosts were preincubated with RL90 specific PDI antibodies for 1 hour at room temperature. 20 μL of ghost suspension with or without RL90 was placed in a 96 well plate in the presence of dieosin-GSSG (500 nM) and DTT (2 μM) and the increase in fluorescence due to the cleavage of GSSG was monitored over time. Rates presented here were corrected for the corresponding control that did not contain ghosts (n=3).

We have previously shown that S-nitrosothiols such as GSNO are capable of inhibiting PDI disulfide exchange activity (Root *et al.*, 2004) due to transnitrosation of protein thiols. Here, we wanted to establish if ghost disulfide exchange activity could be inhibited in the presence of NO donors. Addition of increasing GSNO concentrations (25-1000 nM) to the sample containing ghost suspension resulted in the inhibition of disulfide exchange activity as shown in Figure 4.5 A.

A similar experiment was performed in the presence of spontaneous NO donor DEA-NO which is known to S-nitrosate protein thiols such as PDI (Sliskovic *et al.*, 2005). Addition of increasing DEA-NO concentrations resulted in disulfide reductase inhibition (Figure 4.5 B) that resembled the one observed with GSNO, suggesting that regardless of the NO donor disulfide exchange activity of ghosts can be inhibited.

Next, we wanted to establish the relationship between observed decrease in disulfide reductase activity and total thiol concentration of ghosts. Upon incubation of ghosts with increasing concentrations of GSNO (25-2500 nM, Figure 4.6 diamonds) or DEA-NO (25-2500 nM, Figure 4.6 squares) a concentration dependent decrease in total thiols was observed as determined by the DTNB assay. The thiol inhibition curve resembled the results obtained from disulfide reductase activity experiments, indicating that the decrease in ghost-mediated disulfide reductase activity was due to the disappearance of free thiols.
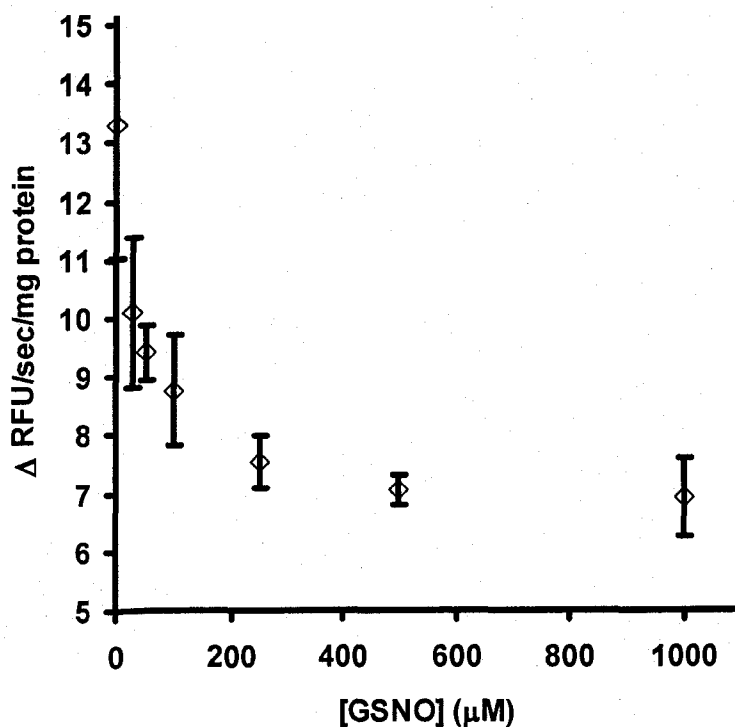
**Figure 4.5: Inhibition of disulfide reductase activity of ghosts**

A. GSNO mediated inhibition of disulfide reductase activity.

Disulfide reductase activity of ghosts (20 µL) was monitored in the presence of 2 µM DTT and 500 nM dieosin-GSSG as a function of increasing GSNO concentrations (25 nM to 1000 nM). The data represented here was obtained by subtracting the initial rates of samples containing ghosts with corresponding control that did not have any ghosts present (n=4).
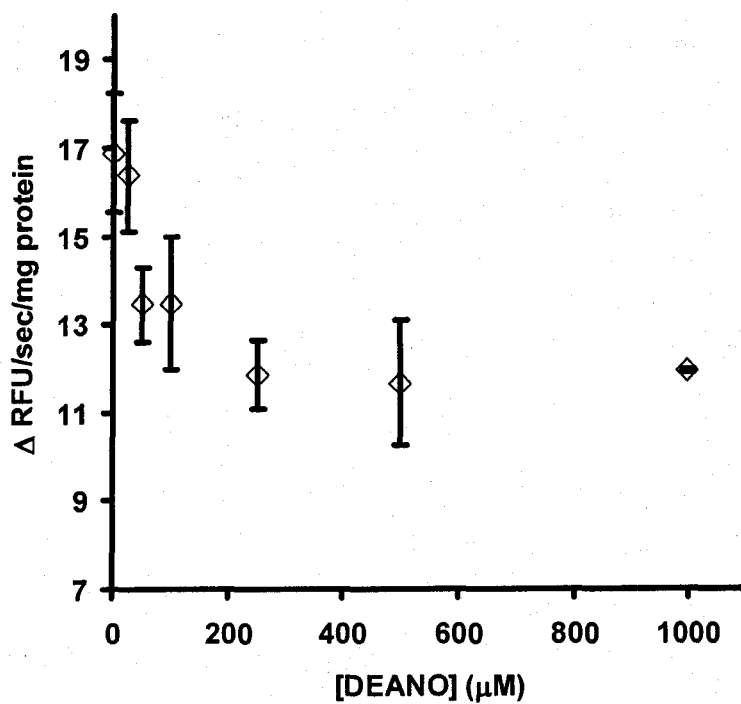
B. DEA-NO mediated inhibition of disulfide reductase activity.

Disulfide reductase activity of ghosts (20 μL) was monitored in the presence of 2 μM

DTT and 500 nM dieosin-GSSG as a function of increasing DEA-NO concentrations (25

nM to 1000 nM). The data represented here was obtained by correcting the initial rates

of samples containing ghosts with corresponding control that did not have any ghosts

present (n=4).
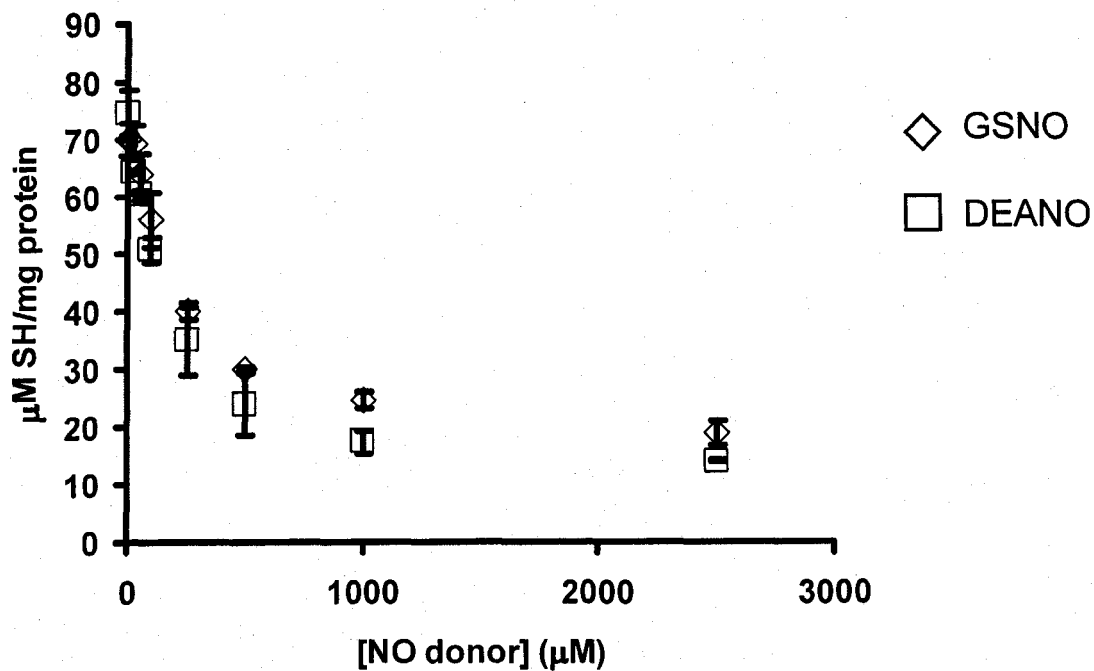
**Figure 4.6: Thiol content estimation by DTNB assay**

Ghosts were incubated in the presence of increasing GSNO (diamond) or DEA-NO (square) concentrations (25-2500 nM) for 1 hour at room temperature. Aliquots of these samples were taken and further incubated with DTNB (1 mM) for 15 minutes, followed by centrifugation at 10000 x g for 10 minutes. The supernatant was removed and the absorbance at 412 nm was measured against corresponding controls that did not contain ghosts. Data is presented as μM of thiols per mg of protein (n=4).

### 4.4.4 S-nitrosation of Ghosts

So far, we have established that ghost membrane-associated PDI contributes to the disulfide reductase activity, which can be inhibited in the presence of increasing GSNO or DEA-NO concentration accompanied with corresponding decrease in total concentration of free thiols. Next, we sought to establish if these observations were due to the thiol oxidation of S-nitrosation.

To this end, ghosts exposed to excess DEA-NO and subsequently washed, were placed in the 96 well plate and the disulfide reductase activity was monitored in the absence and presence of DTT. As shown in Figure 4.7, ghosts exposed to DEA-NO showed a significant decrease in disulfide reductase activity without DTT present. However, upon addition of DTT, there was a ~4-fold increase in activity observed. The same sample was placed in the vial with immersed NO electrode and the current was observed for 60 seconds in order to obtain a stable baseline. At this time, $HgCl_2$ (200 $\mu$M) was added to phosphate buffer (Figure 4.8, light grey trace) control and ghosts not exposed to DEA-NO (Figure 4.8, black trace) resulting in no increase in current, while the concentration dependent increase was observed in the presence of DEA-NO treated ghosts (Figure 4.8, dark grey trace and dashed line). This observation suggested the formation of S-nitrosated proteins occurs within membranes of RBC ghosts.

In order to determine if PDI is one of the potential proteins of S-nitrosation, we performed a biotin switch assay. The biotin switch assay is a widely employed method for detecting S-nitrosated protein, although it is constantly under development (Jaffrey *et*

*al.*, 2001; Martinez-Ruiz and Lamas, 2004; Foster and Stamler, 2004, Zhang *et al.*, 2005).

Upon exposure of ghosts with excess of GSNO or DEA-NO, the strepavidin reactive

signal was observed that corresponded to the bands detected for PDI. Control ghosts also

showed a faint strepavidin-reactive signal which could be due to the partial blocking of

the free thiols or PDI disulfide bond reduction under our experimental conditions.
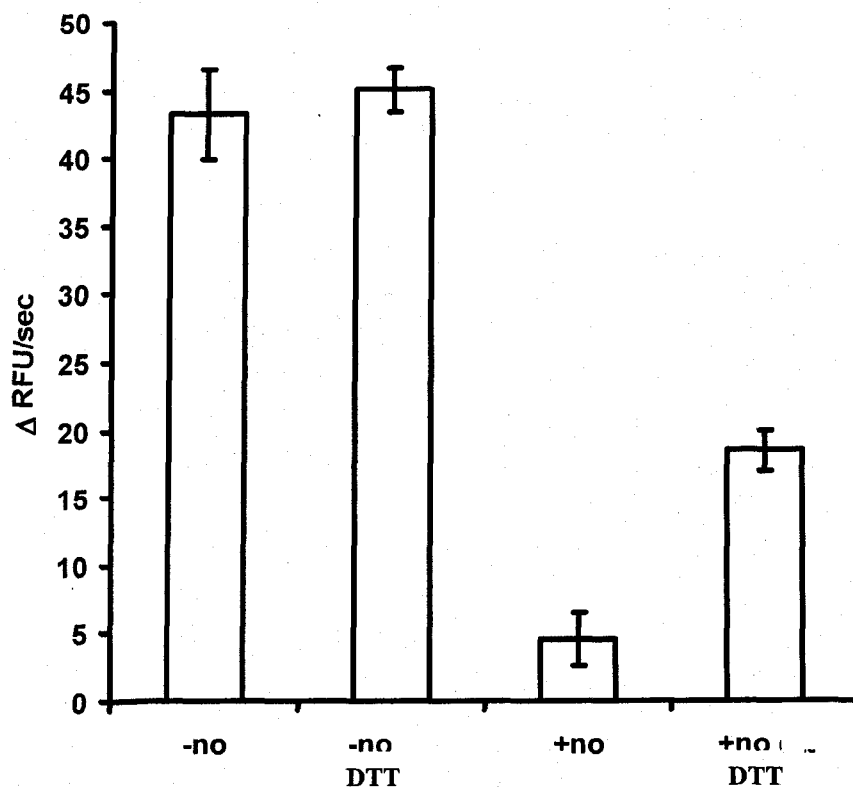
**Figure 4.7: Recovery of disulfide reductase activity by DTT**

Ghosts (20 µL) were incubated in the presence of DEA-NO as described in "Experimental Methods". The disulfide reductase activity was monitored in the presence of 500 nM dieosin-GSSG, using ghost sample without or with DEA-NO exposure and with or without DTT (2 µM, n=4).
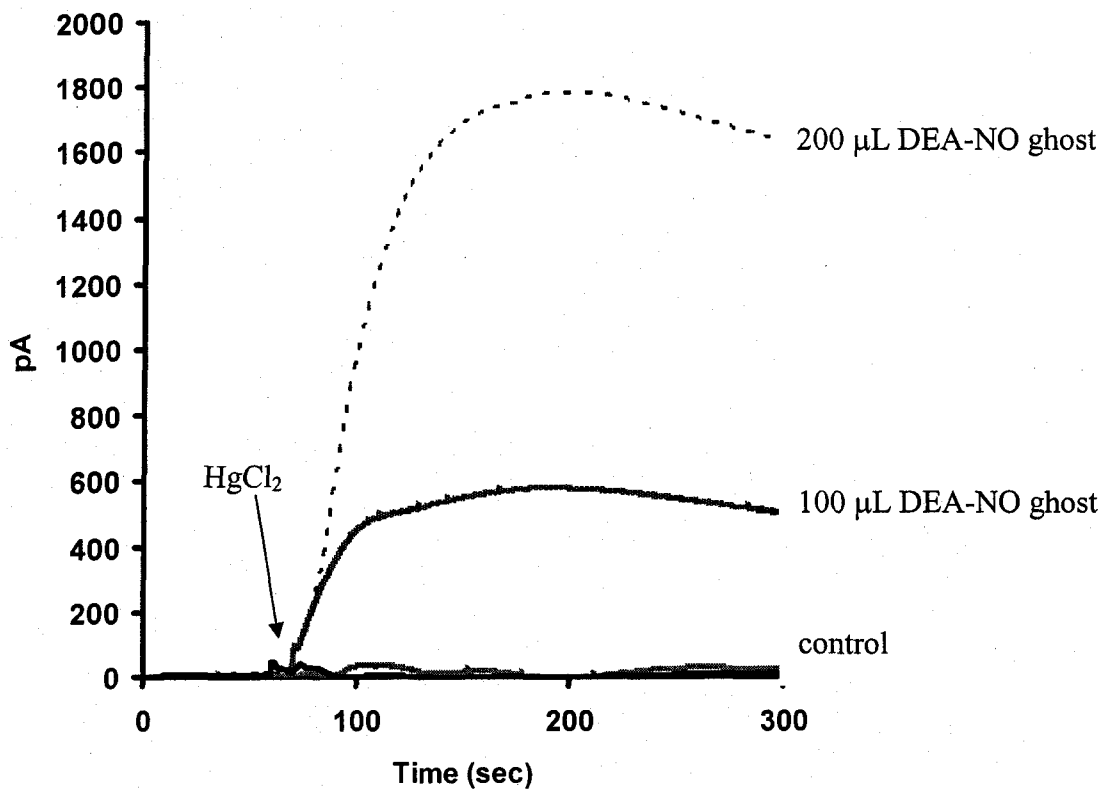
**Figure 4.8: Release of NO from nitrosated ghosts**

Ghosts were incubated in the presence of DEA-NO (1 mM) as described in "Experimental Methods". Control (light grey trace) contained hypotonic buffer only. Ghosts that were not exposed to DEA-NO treatment are shown in the black trace. DAE-NO treated ghosts were added at 100 µL (dark grey trace) or 200 µL (dashed trace) and the current was observed for 60 seconds. At that time $HgCl_2$ was added and the current was monitored until signal was stabilized (n=3).

Strepavidin-HRP        Anti-PDI



1    2    3            1    2    3        ← ~ 58 kDa
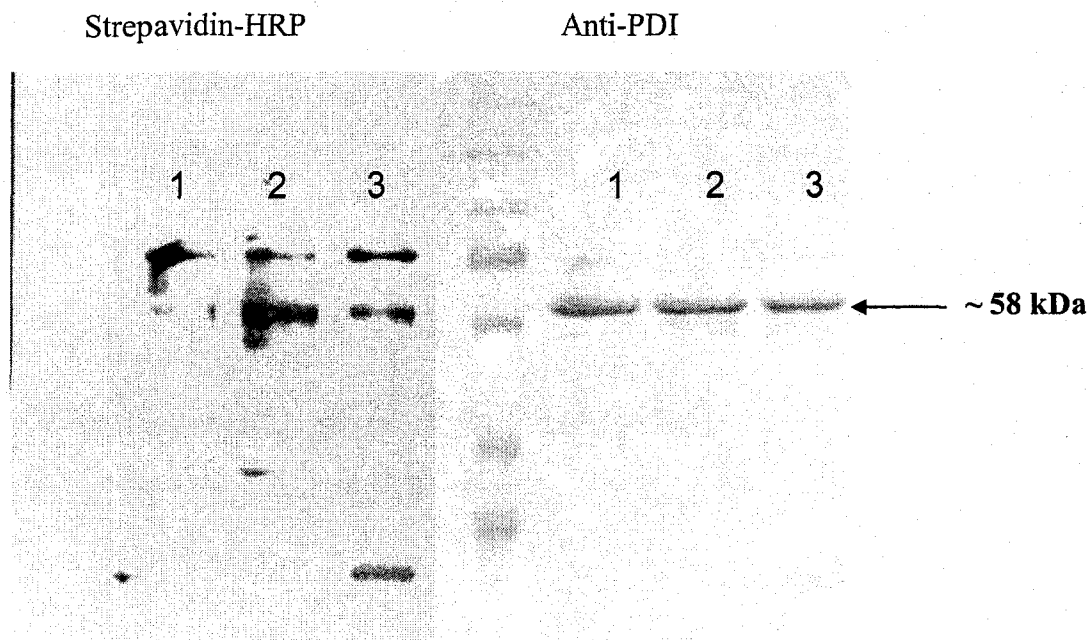
**Figure 4.9: Biotin switch assay of ghosts**

The biotin switch assay was performed as described in "Experimental Methods". Left

blot was probed against biotin using strepavidin-HRP and right blot represents signal due

to the presence of PDI. Lane 1 contained ghosts only, lane 2 ghosts treated with GSNO

and lane 3 ghosts treated with DEA-NO (n=3).

## 4.5 Discussion

Protein S-nitrosation offers a covenient method for transport of NO. Previous studies (Jia et al., 1996) identified Hb-SNO species and AE1-SNO and proposed that NO transfer from the heme iron to β-93 cysteine occurs via allosteric regulation due to the oxygen tension mediated by intracellular small thiol molecules. The export of NO from RBCs is thought to be mediated by the formation of S-nitroso protein that would result in a series of transnitrosation reaction and subsequent export in the form of protein-SNO. The first evidence of ghost membrane-associated PDI came from the study of Alloisio and coworkers (Alloisio et al., 1996) but no known function was assigned to it. Here we showed, using western blotting, that PDI is not only associated with the ghost membrane (Figure 4.1, lane 1) but could also be released from the ghosts by extensive washing (Figure 4.1, lane 2) and is present in cytosol of RBCs as well (Figure 4.1, lane 4).

Disulfide reductase activity of ghosts was performed using a sensitive assay that utilize dieosin-GSSG probe, which has two eosin molecules attached to the N-terminal of GSSG (Raturi and Mutus, 2007). Upon cleavage of disulfide bond of GSSG, the fluorescence quenching due to the close proximity of two eosin molecules is released thus resulting in the increase in fluorescence. Ghost membranes displayed an enzyme-mediated disulfide reductase activity as seen by the saturation curve constructed form initial rates of disulfide cleavage as a function of increasing dieosin-GSSG concentration (Figure 4.2 A and B). Treatment of ghosts with the known vicinal thiol inhibitor PAO resulted in ~80% inhibition confirming that the activity observed is due to proteins that contain vicinal thiols that are present in the ghost membranes (Figure 4.3). However, upon addition of

PDI specific antibodies (RL90) to the ghost suspension, only ~30% inhibition in disulfide exchange activity was observed (Figure 4.4). The remaining disulfide reductase activity initially observed could be due to the presence of other redox active proteins, such as glutaredoxin that have also been identified as the resident of ghost membrane (Papov *et al.*, 1994).

Previous studies in our lab showed that NO donors such as GSNO could inhibit PDI disulfide exchange activity (Root *et al.*, 2004) thus inhibiting platelet aggregation. Our interest in this study was to determine if NO donors like GSNO that participates in transnitrosation, or a spontaneous NO donor DEA-NO could inhibit ghost membrane-mediated disulfide exchange. Both GSNO and DEA-NO, successfully inhibited ghost membrane-mediated disulfide exchange activity (Figure 4.5 A and B respectively) in the concentration dependent manner. Next, we wanted to establish the relationship between decrease in activity and total protein thiol concentration. To this end, a ghost suspension was incubated with increasing GSNO and DEA-NO concentrations and thiols quantification was performed using the DTNB assay. There was a concentration dependent decrease in total thiols observed with both GSNO and DEA-NO (Figure 4.6) that resembled the activity inhibition studies. Results obtained hitherto demonstrated the ability of NO donors to inhibit the disulfide exchange activity and decrease the thiol concentration in ghost membranes.

Next, we wanted to investigate the possibility of PDI to become S-nitrosated upon exposure to the NO donors. To this end, ghosts treated with DEA-NO were tested for

disulfide reductase activity in the absence or presence of reducing agent. The ghosts treated with DEA-NO showed a significant decrease in activity which was recoverable in the presence of DTT (Figure 4.7). When the same sample of NO-loaded ghosts was placed in the NO-meter, a concentration dependent increase in current was observed upon addition of S-NO bond cleaving agent $HgCl_2$. Therefore, these findings suggested that upon treatment of ghosts with a spontaneous NO donor DEA-NO, the disulfide reductase activity inhibition and decrease in the total thiol concentration were most likely due to the proteins S-nitrosation rather than the oxidation of thiols. Lastly, the biotin switch assay was performed in order to unambiguously determine if PDI could be one of the target proteins for S-nitrosation. While PDI protein concentrations were equal between different samples loaded (Figure 4. 9, right blot), the biotin label signal corresponding to the PDI band was significant in the samples that were exposed to either GSNO or DEA-NO. The faint signal observed in the control sample that did not receive any NO treatment could be due to the uncertainties of the assay and experimental condition used (Zhang et al., 2005). A recent study by Forrester (Forrester et al., 2007) showed that while ascorbate treatment used to dissociate S-NO bond may generate a false positive signal, the use of flash photolysis for S-NO bond dissociation appears to be a better approach leading to the improved reproducibility of the assay.

Therefore, based on the findings from this study, we propose the following mechanism (Figure 4.10). PDI-bound NO could potentially enter RBCs via membrane-bound PDI, resulting in the transfer of NO to the Fe(II) of Hb. Once nitrosyl heme is formed, the reaction could proceed in two directions. In reaction 1, during the low oxygen tension,

intramolecular NO transfer can occur resulting in S-nitrosated β-93 Cys of Hb (Jia *et al.*, 1996). This NO moiety could transnitrosate intracellular PDI which in turn could either transnitrosate AE1 (Pawloski *et al.*, 2001) or membrane associated PDI. In reaction 2, intracellular S-nitrosated PDI could transnitrosate β-93 Cys of Hb, subsequently leading to the similar outcome as in reaction 1.
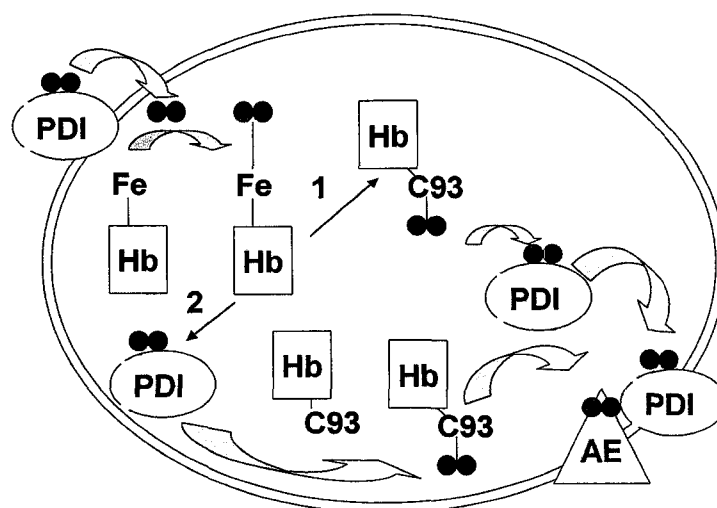


**Figure 4.10: The Role of PDI in NO influx and efflux in RBCs**

PDI is represented by a circle, Hb by squares, anion exchanger (AE1) as a triangle and NO as blue and red circles.

Therefore, here we propose a novel mechanism for PDI-mediated NO influx and efflux in RBCs. PDI appears to be a great target for this particular function since it is widely expressed throughout different locations in the RBCs, and we have previously shown that PDI proteins can communicate between themselves and participate in transnitrosation and denitrosation reactions (Sliskovic *et al.*, 2005).

# CHAPTER 5

**Reversible Inhibition of Caspase-3 Activity by Iron(III)**

**Potential Role in Physiological Control of Apoptosis**

## 5.1 Introduction

So far, we have examined the role of PDI with respect to RSNO denitrosation, platelet aggregation and redox state of its active site thiols. This chapter will deal with the novel activity of PDI and its role in controlling apoptosis.

### 5.1.1 Apoptosis

Programmed cell death, also known as apoptosis, is a highly regulated process in which unwanted cells are eliminated during a regular homeostasis of multicellular organisms (Raff, 1998; Jacobson *et al.*, 1997). Apoptosis is generally accompanied with a series of cellular events including DNA fragmentation, membrane blebbing, cell shrinkage and disassembly into membrane-enclosed vesicles. Also, the loss of apoptotic regulation is found to be closely linked to human diseases including various forms of cancer, ischemic damage, neurodegenerative diseases and immune disorders (Nicholson, 1996). Although the exact mechanism of apoptosis regulation is not fully understood, it is now recognized that the family of proteins called cysteine proteases or caspases play an essential role in the apoptotic process.

### 5.1.2 Caspase-3

Figure 5.1 represents a summary of different roles of caspases in the initiation of apoptosis (Grutter, 2002). Currently there are two major recognized pathways of apoptosis, extrinsic and intrinsic pathway. The extrinsic pathway is triggered upon a ligand binding to the surface receptor resulting in its trimerization and subsequent activation of the initiator caspases-8 or -10. Caspase-8 or -10 are capable of activating

execution caspases-3 and -7, which once activated can perform a series of proteolytic events that eventually result in the apoptosis. However, during the cell stress such as irreparable genome damage, pharmaceuticals or ionizing radiation, the intrinsic pathway is activated and cytochrome c is released from mitochondria, followed by the activation of caspase-9 in complex with Apaf-1. Caspase-9 is another candidate for activation of execution caspases-3 and -7. Finally, caspases-1 and -2, located in the ER can be activated in the presence of calcium under cellular stress, also resulting in caspase-3 and -7 activation. Therefore, by controlling caspase-3 activation, it would be possible to gain control over the overall process of apoptosis.

**Extrinsic pathway**

**Intrisic pathway**
Cellular Stress

Casp-8,10

Apaf-1

Casp-9

Casp-12

pCasp-3,7

Casp-3,7

**Many proteins**

**Apoptosis**
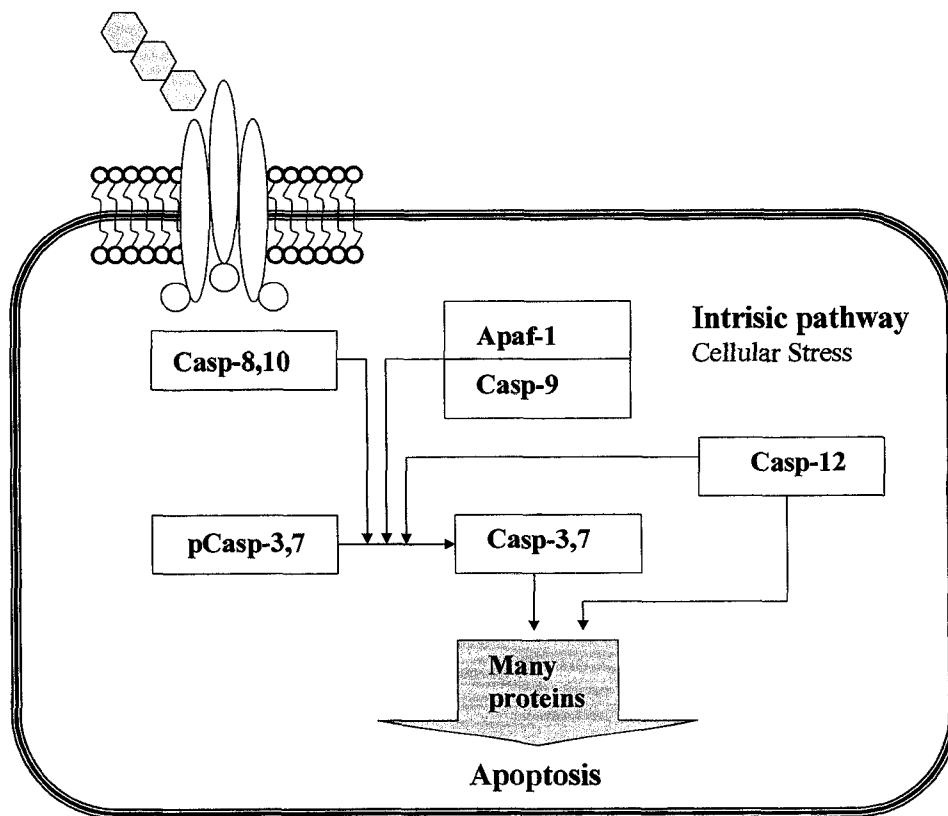
**Scheme 5.1 The role of caspases in the major apoptotic pathways (Grutter, 2000)**

Under normal cellular conditions caspase-3 is synthesized as a single chain precursor and exists in an inactive zymogen form. Upon oxidative stress, procaspase-3 is activated by the cleavage of the N-terminal prodomain peptide at $Asp_{119}$ and the conserved $Asp_{296}$ and $Asp_{316}$ (Scheme 5.2). These proteolytic cleavages result in the formation of a large subunit ($\alpha$ chain) and a small subunit ($\beta$ chain) (Lord *et al.*, 2003), leading to the assembly of a homodimer of heterodimers which represents the active form of the enzyme (Walker *et al.*, 1999).
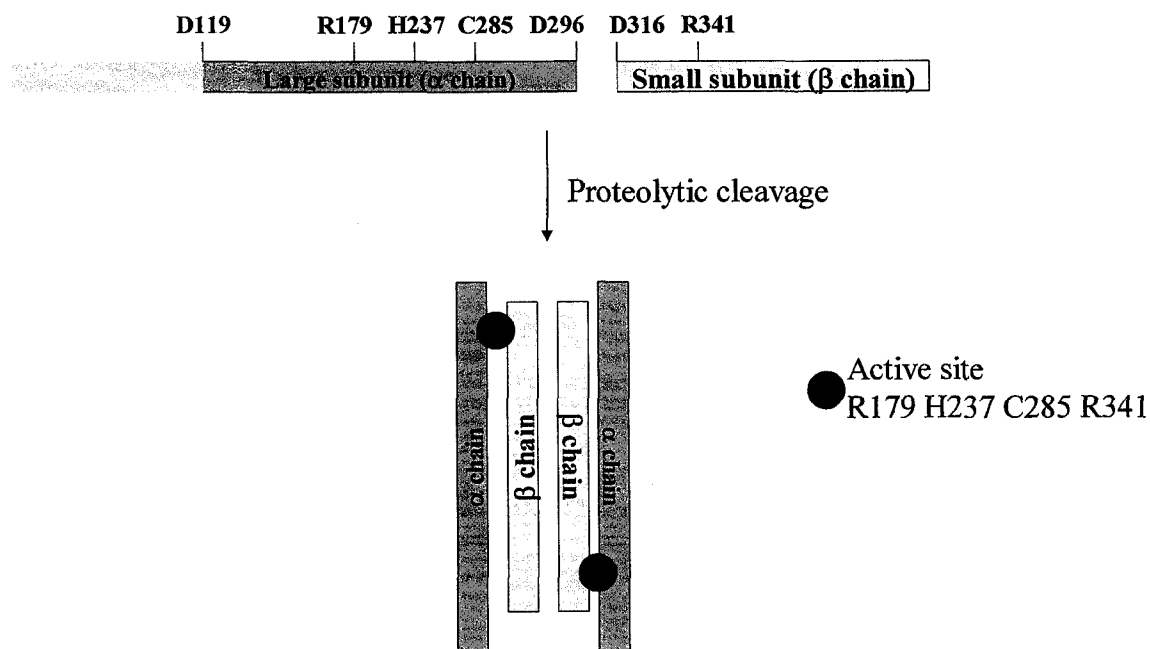


**Scheme 5.2 Proteolytic activation of caspase-3 (Grutter, 2000).**

The activity and the specificity of caspases are determined by the conserved residues which are arranged into a specific structural arrangements required for catalysis. They

consist of $Arg_{179}$, $His_{237}$, $Cys_{285}$ and $Arg_{341}$, with the cysteine residue being a catalytic nucleophile, while histidine acts as a general base.

Once activated, caspase-3 is responsible for a proteolytic cleavage of a large number of substrates containing common Asp-Glu-Val-Asp (DEVD) motif such as PARP (Lazebnik *et al.*, 1994), U1-70 kDa (Song *et al.*, 1996), DNA-$PK_{CS}$ (Waterhouse *et al.*, 1996), PKC δ (Emoto *et al.*, 1995), Huntington (Janicke *et al.*, 1996) and SREBP-1 (Na *et al.*, 1997), to name a few.

### 5.1.3 Regulation of caspase-3 activity

Previous *in vitro* and *in vivo* studies have shown that the active-site cysteine residue is susceptible to oxidative modification which results in caspase-3 inactivation and subsequent inhibition of apoptosis. Nitric oxide (NO) can act as a reversible inhibitor of caspase-3 activity, by nitrosating its active site cysteine (Li *et al.*, 1997; Kim *et al.*, 1997). Reactive oxygen species such as hydrogen peroxide ($H_2O_2$) reversibly inhibit caspase-3 activity (Borutaite and Brown, 2001). The recent discovery of metal ion-dependent regulation of apoptosis suggested new mechanisms for regulating caspase-3 activation (Perry *et al.*, 1997; Troung-Tran *et al.*, 2000).

Iron is an essential component of various biochemical processes including cell proliferation, electron transfer and detoxification (Crichton and Ward, 1992). Intracellular iron trafficking occurs through the cell surface transferrin receptor (TfR) (Klausner *et al*, 1983). While the expression of TfR in healthy cells is low, carcinoma

cell lines are accompanied with overexpression of the iron receptor (Inoue *et al.*, 1993). Consequently, increased iron levels have been observed in various cancer types (Toyokuni, 1996), including HL-60 leukaemic cells, human breast cancer cells and human neuroblastoma cells as detected by the apoptosis markers amongst which is an increased caspase-3 activity. However, there has been no direct evidence of caspase-3 interaction with iron.

Protein disulfide isomerase (PDI) is a multifunctional enzyme expressed throughout various cellular compartments including ER, cell surface, the cytosol and the nucleus (for review on PDI localization, see Turano *et al*, 2002). The main function of PDI is isomerization and rearrangement of disulfide bonds (Darby *et al.*, 1994). As described in Chapter 1, the active site of PDI contains two vicinal thiols that undergo a redox state change during catalysis (Gilbert, 1997). Recent reports suggested that PDI also has a zinc (Solovyev and Gilbert, 2004) and copper (Narindrasorasak *et al.*, 2003) binding ability through its active site thiols. Since PDI active site also resembles [2Fe-2S]-ferrodoxin iron binding domains (Yeh *et al.*, 2000), we speculated that PDI could also bind iron. Therefore, we sought to determine the effects of iron on caspase-3 activity and the role of PDI on caspase-3 activation.

## 5.2 Material and Equipment

### 5.2.1 Materials

7-Amino-4-methylcoumarin, N-acetyl-L-aspartyl-Lglutamyl-L-valyl-l-aspartic acid

| | |
|---|---|
| amide (Ac-DEVD-AMC) | Sigma-Aldrich Canada Ltd., Oakville, Ontario |
| Ammonium persulfate; | Sigma-Aldrich Canada Ltd., Oakville, Ontario |
| Biorad Bradford Reagent; | Bio-Rad Laboratories Ltd., Mississauga, Ontario |
| Bovine Serum Albumin; | Sigma-Aldrich Canada Ltd., Oakville, Ontario |
| Copper (II) sulfate; | Sigma-Aldrich Canada Ltd., Oakville, Ontario |
| Desferoxamine; | Sigma-Aldrich Canada Ltd., Oakville, Ontario |
| Diethylamine NONOate (DEANO); | Sigma-Aldrich Canada Ltd., Oakville, Ontario |
| Dimethyl formamide (DMF); | Sigma-Aldrich Canada Ltd., Oakville, Ontario |
| 5, 5'-dithiobis(2-nitrobenzoic) acid; | Sigma-Aldrich Canada Ltd., Oakville, Ontario |
| Dithiothreitol (DTT); | Sigma-Aldrich Canada Ltd., Oakville, Ontario |
| Ethylene diamine tetraacetic acid; | Sigma-Aldrich Canada Ltd., Oakville, Ontario |
| Ferric Sulfate; | Sigma-Aldrich Canada Ltd., Oakville, Ontario |
| Fluoresceine isothiocyanate; | Sigma-Aldrich Canada Ltd., Oakville, Ontario |
| Imidazole; | Sigma-Aldrich Canada Ltd., Oakville, Ontario |
| Insulin; | Sigma-Aldrich Canada Ltd., Oakville, Ontario |
| Lysozyme; | Sigma-Aldrich Canada Ltd., Oakville, Ontario |
| Neocuproine; | Sigma-Aldrich Canada Ltd., Oakville, Ontario |
| N-ethylmaleimide (NEM) | Sigma-Aldrich Canada Ltd., Oakville, Ontario |
| Ni-Cam™ Resin; | Sigma-Aldrich Canada Ltd., Oakville, Ontario |

Oxidized glutathione;                Sigma-Aldrich Canada Ltd., Oakville, Ontario

Potassium phosphate;                Sigma-Aldrich Canada Ltd., Oakville, Ontario

Reduced glutathione;                Sigma-Aldrich Canada Ltd., Oakville, Ontario

Sephadex G-25;                      Sigma-Aldrich Canada Ltd., Oakville, Ontario

Sodium chloride;                    Sigma-Aldrich Canada Ltd., Oakville, Ontario

Sodium dithionate;                  Sigma-Aldrich Canada Ltd., Oakville, Ontario

Sodium hydroxide;                   Sigma-Aldrich Canada Ltd., Oakville, Ontario

Sodium phosphate monobasic:         Sigma-Aldrich Canada Ltd., Oakville, Ontario

Sodium phosphate dibasic;           Sigma-Aldrich Canada Ltd., Oakville, Ontario

TEMED;                              Bio-Rad Laboratories Ltd., Mississauga, Ontario


## 5.2.2 Equipment

Agilent 8453 UV-VIS spectrophotometer;

   (Agilent Technologies Canada Inc, Mississauga, Ontario)

Beckman J2-HS Centrifuge;

   (Beckman Coulter Canada Inc., Mississauga, Ontario)

BioRad Fraction Collector Model 2110;

   (Bio-Rad Laboratories Ltd., Mississauga, Ontario)

ISO-NO Mark II with WPI MKII Nitric Oxide electrode;

   (World Precision Instruments Inc., Sarasota, Florida)

Jouan CR3i Centrifuge;

   (Jouan Inc, Winchester, Virginia)

Labconco FreeZone 4.5 Liter Benchtop Freeze Dry Systems;

(Labconco Corporation, Kansas City, Missouri)

Mettler AJ100 Balance;

(Mettler Toledo Canada, Mississauga, Ontario)

Microtiter 96-well Solid Plate;

(Thermo Electron Corp. Canada, Burlington, Ontario)

Mini-Protein II Gel Electrophoresis System;

(Bio-Rad Laboratories Ltd., Mississauga, Ontario)

Orion Model 420A pH Meter;

(Thermo Electron Corp. Canada, Burlington, Ontario)

Stir Plate 360 Series;

(VWR International, Mississauga, Ontario)

Varian Eclipse Fluorescence Spectrophotometer;

(Varian Canada, Mississauga, Ontario)

Wallac Victor$^3$TM 1420 Multilabel Counter;

(Perkin Elmer, Waltham, Massachusetts)

## 5.3 Experimental Methods

### 5.3.1 Protein Expression and Purification.

PDI was expressed and purified as described in Sliskovic *et al* (Sliskovic *et al.*, 2005). Briefly, TB medium was used to grow *E. coli* BL21 (DE3) with the expression vector pET-28b containing plasmid that encodes for the entire human PDI sequence with the N-terminal $His_6$ tag (Pihlajaniemi *et al.*, 1987). Induction was initiated with 1 mM isopropyl β-D-thiogalactoside and cells were grown for another 4 hours at 37°C. Bacterial pellet was lysed with 0.1 mg/ml lysozyme, followed by sonication. Purification of PDI was done using Ni-CAM™ HC Resin (Sigma), equilibrated with 50 mM Tris-HCl, pH 8.0. PDI was eluted using 250 mM imidazole. The buffer was exchanged by dialysis against 0.1 M potassium phosphate buffer, pH 7. Protein quantification and purity was preformed using the Bradford assay (Bradford, 1976) and gel electrophoresis and western blotting, respectively.

Human active caspase-3 was expressed in *E. coli* BL21(DE3) with the expression vector pET-28b as previously described (Stennicke and Salvesen, 1997). Briefly, cells grown in TB medium were induced with 1 mM isopropyl β-D-thiogalactoside and harvested after 6 hour incubation at 37°C. Purification of caspase-3, protein quantification and purity was carried out as described in the above paragraph.

### 5.3.2 Caspase-3 Activity.

The conditions used for assay of caspase-3 activity are specified in figure legends. Caspase-3 activity was evaluated by measuring proteolytic cleavage of fluorogenic synthetic substrate Ac-DEVD-AMC. Assay buffer contained 100 mM phosphate buffer, pH 7.0, unless stated otherwise. Fluorescence increase due to AMC release was monitored using 360 nm excitation and 460 nm emission wavelengths. All caspase-3 activity experiments were performed using Wallac Victor$^3$$_{TM}$ 1420 Multilabel Counter (Perkin Elmer) and Varian Cary Eclipse fluorescence spectrometer.

### 5.3.3 Preparation of PDI-bound Iron.

PDI (1 mg) was incubated with 5 x molar excess of $Fe_2(SO4)_3$ for 1 hr at room temperature. Following incubation, excess iron was removed over a Sephadex G-25 column with 100 mM phosphate buffer, pH 7.0. Final PDI concentration was quantified using Bradford assay. PDI-Fe was processed immediately for iron determination.

### 5.3.4 Iron Determination.

Quantification of complexed iron was performed as described by Fish (Fish, 1988). Briefly, PDI and PDI-Fe (50 µg) were mixed with 0.25 mL of reagent A (0.6 M HCl and 0.142 M $KMnO_4$, freshly made) and digested for 2 hrs at 60°C. Following digestion, 0.05 mL of reagent B (6.5 mM ferrozine, 13.1 mM neocuproine, 2 M ascorbic aid and 5 M ammonium acetate) was added and the mixture was vortexed to assure for proper mixing. After 30 min incubation at room temperature, absorbance was measured at 562

nm using an Agilent UV-vis spectrophotometer. The standard curve was obtained using 1 to 6 µg/ml ferrous sulphate in 10 mM HCl.

### 5.3.5 Chemical Blocking of PDI thiols.

PDI active site thiols were chemically modified using N-ethyl maleimide and phenylarsine oxide. Prior to chemical blocking, PDI (1 mg) was incubated with 5 x molar excess DTT for 2 hr at the room temperature to assure full reduction of the active site thiols. Excess DTT was removed over Sephadex G-25 using 100 mM phosphate buffer, pH 7.0. Reduced PDI was immediately incubated with 5 x molar excess NEM and PAO for 2 hr at the room temperature and chromatographed over a Sepadex G-25 column. Thiol blocking was checked with DTNB assay (Jiang *et al.*, 1999).

### 5.3.6 Preparation of oxidized PDI

PDI active site thiols were oxidized as previously described (Raturi *et al.*, 2005). Briefly, PDI (10 µM) was incubated with GSSG (10 mM) overnight at 4°C to fully oxidize PDI thiols. Excess GSSH was removed using a Sephadex G-25 column in phosphate buffer (100 mM, pH 7.0). Oxidized PDI (PDI-SSG) was quantified using the Bradford assay and stored at -80°C.

### 5.3.7 Lysozyme denaturation and refolding

Lysozyme denaturation and refolding was performed as described by Puig and Gilbert (Puig and Gilbert, 1994). Briefly, lysozyme (100 mg/ml) reduction and denaturation was done in a buffer containing 8 M urea, 130 mM 2-mercaptoethanol and 25 mM Tris-HCl,

pH 8.6) for 1.5 hours at 37°C. The reaction was stopped by the addition of 0.1 M acetic acid, pH 4.0 resulting in a working solution of lysozyme of 200 μM. Refolding of lysozyme (5 μM) was performed by means of measuring lysozyme activity as a decrease in absorbance at 650 nm using refolding buffer (100 mM HEPES, 5 mM MgCl₂, 20 mM NaCl and 2 mM EDTA, pH 7) and in the presence of PDI (250 nM) and PDI and caspase-3 (250 nM and 800 μg/ml, respectively). Lysozyme activities are reported as a fold increase in lysozyme refolding with respect to the same molar amount of native lysozyme.

### 5.3.8 PDI disulfide reductase activity

Dieosin-insulin was prepared by insulin (200 μM) with 5 fold molar excess of eosin isothiocyanate. Reaction was left with stirring for 4 hours at the room temperature in phosphate buffer (100 mM sodium phosphate and 2 mM EDTA, pH 8.5), followed with the removal of unreacted eosin by a Sephadex G-25 column. Insulin content was determined by the Bradford assay, while eosin was quantified by monitoring the absorbance at 525 nm with $\varepsilon=88000$ M⁻¹cm⁻¹. PDI disulfide reductase activity was monitored as an increase in fluorescence at 545 nm ($\lambda_{ex}$ 525 nm) due to the cleavage of a and b insulin chains. Inhibition of PDI-mediated insulin cleavage was performed in the presence of increasing caspase-3 concentrations (50-700 μg/ml).

### 5.3.9 S-nitrosation of caspase-3

S-nitrosated caspase-3 (caspase-3-SNO) was prepared as follows. Casapse-3 (1mg/ml) was incubated with the excess of DEA-NO for 1 hour at the room temperature, followed

by the chromatographic separation using Sephadex G-25 and 100 mM phosphate buffer

(pH 7.0). The activity of caspase-3-SNO was assessed by Ac-DEVD-AMC fluorescent

substrate (25 nM) in the absence (blank) and the presence of PDI (2 μM, sample).

Monitoring of NO release form caspase-3-SNO was performed using an NO-meter.

## 5.4 Results

### 5.4.1 Chelating agent dependent caspase-3 activation

Assay conditions for measuring caspase-3 activity in the literature generally employ chelating agents such as EDTA, as well as reducing agent DTT in order to maintain the active site cysteine in its reduced form (Karki *et al.*, 2005). We first sought to determine the kinetic parameters of recombinant caspase-3 in the presence and absence of chelating and reducing agents. As seen in Figure 5.1, EDTA (triangles) totally abolished the need for employing reducing agent such as DTT (diamonds) or GSH (squares), suggesting that the activation of caspase-3 mainly depends on the presence of contaminating metal ions, which could inactivate caspase-3 by interfering with its active site cysteine required for the enzymatic activity. In the absence of EDTA (Figure 5.2), DTT (diamonds) was more successful in activating caspase-3 that GSH (squares). The apparent Km of caspase-3 was estimated to be ~20 ± 2 μM in the presence of EDTA (± DTT, GSH, Figure 5.1) and ~15 ± 2 μM in the absence of EDTA (+ DTT, Figure 5.2).
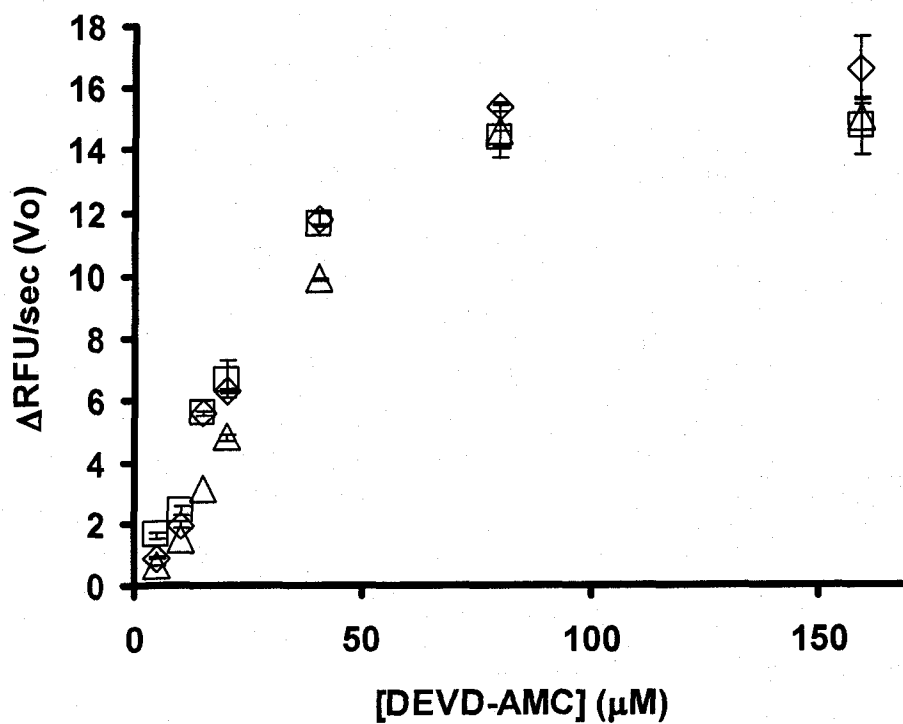
**Figure 5.1: Chelating and reducing agent dependent activation of caspase-3**

A. Caspase-3 (25 nM) activity was monitored over 15 min with increasing concentrations of Ac-DEVD-AMC, in the presence of EDTA (2 mM, △), EDTA and DTT (2 mM and 1 mM, respectively, ◊) and EDTA and GSH/GSSG (2 mM and 1/0.5 mM, respectively, □). All rates were corrected with corresponding blanks which did not contain caspase-3 (n=4). ($\lambda_{ex}$. 360 nm, $\lambda_{em}$. 460 nm)
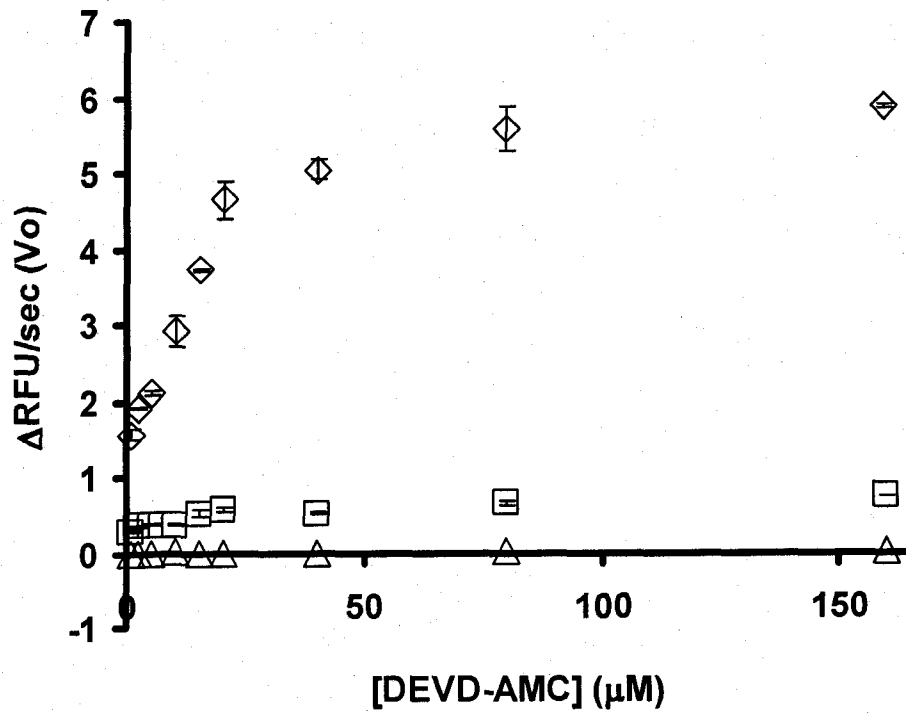
B. Caspase-3 (25 nM) activity was monitored over 15 min with increasing concentrations of Ac-DEVD-AMC, in the absence of reducing agent ($\triangle$), and in the presence of DTT (1 mM, $\lozenge$) and GSH/GSSG (1/0.5 mM, $\square$). All rates were corrected with corresponding blanks which did not contain caspase-3 (n=4).

## 5.4.2 Identification of metal ions responsible for caspase-3 inactivation

In order to identify the metal ions responsible for caspase-3 inhibition, the activity of the enzyme was measured in the presence of different metal ion chelators. As shown in Figure 5.2, besides EDTA, desferoxamine (DFO, 100 μM) was more successful than neocuproine in restoring caspase-3 (25 nM) activity. DFO is the metal chelator with the highest affinity of Fe(III). Therefore, the results obtained here suggested that iron may be responsible for inhibiting caspase-3 activity. To further test this hypothesis, the activity of caspase-3 was measured in a metal free buffer prepared in MiliQ water and treated with Chelex-100 resin. As expected, caspase-3 was active in the absence of metal free ions. Upon addition of 1-100 μM Fe(III) to 25 nM enzyme, ~90% of the initial activity was lost. The $IC_{50}$ estimated for Fe(III) mediated inhibition of caspase-3 was ~7 ± 2 μM (Figure 5.3).
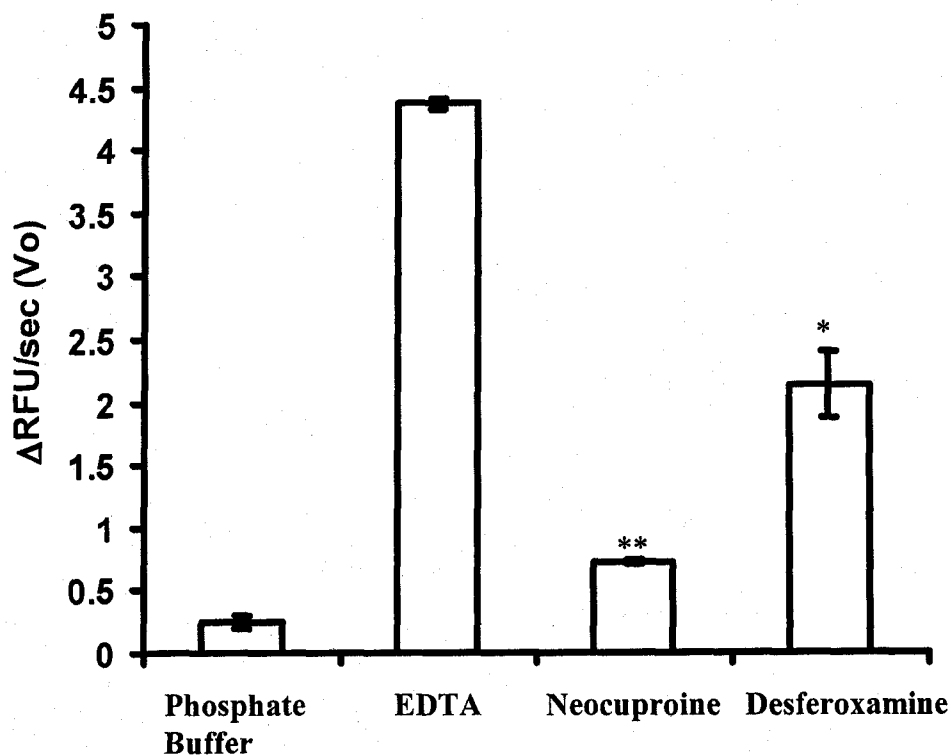
**Figure 5.2: Chelating agent dependent activation of caspase-3.**

Capsase-3 (25 nM) activity was monitored over 15 minutes in the presence of Ac-DEVD-AMC (20 μM). Assay buffer contained 100 mM phosphate, pH 7.0, EDTA (100 μM), neocuproine (100 μM), or desferoxamine (100 μM). Final rates were obtained by correcting for the blank rates without caspase-3 and represented as the percentage of the highest rate (*P=0.01 compared to EDTA, **P=0.001 as compared to phosphate buffer, n=4).
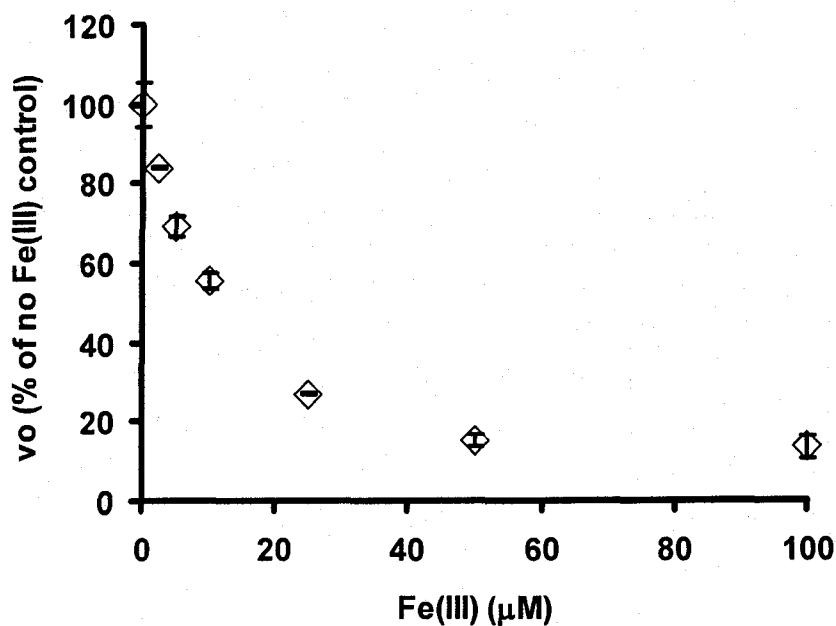
**Figure 5.3: Iron dependent inhibition of caspase-3 activation.**

Caspase-3 (25 nM) activity was assessed by Ac-DEVD-AMC (20 μM) in the presence of increasing iron concentrations (1-100 μM) in the iron-free phosphate buffer (<50 nM as established by the iron determination as described under "Experimental Methods"). The initial rates were measured over 15 minutes and corrected for the corresponding controls without caspase-3. The rates are represented as the percent of caspase-3 without iron (n=4).

### 5.4.3 The ability of PDI to activate caspase-3

Next, we investigated the possibility of PDI to act as a metal chelator since its active site with CXXC motif is similar to [2Fe-2S]-ferrodoxin iron binding domains (Tsukihira *et al.*, 1981). To test this hypothesis, caspase-3 (25 nM) was incubated in a phosphate buffer (100 mM, pH 7.0) and no detectable activity was observed. To this sample, an increasing amounts of PDI (25 nM to 2.5 µM) were added. The result was a PDI-dependent increase in caspase-3 activity (Figure 5. 4 A). In a similar experiment, time dependent caspase-3 activity was monitored in a phosphate buffer (Figure 5.4 B, black diamonds). Addition of DFO (100 µM) gave a rise to an initial rate of 0.3 µM/min (Figure 5.4 B, white diamonds). In the presence of PDI (1 µM) the initial rate was ~ 2.5-fold larger than observed with DFO alone (Figure 5.4 B, black squares). The rate with PDI and DFO (Figure 5.4 B, white squares) was relatively close to the rate with PDI only, suggesting that PDI alone was successful in removing contaminating iron. These results also suggest that PDI was a better chelator than DFO and raises the possibility that DFO bound iron can still bind to the caspase-3 active site to some extent and partially inactivate it.

In a further attempt to demonstrate the PDI-mediated activation of caspase-3 was related to Fe(III), PDI (1 µM) and caspase-3 (25 nM) were added to a metal free buffer and the initial rates of Ac-DEVD-AMC cleavage were monitored as a function of [Fe(III)] (1-100 µM). Under these conditions, PDI-activated caspase-3 activity decreased by ~80% in an [Fe(III)]-dependent manner with an apparent $IC_{50}$ of ~3 ± 1 µM (Figure 5.4 C).
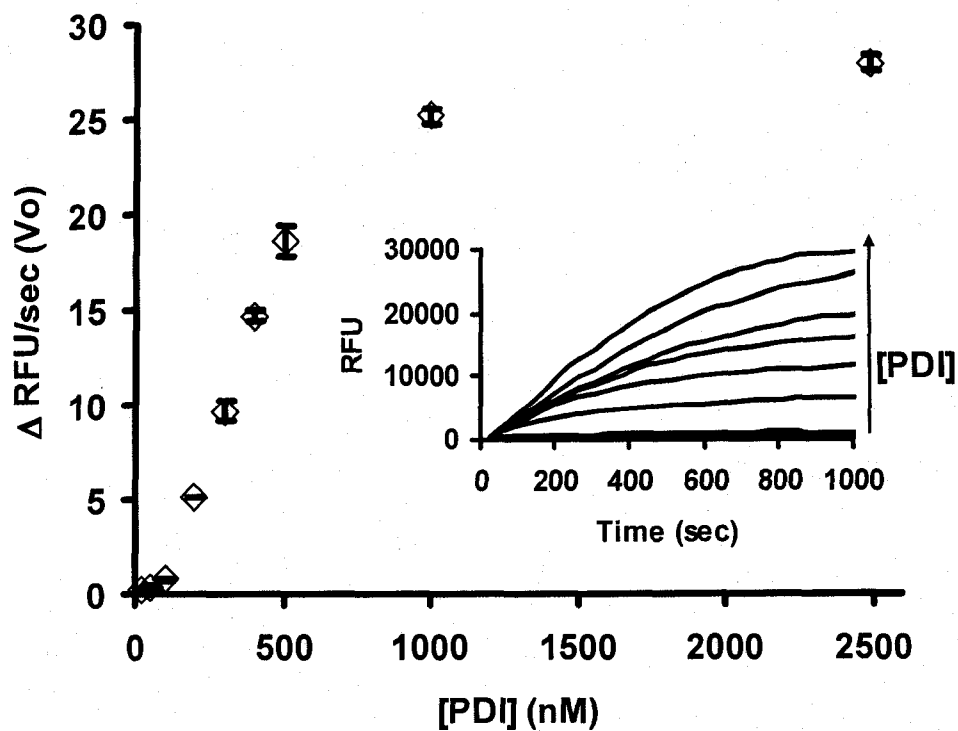
**Figure 5.4: PDI dependent caspase-3 activation.**

A. Initial rates of caspase-3 activation were monitored in the presence of increasing PDI

concentrations (25-2500 nM), using Ac-DEVD-AMC (20 µM) as a caspase-3 substrate,

over 15 minutes (inset). Final rates due to presence of PDI were obtained by subtracting

the blank which contained caspase-3 only (n=4).
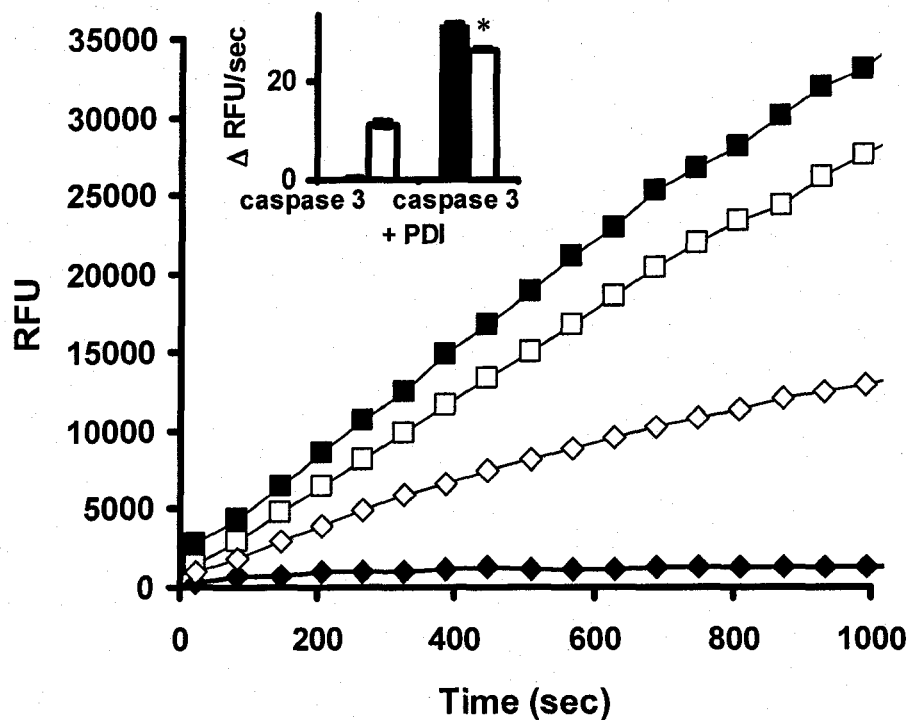
B. The role of PDI (1 μM) dependent caspase-3 (25 nM) activation was measure in the

presence (white bars) and absence (blank bars) of DFO (100 μM), using Ac-DEVD-AMC

(20 μM) as a substrate for caspase-3. Traces shown are representative of caspase-3

activity in phosphate buffer without (black diamonds) or with PDI (black squares), and

DFO (100 μM) containing buffer without (white diamonds) or with PDI (white squares).

The initial rates of caspase-3 activation in the phosphate buffer are represented by the

black bars, and in the presence of DFO by the white bars (inset). ($*P=0.001$, n=4).
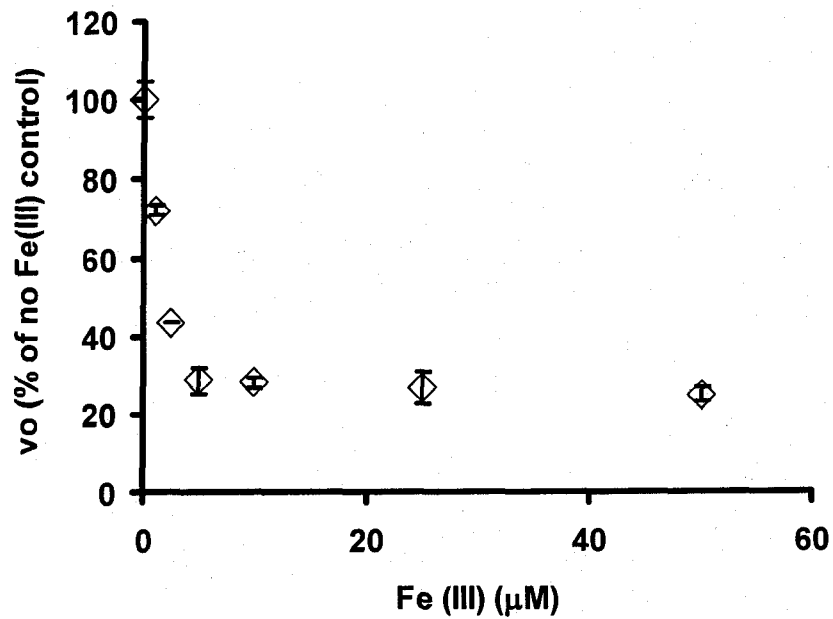
C. Caspase-3 (25 nM) activity was monitored by Ac-DEVD-AMC (20 $\mu$M) in the presence of PDI (1 $\mu$M) and increasing iron concentrations (1-100 $\mu$M). The initial rates of caspase-3 activity were monitored over 15 minutes, and subtracted for the control which did not contain caspase-3 (n=4).

Next we asked if iron-dependent caspase-3 activation was a reversible process. The initial rate of DEVD-AMC cleavage due to a freshly prepared caspase-3 (25 nM) was inhibited by the addition of iron (50 μM) (Figure 5.5 A, grey trace), and the activity was successfully restored by the addition of DFO (100 μM) in the time dependent manner. Similarly, caspase-3 inhibited by the addition of iron, was successfully restored in the presence of DTT (1 mM) (Figure 5.5 B, black trace) or PDI (2 mM) (Figure 5.5 B, grey trace). These findings prompted us to investigate whether active site thiols are essential for PDI-mediated caspase-3 activation.
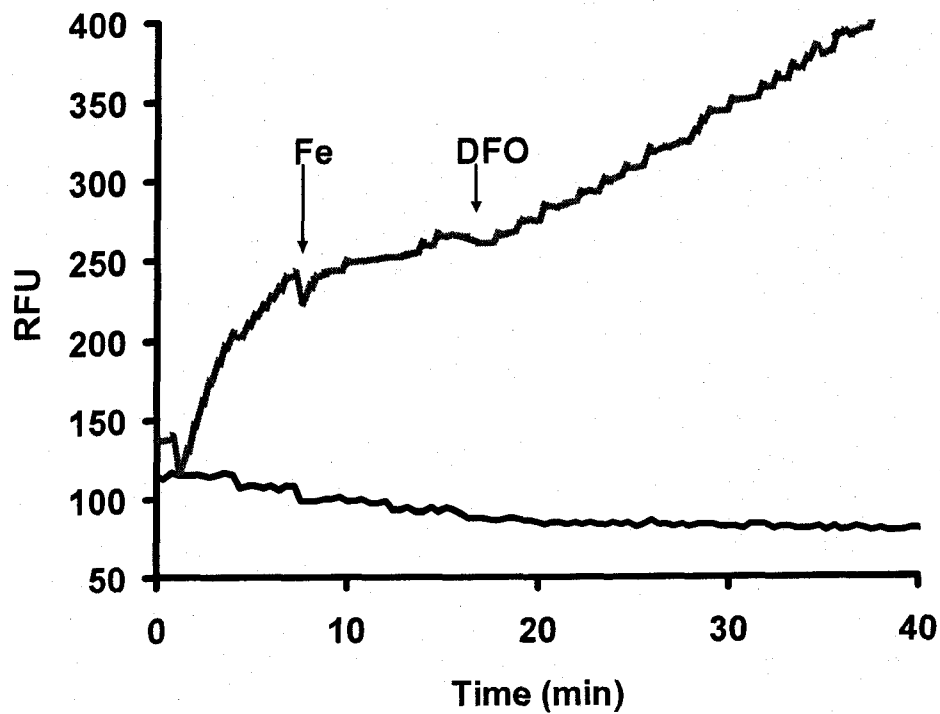
**Figure 5.5: Reversible activation of iron-inhibited caspase-3.**

A. Caspase-3 (25 nM) activity in the iron-free phosphate buffer, pH 7.0, was inhibited by

the addition of iron (50 μM), and followed by the reactivation with DFO (100 μM) (grey

trace). Blank (black trace) received the same treatment and did not contain any caspase-3

(n=3).
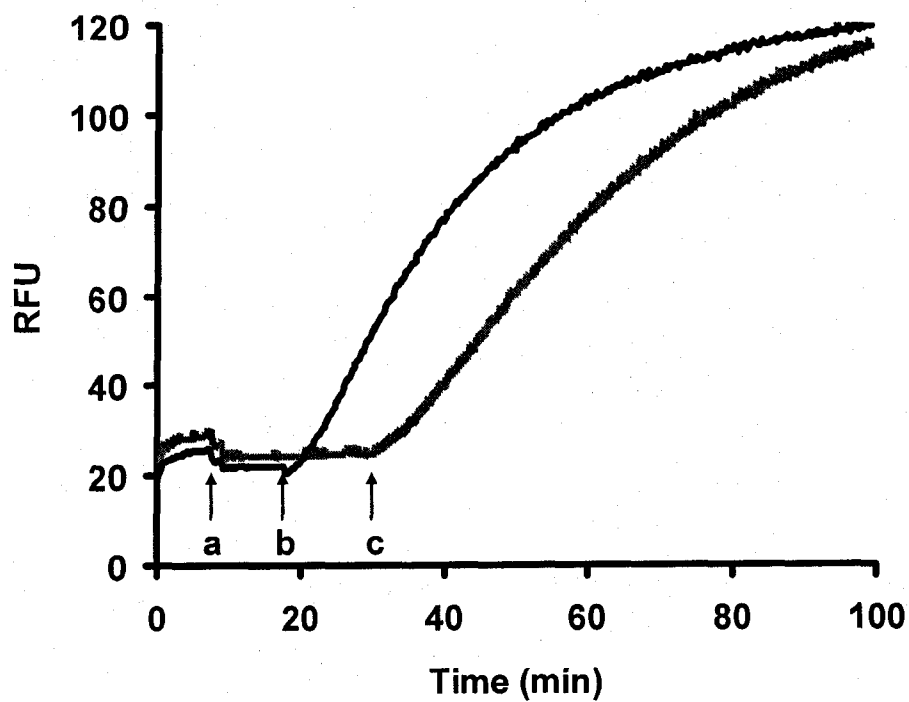
B. Caspase-3 (25 nM) activity was inhibited by addition of iron (50 μM) (*a*), followed

by reactivation by DTT (1 mM) (black trace, *b*) or PDI (2 μM) (grey trace, *c*) (n=3).

## 5.4.4 The role of PDI active site thiols in caspase-3 activation

Caspase-3 activity was monitored in the presence of oxidized PDI (PDI-SSG). As shown in Figure 5.6 A, the activity of caspase-3 in the presence of either DTT (diamonds) or PDI-SSG (line) was not significantly different from the activity of caspase-3 only (asterisk). Addition of DTT (1 mM) to PDI-SSG (1 $\mu$M) significantly increased caspase-3 activity (triangles). Next, we prepared chemically modified PDI using a thiol specific blocker N-ethylmaleimide (NEM). Results obtained demonstrated that modification of PDI active site thiols by NEM prevents caspase-3 activation (Figure 5.6 B). In light of these results, the ability of native PDI to bind iron was tested. PDI pretreated with iron was found to bind ~ 2 moles of iron per mole of active site thiols (Figure 5.7), suggesting that PDI-dependent caspase-3 activation is most likely due to the ability of PDI active site thiols to coordinate with iron.
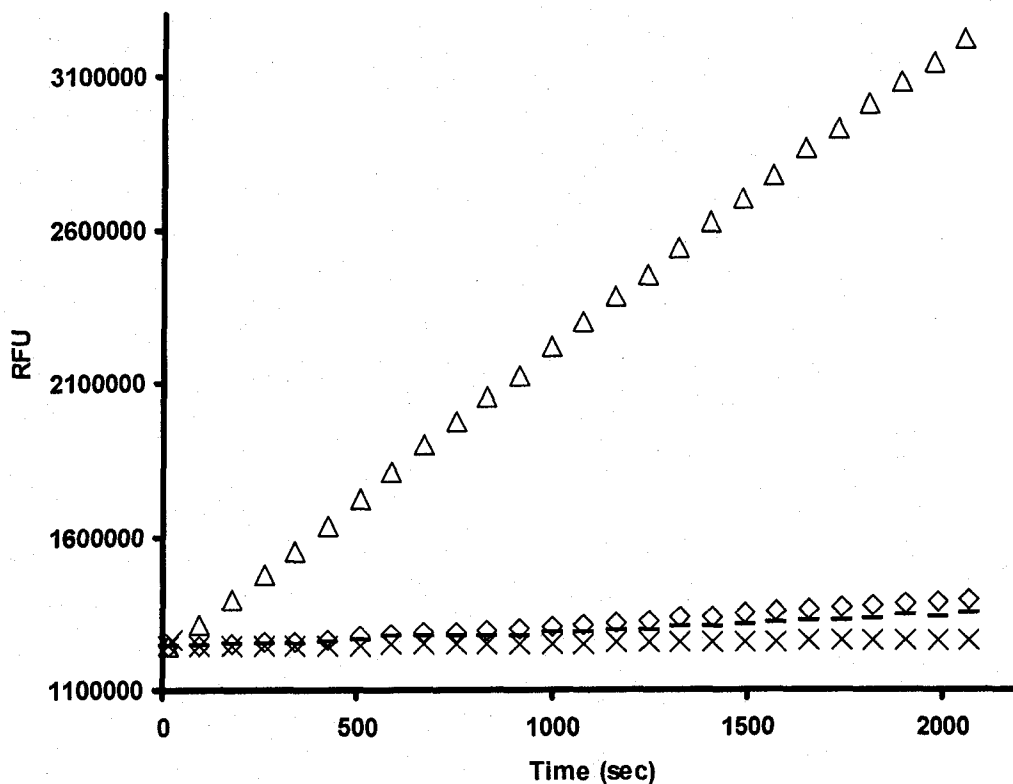
**Figure 5.6: Active site thiols are essential for caspase 3 activation.**

A. Caspase 3 (25 nM) activation was monitored in the presence of oxidized PDI (1 μM) with or without DTT (1 mM), using Ac-DEVD-AMC (20 μM) as a substrate. Caspase-3 (asterisk), caspase-3 and DTT (diamond), caspase-3 and PDI-SSG (black line) and caspase-3 and PDI-SSG in the presence of DTT (triangle). PDI-SSG was prepared as outlined under "Experimental Methods" (n=3).
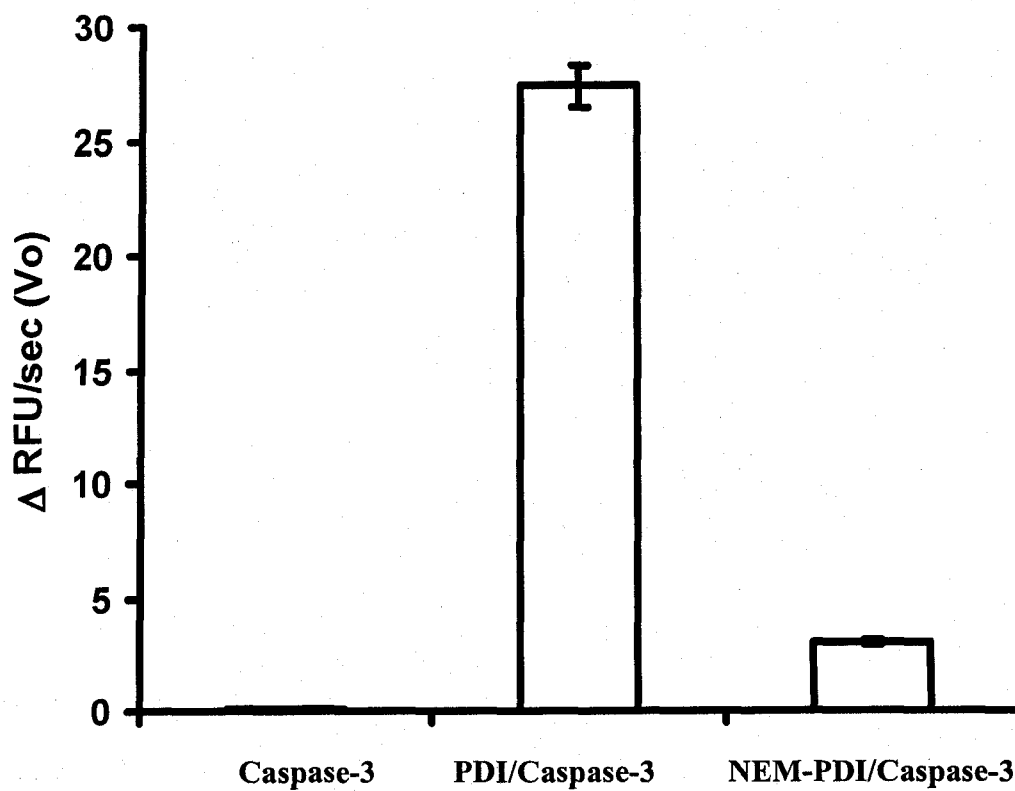
B. Caspase-3 (25 nM) activity was monitored in the absence and presence of PDI and NEM-blocked PDI (1 μM) over 15 minutes, using Ac-DEVD-AMC (20 μM). NEM-blocked PDI was prepared as outlined in "Experimental Methods" (n=4).
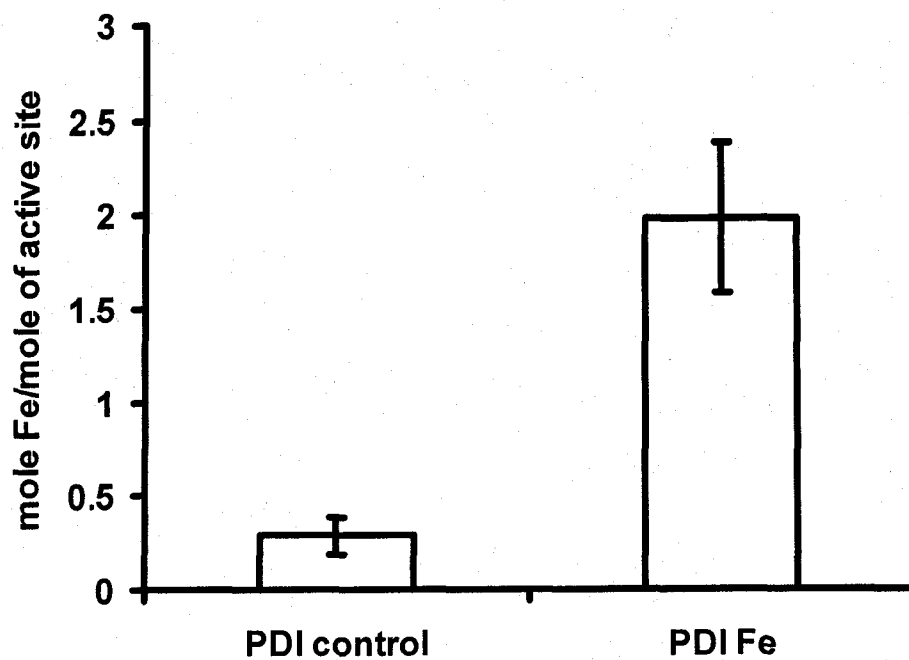
**Figure 5.7: PDI-bound iron detection.**

Iron estimation was performed for the PDI samples without iron (PDI control) and with excess iron incubation (PDI-Fe). Assay was carried out as described in "Experimental Methods" (n=4).

### 5.4.5 The effects of caspase-3 on PDI activity

The effects of caspase-3 on PDI activity was carried out using two different methods. PDI refolding activity was monitored using reduced and denatured lysozyme as a substrate. In the presence of caspase-3 (800 μg/ml) the PDI ability to refold denatured lysozyme decreased ~80% as compared to the control (Figure 5.8 A). Next, we used the PDI reductase activity by means of monitoring insulin cleavage of FITC labeled insulin which results in an increase in fluorescence. As shown in Figure 5.8 B, caspase-3 was able to inhibit PDI-mediated insulin cleavage in a concentration dependent manner (50-700 μg/ml).
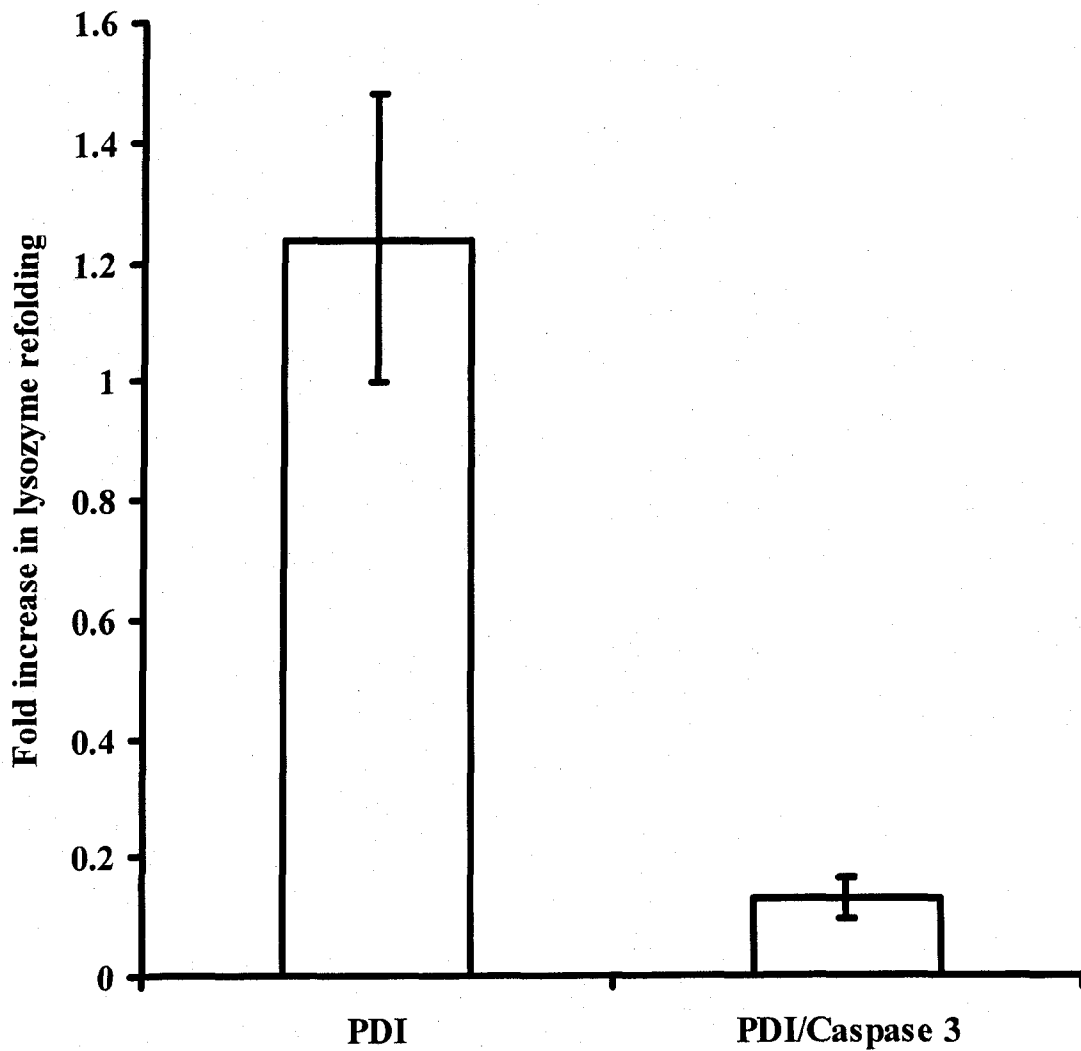
**Figure 5.8: The role of caspase-3 on PDI enzymatic activity.**

A. Lysozyme (5 μM) refolding activity was monitored in the presence of PDI only (250 nM) and PDI and caspase 3 (800 μg/ml). Presence of caspase 3 decreased the PDI refolding activity of lysozyme by ~90% (n=4).
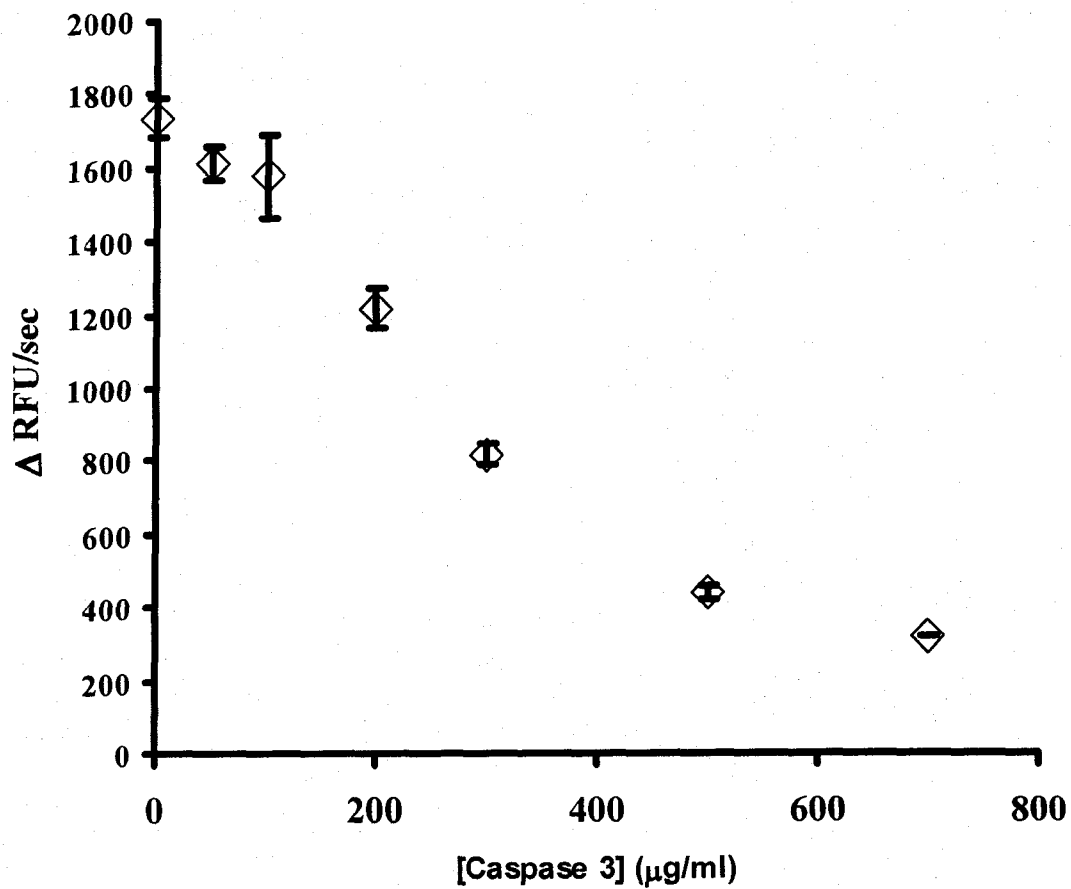
B. Caspase 3 concentration dependent inhibition of PDI insulin disulfide exchange activity was monitored in the presence of caspase 3, PDI (25 nM) and eosin-insulin (25 nM) probe (n=3).

## 5.4.6 The role of nitric oxide in caspase-3 activation

S-nitrosation of caspase-3 results in the reversible inhibition of the enzyme. To test the possibility of PDI to activate S-nitrosated caspase-3 (caspase-3-SNO), the activity due to the cleavage of Ac-DEVD-AMC was monitored in the presence of caspase-3-SNO and caspase-3-SNO and PDI. As seen in Figure 5.9 A, PDI was able to increase caspase-3-SNO activity by ~10 fold. In order to investigate if this activation was due to the NO release from caspase-3-SNO, a NO-meter was employed. Control samples containing caspase-3 only did not change its signal upon the addition of PDI (Figure 5.9 B, black trace). However, when PDI (2.2 $\mu$M) was added to the vial containing caspase-3-SNO, an increase in current was observed (grey trace), a representative of NO generation.
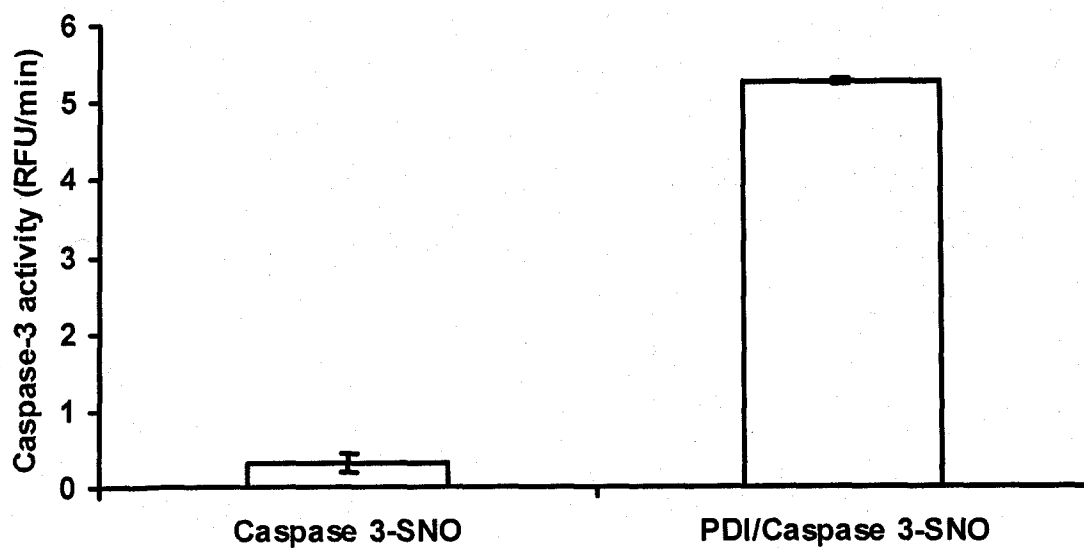
**Figure 5.9: PDI dependent Caspase-3 activation monitored by DEVD-AMC**

**cleavage.**

A. Activation of Caspase 3 and nitrosated Caspase 3 (Caspase 3-SNO) (2 μg/ml) was

monitored in the presence or absence of PDI (2 μM) over time. Fold increase was

obtained by correcting the PDI/caspase 3 rates with respect to caspase 3 rates (n=4).
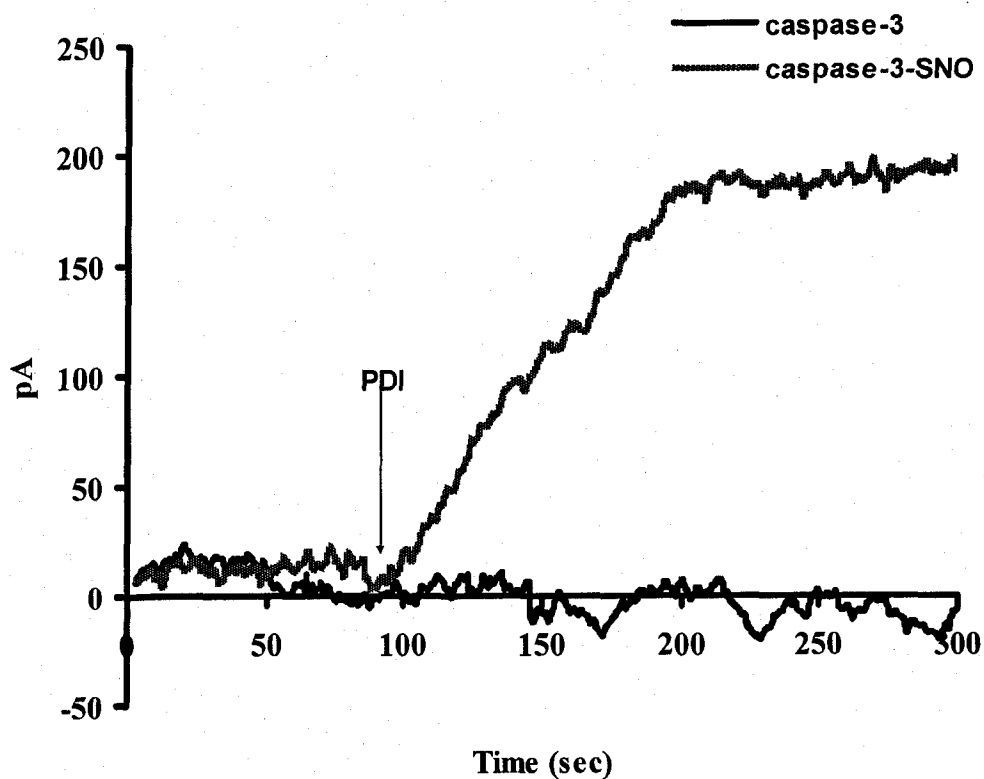
B. Caspase-3-SNO (2 μg/ml) was placed in the vial containing 100 mM phosphate buffer

(pH 7.0) and the current was measured for 100 seconds. At that time PDI (2.2 μM, grey

trace) or buffer (black trace) was added and the increase in current reflecting the release

of NO was monitored until saturation was obtained (n=3).

## 5.5 Discussion

The initial experiments of this study dealt with establishing kinetic parameters for caspase-3 activity with respect to its fluorogenic substrate Ac-DEVD-AMC. Initial findings were unexpected and suggested that caspase-3 activity is mainly dependent on the presence of metal chelators, and the presence of reducing agents such as DTT and GSH did not result in the change in activity (Figure 5.1 A). Next, we performed a set of experiments to determine which metal was responsible for caspase-3 inhibition. For this purpose, caspase-3 activity assay was performed in the presence of a non-specific metal chelator EDTA, as well as iron and copper specific metal chelators desferoxamine (DFO) and neocuproine, respectively. The results obtained showed that the caspase-3 activity was restored in the presence of a specific iron(III) chelating agent DFO (Figure 5.2). This finding was supported by the additional evidence with iron(III) dependent inhibition of caspase-3 activity with $IC_{50}$ of ~7 ± 2 μM which corresponds to a 90% inhibition of the original activity (Figure 5.3).

Activity of caspase-3 was also restored in the presence of PDI in the concentration dependent manner (Figure 5.3 A). In addition, PDI appeared to be a better chelating agent than DFO in that a 100-fold lower concentration of PDI was able to yield a ~2-fold larger activity from fully iron-inactivated caspase-3 (Figure 5.3 B). One possibility for this is that the DFO-Fe(III) complex is relatively small and can still interact with the caspase-3 active site and partially block its activity. On the other hand, this is not possible with a much larger PDI-Fe(III) complex. PDI dependent caspase-3 activation was attenuated by the addition of iron (Figure 5.3 C) with an estimated $IC_{50}$ of ~3 μM.

The results obtained so far provided a direct evidence of caspase-3 inhibition by Fe(III), which supports previous observations that iron chelating agents can induce apoptosis in various cancer cell lines (Jiang *et al.*, 2002; Wang *et al.*, 1999).

Up until now, NO and $H_2O_2$ have been shown to reversibly inactivate caspase-3 (Kim *et al.*, 1997; Borutaite and Brown, 2001; Tannenbaum and Kim, 2005). In this study, we were able to show that iron(III) can also reversibly regulate caspase-3 activity, most likely by interacting with active site $Cys^{285}$ since inactivation is reversible by thiol reductant (Figure 5.1 B) as well as iron chelators (Figure 5.1 A). In addition, our data does not preclude iron interacting at the allosteric sites elsewhere in the molecule. A role of iron(III) in inactivating caspase-3 was established by the effect of iron(III) specific chelator DFO on restoring caspase-3 activity (Figure 5.5 A) and by the direct inhibition of caspase-3 and PDI-activated caspase-3 (Figures. 5.3 and 5.4 C). The fact that the inhibition by iron(III) is reversible with DFO and PDI, suggests that iron does not play a role in altering the oxidation state of the active site $Cys^{285}$.

Next, we attempted to establish if PDI active site thiols are required for caspase-3 activation. Our data demonstrates that either oxidation (Figure 5.6 A) or chemical modification (Figure 5.6 B) of PDI active site thiols inhibits PDI-mediated caspase-3 activation. Previous reports demonstrated that PDI-like proteins such as glutaredoxin are able to form iron-sulfur complexes (Lillig *et al.*, 2005). PDI was found to bind iron at 2:1 iron:cysteine thiol ratio suggesting that PDI most likely binds iron(III) through its active

site thiols, as it was shown to bind zinc and copper (Narindrasorasak *et al.*, 2003; Solovyov and Gilbert, 2004).

In order to be active, caspase-3 forms a heterodimer (Grutter, 2000). We sought to test the possibility of PDI interacting with caspase-3. Caspase-3 was able to inhibit PDI lysozyme refolding activity by 90% (Figure 5.8 A) and disulfide reductase activity of insulin (Figure 5.8 B) in a concentration dependent manner. These results suggest that PDI may be interacting with caspase-3 probably through its active site thiols, since the active site is required for both of the PDI activities tested. Although there is also a possibility of PDI assisting the folding of caspase-3 heterodimer, since previous studies have suggested that PDI requires all of its domains for its chaperone activity (Sun *et al.*, 2000). Therefore, PDI does not only remove iron(III) but likely keeps caspase-3 active site in its reduced state, resulting in improved caspase-3 activity. Lastly, the possibility of PDI activating caspase-3-SNO was tested. Previous studied showed that S-nitrosated caspase-3 is reversibly inhibited (Kim *et al.*, 1997; Tannenbaum and Kim, 2005), and also that PDI is able to denitrosate small molecular weight thiols and S-nitrosated proteins (Sliskovic *et al.*, 2005). Therefore, it was of a great interest to test whether PDI is able to restore the activity of S-nitrosated caspase-3. The results obtained using a fluorogenic caspase-3 substrate demonstrated that PDI was able to reactivate caspase-3-SNO (Figure 5.9 A) by removing NO moiety from caspase-3 active site (Figure 5.9 B).

Based on our findings, we are proposing a physiological role for both iron(III) and PDI in the modulation of caspase-3 activity and in the process regulating apoptosis. Previous

studies showed a correlation between cancer cells and increased iron levels due to i)

increased expression of transferrin receptor (Inoue *et al.*, 1993), ii) increased ferritin (iron

storage) secretion (Toyokuni, 1996), and iii) ability of desferoxamine to induce apoptosis

in cancer cells (Crichton and Ward, 1992). Here we show that a potential target of

iron(III) is caspase-3, a central regulator of apoptosis. Therefore, we propose the

mechanism illustrated in Scheme 5.3 for the regulation of apoptosis by Fe(III) and PDI.
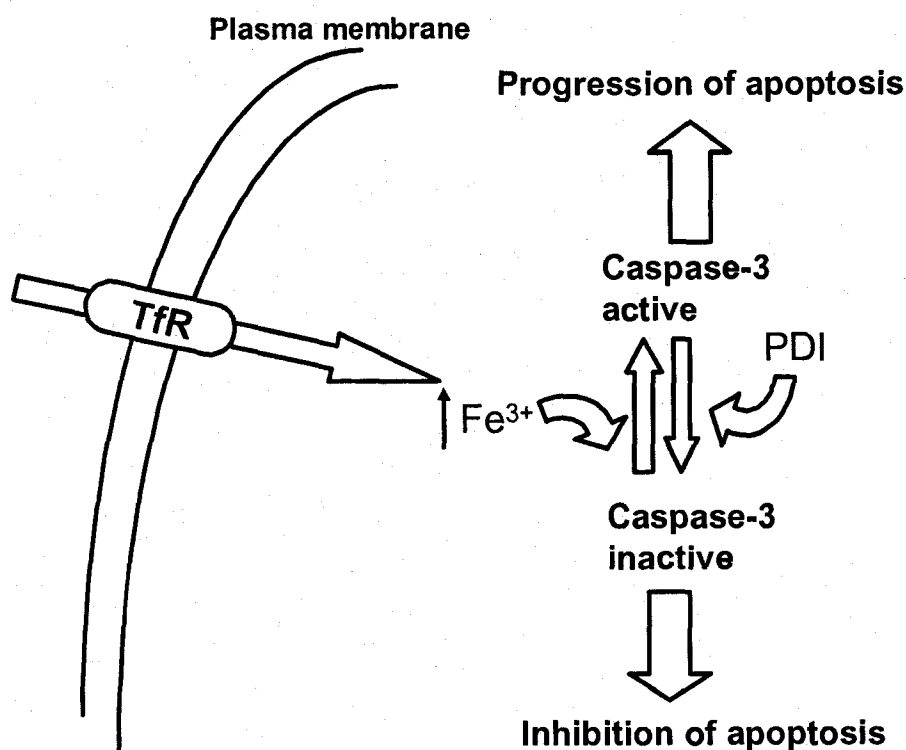


**Scheme 5.3 Proposed mechanism of caspase-3 regulation in cancer cells.**

Cells upon becoming cancerous, upregulate transferrin receptor resulting in an increase of

intracellular iron(III), which subsequently inactivates caspase-3 thus arresting apoptosis.

In cells that successfully upregulate and secrete PDI, blocking of caspase-3 activity by iron(III) could result in re-initiation of apoptosis and cell death. This suggests that substances that induce PDI overexpression (Tanaka *et al.*, 2000) could potentially be employed as a new anti-cancer therapeutics.

# CHAPTER 6

# Conclusions

Protein disulfide isomerase (PDI) is a multifunctional eukaryotic protein expressed throughout the cell. The most studied function of PDI is its ability to participate in disulfide bond isomerization of newly synthesized proteins in the endoplasmic reticulum. However, recent findings from our lab suggested that cell surface-associated PDI mediates nitric oxide ($\bullet$NO) release from extracellular S-nitrosothiols (RSNO) thus participating in the $\bullet$NO transport across the membrane. $\bullet$NO is the small signaling molecule involved in many cellular processes such as smooth muscle relaxation, modulation of neurotransmission, platelet activation, to name a few. The work presented here focused on the role of csPDI in mediating $\bullet$NO regulated processes.

In Chapter 2, we characterized the S-denitrosation activity of PDI using S-nitrosoglutathione (GSNO) as a model. The hemoglobin assay provided strong evidence that the main product of PDI denitrosation activity is $\bullet$NO. Based on our findings, we proposed a novel catalytic mechanism for PDI-dependent GSNO consumption which involves the formation of a nitroxyl disulfide intermediate that undergoes a one-electron oxidation resulting in the generation of $\bullet$NO and dithiyl radical. The evidence for generation of thiyl/dithiyl radicals was provided using a specific thiyl/dithiyl radical probe. In the presence of excess $\bullet$NO, PDI becomes an $\bullet$NO carrier via an $N_2O_3$-mediated auto-S-nitrosation of its active site thiols (PDI-SNO). This PDI-SNO could then be denitrosated by another PDI, suggesting that this enzyme may be intimately involved in mediating the $\bullet$NO influx and efflux across the membrane.

In Chapter 3, we demonstrated the role of platelet csPDI-dependent GSNO consumption resulting in •NO generation. Previous studies have shown that platelet csPDI facilitates platelet aggregation through its disulfide exchange activity. On the contrary, •NO can inhibit platelet aggeration through the GC/PKC pathway. Our study demonstrated that platelet GSNO can inhibit platelet aggregation by occupying active site thiols of PDI which are required for ligand-integrin disulfide exchange reaction. It has been observed that platelets of both diabetic humans and animal model of diabetes have elevated reactive oxygen species (ROS) levels that promote platelet aggregation. Our results suggested that there is a relationship between increased ROS levels and PDI-regulated activities. Platelets obtained from an animal model of pre-diabetes had significantly higher ROS levels relative to control, accompanied by diminished PDI denitrosation activity and increased platelet aggregation rates. All of the activities monitored were successfully restored in the presence of rosuvastatin an HMG-CoA reductase inhibitor, suggesting that this drug might have beneficial effects other than the lowering of cholesterol. The redox state of PDI active sites directs its catalytic functionality. Therefore, the ability to monitor and identify the dynamic changes in redox state of PDI active site thiols may provide insight into how this enzyme is regulated. Our results demonstrated that ICAT-MALDI technology may be a suitable method for detecting the changes in **a** domain active site thiols, while active site thiols in **a'** domain appears to exist mainly in oxidized form.

Chapter 4 investigated the role of ghost-associated PDI in the transport of NO. Currently, it is believed that •NO exits red blood cells (RBC) via formation of S-NO proteins such

as anion transporter (AE1). Our results showed that in the presence of excess •NO, PDI disulfide exchange activity and thiols concentration decrease due to formation of PDI-SNO. Based on our findings we proposed the PDI-mediated •NO efflux from RBC, where the cytosolic PDI could be nitrosated by hemoglobin-SNO and transport the NO equivalents to the ghost-associated PDI which, in turn, could exit the RBC and deliver NO to nearby cells.

In Chapter 5 we described a novel role of PDI in regulation of apoptosis. Caspase-3 activity was inhibited in the presence of iron(III), which could be reversed by the addition of iron(III) specific chelator desferoxamine or by PDI. PDI was able to activate iron(III) inhibited caspase-3 in a concentration dependent manner, most likely through the formation of iron-sulfur complexes through its active site thiols. Therefore, our results suggest that iron(III) could be a potential inhibitor of apoptosis through caspase-3 dependent inhibition, with a possibility of recovery through PDI overexpression in cells.

# REFERENCES

Abu-Soud, H. M., Stuehr, D. J. (1993), *Proc. Natl. Acad. Sci. U.S.A*, **90**, 10769-10772.

Alderton, W. K., Cooper, C. E., Knowles, R. G. (2001), *Biochem. J.* **357**, 593-615.

Alloisio, N., Texier, P., Denoroy, L., Berger, C., Miraglia del Giudice, E., Perrotta, S., Iolascon, A., Gilsanz, F., Berger, G., Guichard, J., Masse, J. M., Debili, N., Breton-Gorius, J., Delaunay, J. (1996), *Blood.* **87**, 4433-4439.

Alonso, D., and Radomski, M. W. (2003), *Heart Failure Rev.* **8**, 47-54.

Ando, S., Kaibuchi, K., Sasaki, T., Hiraoka, K., Nishiyaa, T., Mizuno, T., Asada, M., Nunoi, H., Matsuda, I., Matsuura, Y., Polakis, P., McCormic, F., Takai, Y. (1992), *J. Biol. Chem.* **267**, 25709-25713.

Arnelle, J. S., and Stamler, J. S. (1995), *Arch. Biochem. Biophys.* **318**, 279–285.

Aslund, F., Berndt, K. D., Holmgren, A. (1997), *J. Biol. Chem.* **272**, 30780-30786.

Balbatun A, Louka, F. R., Malinski, T. (2003), *Acta Biochimi. Pol.* **50**, 61-68.

Bassuk, J. A., Kao, W. W., Herzer, P., Kedersha, N. L., Seyer, J., DeMartino, J. A., Daugherty, B.L., Mark, G. E. 3rd., Berg, R. A. (1989), *Proc Natl Acad Sci U S A.* **86**,7382-7386.

Bath, P. M. V., Hassall, D. G., Gladwin, A. M. (1991), *Atherioscler. Thromb. 11*, 254-260.

Bazylinski, D. A., and Hollocher, T. C. (1985), *J. Am. Chem. Soc.* **107**, 79828–79860.

Bendtzen, K., Mandrup- Poulsen, T., Nerup, J., Nielsen, J. H., Dinarello, C. A., Svenson, M. (1986), *Science.* **232**, 1545-1547.

Bennett, T. A., Edwards, B. S., Sklar, L. A., Rogelj, S. (2000), *J. Immunol.* **164**, 4120-4129.

Berger, E.A., Murphy, P. M., Farber, J. M. (1999), *Annu. Rev. Immunol.* **17**, 657–700.

Borisenko, G. G., Martin, I., Zhao, Q., Amoscato, A. A., Kagan, V. E. (2004), *J. Am. Chem. Soc.* **126**, 9221–9232.

Borutaite, V., and Brown, G. C. (2001), *FEBS Lett.* **500**, 114-118.

Bradford, M. M. (1976), *Anal. Biochem.* **72**, 248–254.

Brewer, D. B. (2006), *Br. J. Haematol.* **133**, 251-258.

Buga, G. M., and Ignarro, L. J. (2000), *In* "Nitric Oxide: Biology and Pathobiology", (L. J. Ignarro, ed), pp. 895-920, Academic Press, San Diego.

Bulleid, N. J. (1993), *Adv Protein Chem.* **44**, 125-150.

Cai, H., Wang, C. C., Tsou, C. L. (1994), *J. Biol. Chem.* **269**, 24550-24552.

Calmels, S., Hainaut, P., Ohshima, H. (1998), *In* "Nitric Oxide and the Cell", (Moncada, S., Nistico, G., Bagetta, G., Higgs, E. A., eds), pp. 277-292, Portland Press, London.

Cassoly, R., and Gibson, Q. H. (1975), *J. Mol. Bio.* **91**, 301-313.

Chen, K., Detwiler, T. C., and Essex, D. V. (1995), *Br. J. Haematol.* **90**, 425–431.

Chen, K., Lin, Y., Detwiler, T. C. (1992), *Blood.* **79**, 2226-2228.

Clancy, R. M., Leszczynska, P., Piziak, J., Abramson, S. B. (1992), *J. Clin. Invest.* **90**, 1116-1121.

Clancy, R. M., Levartivsky, D., Leszczynska-Piziak, J., Yegudin, J., Abrason, S. B. (1994), *Proc. Natl. Acad. Sci. U.S.A.* **91**, 3680-3684.

Collet, J.-F., Riemer, J., Bader, M. W., and Bardwell, J. C. A. (2002), *J. Biol. Chem.* **277**, 26886–26892.

Collins, R., Armitage, J., Parish, S., Sleight, P., Peto, R. (2004), *Lancet.* **363**, 757–767.

Cook, J. A., Kim, S. Y., Teague, D., Krishna, M. C., Pacelli, R., Mitchell, J. B., Vodovotz, Y., Nims, R. W., Christodoulou, D., Miles, A. M. et al. (1996) *Anal. Biochem.* **238**, 150–158.

Corbett, J. A., Lancaster, J. R., Jr., Sweetland, M. A., McDaniel, M. L. (1991), *J. Biol. Chem.* **266**, 21351-21354.

Corbett, J. A., and McDaniel, M. L. (1992), *Diabetes.* **41**, 897-903.

Crichton, R. R. and Ward, R. J. (1992), *Biochemistry.* **31**, 11255-11264.

Dai, Y., Wang, C. C. (1997), *J. Biol. Chem.* **272**, 27572-27576.

Danley, D. E. (1996), *J. Biol. Chem.* **271**, 11209-11213.

Darby, N. J., Freedman, R. B., Creighton, T. E. (1994), *Biochemistry.* **33**, 7937-7947.

Darby, N. J., Kemmink, J., Creighton, T. E. (1996), *Biochemistry,* **34**, 10517-10528.

Darby, N. J., Penka, E., Vincentelli, R. (1998), *J. Mol. Biol.* **276**, 239-247.

DeLorenzo, F., Goldberger, R. F., Steers, E., Givol, D., Anfinsen, C. B. (1966), *J. Biol. Chem.*, **241**, 1562-1567.

Dodge, J. T., Mitchell, C., Hanahan, D. J. (1963), *Arch. Biochem. Biophys.* **100**, 119-130.

Donoghue, N., Yam, P. T., Jiang, X. M., Hogg, P. J. (2000), *Protein Sci.* **9**, 2436-2445.

Eich, R. F., Li, T., Lemon, D. D., Doherty, D. H., Curry, S. R., Aitken, J. F., Mathews, A. J., Johnson, K. A., Smith, R. D., Phillips, G. N., Olsoon, J. S. (1996), *Biochemistry.* **35**, 6976-6983.

Ellgaard, L. (2004), *Biochem. Soc. Trans.* **32**, 663-667.

Ellgaard, L., and Ruddock, L. W. (2005), *EMBO reports.* **6**, 28-32.

Ellman, G. L. (1959), *Arch. Biochem. Biophys.* **82**, 70-77.

Emoto, Y., Manoe, Y., einhardt, G., Kisaki, H., Kharbande, S., Robertson, M., Ghayur, T., Wong, W. W., Kamen, R., Weichselbaum, R., Kufe, D. (1995), *EMBO J.* **14**, 6148-6156.

Essex, D. W. (2004), *Antiox. Red. Signal.* **6**, 736-746.

Essex, D. W. and Li, M. (1999), *Br. J. Haematol.* **104**, 448-454.

Essex, D. W., and Li, M. (2003), *Biochemistry.* **42**, 129-136.

Essex, D. W., Miller, A., Swiathowska, M., Feinman, R. D. (1999), *Biochemistry.* **38**, 10398-10405.

Feelisch, M. (1998), *Naunyn-Schmeideberg's Arch. Pharamcol.* **358**, 113-122.

Ferrari, D. M., Nguyen Van, P., Kratzin, H. D., Söling, H. D. (1998), *Eur. J. Biochem.* **255**: 570-579.

Ferrari, D. M., Söling, H. D. (1999), *Biochem. J.* **339**, 1-10.

Fish W. W. (1988), *Meth. Enzymol.* **54**, 357-364.

Forrester, M. T., Foster, M. W., Stamler, J. S. (2007), *J. Biol. Chem.* **282**, 13977-13983.

Forstermann, U., and Ishii, K. (1996), *In* "Methods of Nitric Oxide Research" (M. Feelisch and J. Stamler, eds), pp 556-566. Wiley, New York.

Foster, M. W., and Stamler, J. S. (2004), *J. Biol. Chem.* **279**, 25891-25897.

Franklin, S., Ghayur, T., Hackett, M. C., Hammill, L. D. (1994), *Cell.* **78**, 343-352.

Freedman, R. B., Hirst, T. R., Tuite, M. F. (1994), *Trends Biochem. Sci.* **19**, 331-336.

Freedman, R. B., Hawkins, H. C., McLaughlin, S. H. (1995), *Methods Enzymol.* **251**, 397-406.

Fuse, I. (1996), *Critical Rev. In Oncol/Hematolo.* **22**, 1-25.

Garg, U. C., Hassid, A. (1989), *J. Clin. Invest.* **83**, 1774-1777.

Gaston, B., Reilly, J., Drazen, J. M., Fackler, J., Ramdev, P., Arnelle, D., Mullins, M. E., Sugarbaker, D. J., Chee, C., Singel, D. J., Loscalzo, J., Stamler, J. S. (1993), *Proc. Natl. Acad. Sci. U.S.A.* **90**, 10957-10961.

Gilbert, H. F. (1997), *J. Biol. Chem.* **272**, 29399-29402.

Girard, P., Potier, P. (1993) *FEBS Lett.* **320**, 7–8.

Gobert, A. P., Vincendeau, P., Mossalayi, D., Veyret, B. (1999), *Nitric Oxide: Biol. and Chem.* **3**, 467-472.

Goldberger, R., Epstein, C., Anfinsen, C. B. (1963), *J. Biol. Chem.*, **238**, 628-635.

Gorren, A. C. F., Marchal, S., Sørlie, M., Andersson, K. K., Lange, R., Mayer, B. (2006), *Biochim. Biophys. Acta.* **1764**: 578-585.

Gregg, D., de Carvalho, D. D., Kovacic, H. (2004), *Antioxid. Redox Signal.* **6**, 757-764.

Grutter, M. G. (2000), *Curr. Opinion Struct. Biol.* **10**: 649-655.

Hart, T. W. (1985), *Tetrahedron Lett.* **26**, 2013-2016.

Hayano, T., Hirose, M., Kikuchi, M. (1996), *FEBS Lett.* **377**, 505-511.

Herold, S., Exner, M., Nausser, T. (2001), *Biochemistry.* **40**, 3385-3395.

Hevel, J. M., Marletta, M. A, (1994), *Methods Enzymol.* **233**, 250-258.

Hillson, D. A., Lambert, N. and Freedman, R. B. (1984), *Methods Enzymol.* **107**, 281–294.

Hobbs, A. J., and Ignarro, L. J. (1996), *Methods Enzymol.* **269**, 134-149.

Hobbs, A. J. (1997), *Trends Pharmacol. Sci.* **18**, 484-491.

Holmgren, A. (1979), *J. Biol. Chem.* **254**, 9627–9632.

Hotchkiss, K. A., Matthias, L. J., Hogg, P. J. (1998), *Biochim. Biophys. Acta.* **1388**, 478-488.

Houk, K. N., Hietbrink, B. N., Bartberger, M. D., McCarren, P. R., Choi, B. Y., Voyksner, R. D., Stamler, J.S., Toone, E. J. (2003), *J Am Chem Soc.* **125**,6972-6976.

Ignarro, L. J. (2000), *In* "Nitric Oxide: Biology and Pathobiology" (L. J. Ignarro, ed), pp. 3-19, Academic Press, San Diego.

Inoue, T., Cavanaugh, P. G., Steck, P. A., Brunner, N., Nicolson, G.L. (1993), *J. Cell. Physiol.* **156**, 212-217.

Jacobson, M. D., Well, M., Raff, M. C. (1997), *Cell.* **88**, 347-354.

Jaffrey, S. R., Erdjument-Bromage, H., Ferris, C. D., Tempst, P., Snyder, S. H. (2001), *Nat. Cell Biol.* **3**, 193-196.

Janicke, R. U., Walker, P. A., Lin, X. Y., Porter, A. G. (1996), *EMBO J.* **15**, 6969-6978.

Jensen, D., Belka, G., DuBois, G. (1998), *Biochem. J.* **331**, 659-668.

Jia, L., Bonaventura, C., Bonaventura, J., Stamler, J. S. (1996), *Nature.* **380**, 221-226.

Jiang, X. M., Fitzgerald, M., Grant, C. M., and Hogg, P. J. (1999), *J. Biol. Chem.* **274**, 393–399.

Jiang, X. P., Wang, F., Yang, D. C., Elliott, R. L., Head, J. F. (2002), *Anticancer Res.* **22**, 2685-2692.

Johnson, M.A., Macdonald, T. L., Mannick, J. B., Conaway, M. R., Gaston, B. (2001), *J. Biol. Chem.* **276**, 39872-39878.

Johnson, S., Michalak, M., Opas, M., Eggleton, P. (2001), *Cell Biol.* **11**, 122-129.

Jourd'heuil, D., Hallen, K., Feelisch, M., and Grisham, M. B. (2000), *Free Radic. Biol. Med.* **28**, 409–417.

Karki P., Lee J., Shin S. Y., Cho B., Park S. *Arch. Biochem. Biophys.* (2005), **442**: 125-132.

Keefer, L. K., Nis, R. W., Davies, K. M., Wink, D. A. (1996), *Methods Enzymol.* **268**: 281-293.

Kemmink, J., Darby, N. J., Dijkstra, K., Scheek, R. M., Creighton, T. E. (1995), *Protein Sci.* **4**, 2587-2593.

Kemmink, J., Darby, N. J., Dijkstra, K., Nilges, M., Creighton, T. E. (1996), *Biochemistry.* **35**, 7684-7691.

Kemmink, J., Darby, N. J., Dijkstra, K., Nilges, M., Creighton, T. E. (1997), *Curr. Biol.* **7**, 239-245.

Kemmink, J., Dijkstra, K., Mariani, M., Scheek, R. M., Penka, E., Nilges, M., Darby, N. J. (1999), *J. Biomol. NMR.* **13**, 357-368.

Kim, Y. M., Talanian, R. V., Billiar, T. R. (1997), *J. Biol. Chem,* **272**, 31138-31148.

Kinoshita, H., Milstein, S., Wambi, C., Katusic, Z. S. (1997), *Am. J. Physiol.* **273**, H718-H724.

Kivirikko, K. I., Myllyla, R., Pihlajaniemi, T. (1989), *FASEB J.* **3**,1609-17.

Klappa, P., Ruddock, L.W., Darby, N.J., Freedman, R.B. (1998), *EMBO J.* **17**, 927–935.

Klatt, P., Schmidt, K., Lehner, D., Glatter, O., Bachinger, H. P., Mayer, B. (1995), *EMBO J.* **14**, 3687-3695.

Klausner, R. D., Ashwell, G., Van Renswoude, J., Harford, J. B., Bridges, K. R. (1983), *Proc. Natl. Acad. Sci. U.S.A.* **80**, 2263-2266.

Klausner, R. D., Van Rebswoude, J., Ashwell, G., Kempf, C., Schechter, A. N., Dean, A., Bridges, K. R. (1983), *J. Biol. Chem.* **258**, 4715-4724.

Kleinhenz, D. J., Fan, X., Rubin, J., and Hart, C. M. (2003), *Free Radic. Biol. Med.* **34**, 856–861.

Korteme, T., Darby, N. J., Creighton, T. E. (1996), *Biochemistry.* **35**, 14503-14511.

Krause, S., Scholz, T., Temmler, U. and Losche, W. (2001) *Platelets* **12**, 423–430.

Lahav, J., Jurk, K., Hess, O., Barnes, M. J., Farndale, R. W., Luboshitz, J. and Kehrel, B. E. (2000), *Blood.* **100**, 2472–2478.

Lancaster, J. R. (1994), *Proc. Natl. Acad. Sci. U.S.A.* **91**, 8137-8141.

Lazebnik, Y. A., Kaufmann, S. H., Desnoyers, S., Poirier, G. G., Earnshaw, W. C. (1994), *Nature.* **371**, 346-347.

Leopold, J. A., and Loscalzo, J. (1995), *Coron. Artery. Dis.* **6**, 923-939.

Li, J., Billiar, T. R., Talanian, R. V., Kim, Y. M. (1997), *Biochem. Biophys. Res. Commun.* **240**, 419-424.

Lillig, C. H., Berndt, C., Vergnolle, O., Lonn, M. E., Hudemann, C., Bill, E., Holmgren, A. (2005), *Proc. Natl. Acad. Sci. U.S.A.* **120**, 8168-8173.

Lipton, A. J., Johnson, M. A., Macdonald, T., Lieberman, M. W., Gozal, D., Gaston, B. (2001), *Nature.* **413**, 171-174.

Liu, L., Hausladen, A., Zeng, M., Que, L., Heitan, J., Stamler, J. S. (2001), *Nature.* **410**, 490-494.

Liu, X., Miller, M. J., Joshi, M. S., Thomas, D. D., Lancaster, J. R. (1998), *Proc. Natl. Acad. Sci. U.S.A.* **95**, 2175-2179.

Lord, S. J., Rajotte, R. V., Korbutt, G. S., Bleackley, R. C. (2003), *Immunol. Rev.* **193**, 31-38.

Lyles, M. M., Gilbert, H. F. (1994), *J. Biol. Chem.* **269**, 30946-30952.

Macer, D. R. and Koch, G. L. (1988) *J. Cell. Sci.* **91**, 61-70.


Mandrup- Poulsen, T., Bendtzen, K., Nielsen, J. H., Bendixen, G, Nerup, J. (1985), *Allergy.* **40**, 1418-1422.

Maron, D. J., Fazio, S., Linton, M. F. (2000), *Circulation.* **101**, 207-213.

Martinez-Ruiz, A. and Lamas, S. (2004), *Arch. Biochem. Biophys.* **423**, 192-199.

McMahon, T. J., Stone, A. E., Bonaventura, J. Singel, D. J., Stamler, J. S. (2000), *J. Biol. Chem,* **275**, 16738-16745.

McMahon, T. J., Moon, R. E., Luschinger, B. P., Carraway, M. S., Stone, A. E., Stolp, B. W., Gow, A. J., Pawloski, J. R., Watke, P., Singel, D. J., Piantadosi, C. A., Stamler, J. S. (2002), *Nat. Med.* **8**, 711-717.

Miranda, K. M., Espey, M. G., Jourd'heuil, D., Grisham, M. B., Fukuto, J. M., Feelisch, M., Wink, D. A. (2000), *In* "Nitric Oxide: Biology and Pathobiology" (L. J. Ignarro, ed), pp. 41-55, Academic Press, San Diego.

Moncada, S., Palmer, R. M. J., Higgs, E. A., (1991), *Pharacol. Rev.* **43**, 109-142.

Moore, E. C., Reichard, P., Thelander, L. (1964), *J. Biol. Chem.* **239**, 3445-3452.

Moro, M. A., Russel, R. J., Cellek, S., Lizasoain, I., Su, Y., Darley-Usmar, V. M., Radomski, M. W. and Moncada, S. (1996) *Proc. Natl. Acad. Sci. U.S.A.* **93**, 1480–1485.

Munoz-Fuentes, R. M., Vargas, F. and Bobadilla, N. A. (2003), *Rev. Invest. Clin.* **55**, 670–676.

Murad, F. (1994), *Rec. Prog. in. Hor. Res.* **49**, 239-248.

Murrell, W. (1879), *Lancet.* **1**, 8-81, 113-115, 151-152, 225-227.

Mustard, J. F., Kinlough-Rathborne, R. L. and Packham, M. A. (1989), *Methods Enzymol.* **169**, 3-11.

Na, S., Chuang, T.-H., Cunningham, A., Turi, T. G., Hanke, J. H., Bokoch, G. M., Perry, D. K., Smyth, M. J., Stennicke, H. R., Salvesen, G. S., Duriez, P., Poirier, G. G., Hannun, Y. A. (1997), *J. Biol. Chem.* **272**, 18530-18533.

Narindrasorasak, S., Yao, P., Sarkar, B. (2003), *Biochem. Biophys. Res. Comm.* **311**, 405-414.

Nedospasov, A., Rafikov, R., Beda, N., Nudler, E. (2000), *Proc. Natl. Acad. Sci. U.S.A.* **97**, 13543-13548.

Nicholson, D. (1996), *Nat. Biotechnol.* **14**, 297-301.

Nikitovic, D., Holmgren, A. (1996), *J. Biol. Chem.* **271**, 19180-19185.

Noble, D. A., and Williams, D. L. H. (2001), *J. Chem. Soc., Perkin Trans.* **2**, 13-17.

Noiva, R., and Lennarz, W. J. (1992), *J. Biol. Chem.* **267**, 3553–3556.

Noiva, R. (1994), *Prot. Expr. Purif.* **5**, 1-13.

Packhma, M. A. (1994), *Can. J. Physiol. Pharmacol.* **72**, 278-284.

Pfeiffer, S., Schrammel, A., Schmidt, K. and Mayer, B. (1998), *Anal. Biochem.* **258**, 68-73.

Papov, V. V., Gravina, S. A., Mieyal, J. J., Biemann, K. (1994), *Prot. Sci.* **3**, 428-434.

Pawloski, J. R., Hess, D. T., Stamler, J. S. (2001), *Nature.* **409**, 622-626.

*Perry, D. K., Smyth, M. J., Stennicke, H. R., Salvesen, G. S., Duriez, P., Poirier, G. G., Hannun, Y. A. (1997)*, J Biol Chem. *272, 18530-18533.*

Pihlajaniemi, T., Helaakoski, T., Tasanen, K., Myllyla, R., Huhtala, M. L., Koivu, J., Kivirikko, K. I. (1987), *EMBO J.* **6**, 643–649.

Ponte, J. F., and Huot, A. E. (1996), *In* "Biology of Nitric Oxide", part 5 (Moncada, S., Stamler, J. S., Gross, S., Higgs, E. A., eds), pp. 134, Portland Press, London.

Ponte, J. F., and Huot, A. E. (1996), *In* "Nitric Oxide and the Cell",(Moncada, S., Nistico, G., Bagetta, G., Higgs, E. A., eds), pp. 293-300, Portland Press, London.

Puig, A., and Gilbert, H. F. (1994), *J. Biol. Chem.* **269**, 7764-7771.

Raff, M. (1998), *Nature.* **396**, 119-122.

Rafikova, O., Rafikov, R., Nudler, E. (2002), *Proc. Natl. Acad. Sci. U.S.A.* **99**, 5913-5918.

Ramachandran, N., Root, P., Jiang, X.-M., Hogg, P. J., Mutus, B. (2001), *Proc. Natl. Acad. Sci. U.S.A.* **98**, 9539-9544.

Raturi, A. (2007), *In* PhD Thesis (University of Windsor, Department of Chemistry and Biochemmistry, Windsor, ON), pp. 100-141.

Raturi, A., and Mutus, B. (2007), *FRBM.* doi:10.1016/j.freeradbiomed.2007.03.025 (*In Press*).

Raturi, A., Vacratsis, P. O., Seslija, D., Lee, L., Mutus, B. (2005), *Biochem J.* **391**, 351–357.

Redondo, P. C., Jardin, I., Hernandez-Cruz, J. M., Pariente, J. A., Salido, G. M., Rosado, J. A. (2005), *Biochem. Biophys. Res. Commun.* **333**, 794-802.

Rietsch, A., Bessette, P., Georgiou, G., and Beckwith, J. (1997), *J. Bacteriol.* **179**, 6602–6608.

Romeo, A. A., Capobianco, J. A., English, A. M. (2003), *J. Am. Chem. Soc.* **125**, 14370-14378.

Root, P. (2004), *In* PhD Thesis (University of Windsor, Department of Chemistry and Biochemmistry, Windsor, ON), pp. 141-166.

Root, P., Sliskovic, A., Mutus, B. (2004), *Biochem. J.* **382**, 575-580.

Roy, C., Brown, D., Little, J. E., Valentine, R. K., Walker, P. R., Sikorska, M., LeBlanc, J., Chaly, N. (1992), *Exp. Cell Res.* **200**, 416-424.

Ryser, H. J.-P. and Fluckiger, R. (2005), *Drug Disc. Today.* **10**, 1085-1094.

Schwaller, M., Wilkinson, B., and Gilbert, H. F. (2003), *J. Biol. Chem.* **278**, 7154–7159.

Schwaller, M., Wilkinson, B., Gilbert, H. F. (2003), *J. Biol. Chem.* **278**, 7154-7159.

Schwoch, G., and Passow, H. (1973), *Mol. Cell. Biochem.* **2**, 197-217.

Seslija, D. (2005), *In* M. Sc. Thesis. (University of Windsor, Department of Chemistry and Biochemmistry, Windsor, ON), pp. 31-32.

Sexton, D. J., Muruganandam, A., McKenney, D. J., Mutus, B. (1994), *Photochem. Photobiol.* **59**, 463-367.

Shah, C., Locke, I. C., Chowdrey, H. S., Gorrge, M. P. (2003), *Biochem. Soc. Trans.* **31**, 1450-1452.

Shapiro, A. D. (2000), *Haemophilia.* **6 Suppl 1**, 120-127.

Shikama, K., and Matsuoka, A. (2003), *Eur. J. Biochem.* **270**, 4041-4051.

Sliskovic, I., Raturi, A., and Mutus, B. (2005), *JBiol Chem.* **280**,8733-8741.

Smith, S. C. (2007), *Am. J. Med.* **120**, S3-S11.

Smolka, M. B., Zhou, H., Purkayastha, S., Aebersold, R. (2001), *Anal. Biochem.* **297**, 25-31.

Solovyov, A., Gilbert, H. F. (2004) *Prot. Sci.* **13**, 1902-1907.

Song, J. L. and Wang, C. C. (1995), *Eur. J. Biochem.* **231**, 312-316.

Song, Q., Lees-Miller, S. P., Kumar, S., Zhang, N., Chan, D. W., Smith, G. C. M., Jackson, S. P., Alneri, E. S., Litwack, G., Khanna, K. K., Lavin, M. F. (1996), *EMBO J.* **15**, 3238-3246.

Sonta, T., Inoguchi, T., Tsubouchi, H., Sekiguchi, N., Kobayashi, K., Matsumoto, S., Utsumi, H., Nawata, H. (2004), *Free Radic. Biol. Med.* **37**, 115–123.

Spitaler, M. M., and Graier, W. F. (2002), *Diabetologia.* **45**, 476–494.

Springer, T. A. (1995), *Annu. Rev. Physiol.* **57**, 827-872.

Stamler, J. S., Medelsohn, M. E., Amarante, P., Smick, D., Andon, N., Davies, P. F., Cooke, J. P., Loscalzo, J. (1989), *Circ. Res.* **65**, 789-795.

Stamler, J. S., Jaraki, O., Osborne, J., Simon, D. I., Keaney, J., Vita, J., Singel, D., Valeri, C. R., Loscalzo, J. (1992), *Proc. Natl. Acad. Sci. U.S.A.* **89**, 7674-7677.

Stamler, J. S., Jia, L., Eu, J. P., McMahon, T. J., Demchenko, I. T., Bonaventura, J., Gernert, K., Piantadosi, C. A. (1997), *Science.* **276**, 2034-2037.

Stanbury, D. (1989), *Adv. Inorg. Chem.* **33**, 69-138.

Stennicke H. R., Salvesen G. S. (1997), *J. Biol. Chem.* **272**, 25719-25723.

Stone, J. R., and Marletta, M. A. (1994), *Biochemistry.* **33**, 5636-5640.

Sun, X.-X., Dai, Y., Liu, H.-P., Chen, S.-M., Wang, C.-C. (2000), *Biochem. Biophys. Acta.* **1481**, 45-54.

Taghibiglou, C., Rashid-Kolvear, F., Van Iderstine, S., C., Le-Tien, H., Fantus, I. G., Lewis, G. F., Adeli, K. (2002), *J. Biol. Chem.* **277**, 793-803.

Tanaka, S., Uehara, T., Nomura, Y. (2000), *J. Biol. Chem.* **275**, 10388-10393.

Tannenbaum, S. R., and Kim, J.-E. (2005), *Nat. Chem. Biol.* **1**, 126-127.

Tedder, T. F., Steeber, D. A., Pizcueta, P. (1995), *J. Exp. Med.* **181**, 2259-2264.

Terada, K., Manchikalapudi, P., Noiva, R., Jauregui, H. O., Stockerrt, R. J., Schilsky, M. L. (1995), *J. Biol. Chem.* **270**, 20410-20416.

Tian, G., Xiang, S., Noiva, R., Lennarz, W. J, Schindelin, H. (2006) *Cell.* **124**, 61-73.

Toyokuni, S. (1996), *Free Radical Biol. Med.* **20**, 553-566.

Troung-Tran, A. Q., Ruffin, R. E., Zalewski, P. D. (2000), *Am. J. Physiol.* **279**, L1172-L1183.

Trujillo, M., Alvarez, M., Peluffo, G., Freeman, B., Radi., R. (1998), *J. Biol. Chem.* **273**, 7929-7934.

Tsuji, S., Sugimoto, M., Miyata, S., Kuwahara, M., Kinoshita, S., Yoshioka, A. (1999), *Blood.* **94**, 968-975.

Tsukihira, T., Fukuyama, K., Nakamura, M., Katsube, Y., Tanaka, N., Kakudo, M., Wada, K., Hase, T., Matsubara, H. (1981), *J. Biochem.* **90**, 1763-1773.

Tuderman, L., Kuutti, E. R., Kivirikko, K. I. (1975), *Eur J Biochem.* **52**, 9-16.

Turano, C., Coppari, S., Altieri, F., Ferraro, A. (2002), *J. Cell. Physiol.*, **193**, 154-163.

Uehara, T., Nakamura, T., Yao, D., Shi, Z. Q., Gu, Z., Ma, Y., Masliah, E., Nomura, Y., and Lipton, S. A.(2006), *Nature.* **441**, 513–517.

Vanin, A. F., Malenkova, I. V., Serezhenkov, V. A. (1997), *Nitric Oxide.* **1**, 191-203.

Venkataraman, S., Martin, S. M., Schafer, F. Q., Buettner, G. R. (2000), *Free Radic. Biol. Med.* **29**, 580-585.

Vinik, A. I., Erbas, T., Park, T. S., Nolan, R., Pittenger, G. L. (2001), *Diabetes Care.* **24**, 1476-1485.

Walker, N. P., Talanian, R. V., Brady, K. D., Dang, L. C., Bump, N. J., Ferenz, C. R., Wang, F, Elliott, R. L., Head, J. F. (1999), *Anticancer Res.* **19**, 445-450.

Wang, G.-R., Zhu, Y., HAlushka, P. V., Lincoln, T. M., Mendelsohn, M. E. (1998), *Proc. Natl. Acad. Sci. U.S.A.* **95**, 4888-4893.

Wang, X., Wang, W., Li, Y., Bai, Y., Fiscus, R. R. (1999), *J. Mol. Cell. Cardiol.* **31**, 1599-1606.

Ware, J. A., Smith, M., Salzman, E. W. (1987), *Blood.* **94**, 968-975.

Waterhouse, N., Kumar, S., Song, Q., Strike, P., Sparrow, L., Dreyfuss, G., Alneri, E. S., Litwack, G., Lavin, M., Watters, D. (1996), *J. Biol. Chem.* **271**, 29335-29341.

Wetterau, J. R., Combs, K. A., Spinner, S. N., Joiner, B. J. (1990), *J. Biol. Chem.* **265**, 9800-9807.

Wetterau, J. R., Aggerbeck, L. P., Laplaud, P. M., McLean, L. R. (1991), *Biochemistry.* **30**, 4406-4412

Whiteside, W. M., Sears, D. N., Young, P. R., Rubin, D. B. (2002), *Radiation Res.* **157**, 578-588.

Williams, D. L. (1996), *Methods Enzymol.* **268**, 299–308.

Wilkinsin, B., and Gilbert, H. F. (2004), *Biochim. Biophys. Acta.* **1699**, 35-44.

Wink, D. A., Darbyshire, J. F., Nims, R. W., Saveedra, J. E., Ford, P. C. (1993), *Chem. Res. Toxicol.* **6**, 23-27.

Wink, D. A., Kim, S., Coffin, D., Cook, J. C., Vodovotz, Y., Chistodoulou, D., Jourd'heuil, D., and Grisham, M. B. (1999), *Methods Enzymol.* **301**, 201–211.

Wright, S. K., Viola, R. E. (1998), *Anal. Biochem.* **265**, 8–14.

Wylie, A. H., Kerr, J. F. R., Currie, A. R. (1980), *Int. Rev. Cytol.* **68**, 251-306.

Xu, X., Cho, M., Spencer, N. Y., Patel, N., Huang, Z., Shields, H., King, S. B., Gladwin, M. T., Hogg, N., Kim-Shapiro, D. (2003), *Proc. Natl. Acad. Sci. U.S.A.* **100**, 11303-11308.

Yao, Y., Zhou, Y. C., Wang, C. C. (1997), *EMBO J.* **16**, 651-658.

Yeh, A. P., Chatelet, C., Soltis, S. M., Kuhn, P., Meyer, J., Rees, D. C. (2000), *J. Mol. Biol.* **300**, 587-595.

Yoshimori, T., Semba, T., Takemoto, H., Akagi, S., Yamamoto, A., Tashiro, Y. (1990), *J. Biol. Chem.* **265**, 15984-15990.

Yubisui, T., Miyata, T., Iwanaga, S., Tamura, M., Takeshita, M. (1986), *J. Biochem.* **99**, 407-422.

Zai, A., Rudd, A. M., Scribner, A. W., and Loscalzo, J. (1999), *J. Clin. Investig.* **103**, 393-399.

Zapun, A., Bardwell, J. C., Creighton, T. E. (1993) *Biochemistry.* **32**, 5083-5092.

Zhang, X., and Broderick, M. (2000), *Mod. Asp. Immunobiol.* **4**, 160-165.

Zhang, Y., Keszler, A., Broniowska, K. A., Hogg, N. (2005), *Free Rad. Biol. Med.* **38**, 874-881.

# APPENDIX

## A. Buffers

### i) Acid Citrate Dextrose (ACD)

25 g/L trisodium citrate dehydrate
15 g/L citric acid monohydrate
20 g/L dextrose

### ii) Hypotonic Phosphate Buffer

1.38 g/L $NaH_2PO_4$
0.943 g/L $Na_2HPO_4$
pH 7.4

### iii) Isotonic Phosphate Buffer

21.39 g/L $NaH_2PO_4$
14.62 g/L $Na_2HPO_4$
pH 7.4

### iv) Lysis Buffer

100 mM Tris-HCl
200 mM NaCl
2 mM EDTA
100 μg/mL Lysozyme
50 μg/mL DNase I
50 μg/mL RNase
2 mM PMSF
1% Triton X-100
pH 8

### v) Phosphate Buffered Saline (PBS)

8 g/L NaCl
1.44 g/L $Na_2HPO_4$
0.24 g/L $KH_2PO_4$

02 g/L KCl
pH 7.4

### vi) PDI Assay Buffer

14.2 g/L $Na_2HPO_4$
0.58 g/L EDTA
pH 7.0

### vii) Terrific Broth (TB)

12 g/L Tryptone
24 g/L Yeast Extract
9.4 g/L $K_2HPO_4$
2.0 g/L $KH_2PO_4$
35 mg/L kanamycin
pH 7.2

### viii) Tyrode Buffer

8.0 g/L NaCl
0.2 g/L KCl
1.0 g/L $NaHCO_3$
0.05 g/L $NaH_2PO_4$
0.2 g/L $MgCl_2 \cdot 6H_2O$
0.44 g/L $CaCl_2 \cdot 6H_2O$
3.5 g/L bovine serum albumin
1 g/L dextrose
pH 7.4

## B. Deterimination of thiol using Ellman's Reagent

All DTBN assays were performed using a stock solution (10 mM) in 100 mM phosphate buffer, pH 8.0. Free thiols in the sample were quantified by addition of DTNB to a final concentration of 1 mM followed by the absorbance measurements of nitrothiolbenzoate anion at 412 nm, using the extinction coefficient of 13 600 L $mol^{-1}$ $cm^{-1}$ (Ellman, 1959).

## C. Griess Assay

A standard curve was constructed by adding 100 µL of increasing sodium nitrite concentrations to 100 µL of 4.0 M HCl and sulfanilic acid (dissolved in 40 mM HCl) each. The standards were thoroughly mixed for 10 minutes and 100 µL of N-(-1-naphthyl)ethylenediamine dihydrochloride (2 g/L) was added and left to react for 15 minutes. The absorbance at 540 nm was measured and plotted over the range of sodium nitrite concentrations. Unknown nitrite concentrations were determined in the same way as the described above.

## D. Protein Quantification Using Bradford Assay

A standard curve was generated using 200 µL of Bradford Protein Assay with a series of bovine serum albumin concentrations ranging from 0-20 µg/mL in a phosphate buffer, pH 7.0 to a final volume of 1 mL. The mixture was allowed to react for 10 minutes at the room temperature and the absorbance was measured at 595 nm. Unknown protein concentration was determined in the same way, with appropriate dilutions made in order to obtain the absorbance within the range of the standard.

## E. SDS-Polyacrylamide Gel Electrophoresis

Resolving gel was prepared as follows:

    4.0 mL of H$_2$O
    3.3 mL of 30 % acrylamide mix
    2.5 mL of 1.5 M Tris (pH 8.8)
    0.1 mL of 10 % SDS
    0.1 mL of 10 % ammonium persulfate
    0.002 mL of TEMED

This combination is sufficient for preparation of two gels. The mixture was added to the gel casting cassettes and covered with tert-butanol until the gel polymerized.

Next, stacking gel was prepared as follows:

    3.4 mL of $H_2O$
    0.83 mL of 30 % acrylamide ix
    0.63 mL of 1.0 M Tris (pH 6.8)
    0.05 mL of 10 % SDS
    0.05 mL of 10 % ammonium persulfate
    0.005 mL of TEMED

This mixture was poured on top of the resolving gel and the lane comb was inserted until the stacking gel was polymerized.

Samples were prepared by combining 20 μL of protein sample with 20 μL loading dye and heated at 100°C for 5 minutes.

The gel was generally run at 60 V until the sample had passed through the stacking gel when the voltage was increased to 120 V.

Staining was performed using a staining solution containing 0.25 g of Coomassie Brilliant Blue, 90 mL of methanol: $H_2O$ (1:1 v/v) and 10 mL of stock glacial acetic acid, for 1 hour at the room temperature.

Destaining was performed in the same solution lacking Coomassie Brilliant Blue dye, until background was brought to the minimum.

# VITA AUCTORIS

## Inga Slišković

**PLACE OF BIRTH:**

Sarajevo, Bosna i Hercegovina

**DATE OF BIRTH:**

May 9, 1978

**EDUCATION:**

2002-2007          Ph.D. Biochemistry
Department of Chemistry and Biochemistry
University of Windsor, Windsor, Ontario

1998-2002          B. Sc. Chemistry
Department of Chemistry
University of Winnipeg, Winnipeg, Manitoba

**EXPERIENCE:**

2002-2007          Research Assistant in Dr. Bulent Mutus Lab
Department of Chemistry and Biochemistry
University of Windsor, Windsor, Ontario

2002-2007          Graduate Assistant
Department of Chemistry and Biochemistry
University of Windsor, Windsor, Ontario

Summer 2002          Research Assistant in Dr. Michael Eze Lab
                     Department of Chemistry
                     University of Winnipeg, Winnipeg, Manitoba

2001-2002            Laboratory Demonstrator
                     Department of Chemistry
                     University of Winnipeg, Winnipeg Manitoba

## AWARDS:

Tuition Scholarship, University of Windsor, Windsor, ON; 2003-2007

Pre-Doctoral Travel Award, Society of Free Radical Biology and Medicine, 2005

Pre-Doctoral Travel Award, American Society for Photobiology; 2003

Conference Travel Award, University of Windsor, Windsor, ON, 2003, 2004, 2006

Entrance scholarship from the University of Winnipeg, MB 1998/1999

## PUBLICATIONS:

1. Miersch S., **Sliskovic I.**, Vignini A., Mazzanti L., Mutus B. Extracellular NO-Mediated Platelet-cGMP Production in T2D Correlates Indirectly with Plasma Membrane Cholesterol Levels (*Submitted to Diabetologia*).

2. Miersch S., **Sliskovic I.**, Raturi A., Mutus B. (2007), Anti-oxidant and Anti-platelet effects of Rosuvastatin in a hamster model of pre-diabetes. *Free Radical Biology and Medicine*. 42(2): 270-279.

3. Kozareva A., **Sliskovic I.**, Mutus B., Vacratsis P. (2007), Identification of redox sensitive thiols of protein disulfide isomerase using isotope coded affinity technology and mass spectrometry. *Journal of the American Society for Mass Spectrometry*. 18(2):260-9.

4. **Sliskovic I.**, Mutus B. (2006), Reversible inhibition of caspase-3 activity by iron (III)-Potential role in physiological control of apoptosis. *FEBS Letters*. 580: 2233-2237.

5. Larsen A., **Sliskovic I.**, Juric D., Pinnock C. L., Kullman H., Segstro E., Reinfelds G., Eze M. O. (2005), The fatty acid profile of vegetative Azotobacter vinelandii ATCC 12837: growth phase-dependence. *Applied Microbiology and Biotechnology*. 68(4):548-553.

6. **Sliskovic I.**, Raturi A. and Mutus B. (2005), Characterization of the S-Denitrosation Activity of Protein-Disulfide Isomerase. *Journal of Biological Chemistry*. 280(10):8733-41.

7. Root, P., **Sliskovic, I**, and Mutus, B. (2004), Platelet Cell Surface Protein Disulfide Isomerase-Mediated S-Nitrosothiol Consumption. *Biochemical Journal.* 382, 575–580.

## PRESENTATIONS:

1. Society of Free Radical Biology and Medicine, 13th Annual Meeting, Denver, CO, November 2006. *Characterization of Nitric Oxide Efflux and Influx in Red Blood Cells-The role of protein disulfide isomerase (Poster)*

2. Society of Free Radical Biology and Medicine, 12th Annual Meeting, Austin TX, November 2005. *Control of Caspase-3 activation by Protein Disulfide Isomerase (Poster)*

3. Canadian Federation of Biological Societies, 48th Annual Meeting, Guelph ON, June 2005. *Quantification of cell-surface Protein Disulfide Isomerase active site oxidation by ICAT MALDI-TOF (Poster)*

4. 75th European Atherosclerosis Society Congress, Prague, Czech Republic, April 2005 *Rosuvastatin-dependent anti-oxidant and anti-platelet effects in Syrian hamster model of Type II diabetes (Poster)*

5. Free Radical Biology and Medicine, Virgin Islands, Nov 2004 *Characterisation of S-denitrosation activity of Protein Disulfide Isomerase (Poster)*

6. Canadian Diabetis Association, Montreal 2004 *Platelet Cell Surface Protein-Disulfide Isomerase Mediated S-Nitrosothiol Consumption* (Poster)

7. American Society for Photobiology, 31th Annual Meeting, Baltimore, MD; July 2003 *Characterizing the denitrosation activity of Protein Disulfide Isomerase using Fluorescent probes* (Presentation)

8. University of Windsor, Department of Chemistry and Biochemistry Mini-symposium, Windsor, Ontario; May 2003 *Fluorescent RSNOs as Substrates for Studying PDI Denitrosation Activity* (Presentation)

9. Nitric Oxide Conference, Ventura Beach, CA; February 2003 *Mechanism of NO transfer to cytosol from extracellular SNO-proteins* (Presentation)

10. Western Canada Undergraduate Conference, Calgary, Alberta; May 2002 *Effects of Cerulenin and Nitric Oxide on Fatty Acid Synthesis in Escherichia coli.* (Presentation)